PKCδ-mediated SGLT1 upregulation confers the acquired resistance of NSCLC to EGFR TKIs

Chia-Hung Chen[1,2,3,†], Bo-Wei Wang[4,5,†], Yu-Chun Hsiao[4,5,6,†], Chun-Yi Wu[7], Fang-Ju Cheng[6,8,9], Te-Chun Hsia[1,3,10], Chih-Yi Chen[11], Yihua Wang[12,13], Zhang Weihua [14], Ruey-Hwang Chou[4,6], Chih-Hsin Tang[2,8], Yun-Ju Chen[15,16,17], Ya-Ling Wei[4], Jennifer L. Hsu[4,9], Chih-Yen Tu[1,2,*], Mien-Chie Hung[4,5,6,*], Wei-Chien Huang[4,5,6,18,*]

[1]Division of Pulmonary and Critical Care Medicine, Department of Internal Medicine, China Medical University Hospital, Taichung 404, Taiwan.

[2]School of Medicine, China Medical University, Taichung 404, Taiwan.

[3]Department of Respiratory Therapy, China Medical University, Taichung 404, Taiwan.

[4]Center for Molecular Medicine, Research Center for Cancer Biology, and Graduate Institute of Biomedical Sciences, China Medical University, Taichung 404, Taiwan.

[5]Drug Development Center, China Medical University, Taichung 404, Taiwan.

[6]The Ph.D. program for Cancer Biology and Drug Discovery, China Medical University and Academia Sinica, Taichung 404, Taiwan.

[7]Department of Biomedical Imaging and Radiological Sciences, National Yang-Ming University, Taipei, 112, Taiwan.

[8]Graduate Institute of Basic Medical Science, China Medical University, Taichung, 404, Taiwan.

[9]Department of Molecular and Cellular Oncology, The University of Texas MD Anderson Cancer Center Houston, Texas, 77030.

[10]Department of Internal Medicine, Hyperbaric Oxygen Therapy Center, China Medical University Hospital, Taichung 404, Taiwan.

[11]Institute of Medicine, Chung Shan Medical University; Division of Thoracic Surgery, Department of Surgery, Chung Shan Medical University Hospital, Taichung , 402, Taiwan

[12]Biological Sciences, Faculty of Environmental and Life Sciences, University of Southampton SO17 1BJ, UK.

[13]Institute for Life Sciences, University of Southampton SO17 1BJ, UK.

[14]Department of Biology and Biochemistry, University of Houston, Texas, 77030.

[15]Department of Medical Research, E-Da Hospital, Kaohsiung, 824, Taiwan

[16]School of Medicine for International Students, I-Shou University, Kaohsiung, 824, Taiwan

[17]Department of Pharmacy, E-Da Hospital, Kaohsiung, 824, Taiwan

[18] Department of Medical Laboratory Science and Biotechnology, Asia University, Taichung 41354, Taiwan.

[†]These authors contributed equally to this study.

[*]Corresponding authors: To whom correspondence should be addressed.

***Correspondence:** Wei-Chien Huang, Graduate Institute of Biomedical Science, China Medical University, 6, Hsueh-Shih Road, Taichung, Taiwan, 40402, R.O.C. Tel: 886-4-22052121 #7931, Email: whuang@mail.cmu.edu.tw. ORCID ID: https://orcid.org/0000-0001-6467-8716; Mien-Chie Hung, China Medical University, 100, Sec. 1, Jingmao Road, Taichung, 406, Taiwan. Tel: 886-4-22057153, Email: mhung@cmu.edu.tw, ORCID ID: https://orcid.org/0000-0003-4317-4740; or Chih-Yen Tu, Department of Internal Medicine, China Medical University Hospital, No. 2, Yude Road, Taichung 404, Taiwan. Phone: +886-4-22052121. E-mail: chesttu@gmail.com. ORCID ID: https://orcid.org/0000-0002-8126-6171.

Keywords: EGFR, SGLT1, glucose uptake, PKCδ, lung cancer, acquired resistance

Running title**:** SGLT1 mediates EGFR TKI resistance

Abstract

The tyrosine kinase inhibitors (TKIs) targeting epidermal growth factor receptor (EGFR) have been widely used for non-small cell lung cancer (NSCLC) patients, but the development of acquired resistance remains a therapeutic hurdle. The reduction of glucose uptake has been implicated in the anti-tumor activity of EGFR TKIs. In this study, the upregulation of the active sodium/glucose co-transporter 1 (SGLT1) was found to confer the development of acquired EGFR TKI resistance, and was correlated with the poorer clinical outcome of the NSCLC patients who received EGFR TKI treatment. Blockade of SGLT1 overcame this resistance *in vitro* and *in vivo* by reducing glucose uptake in NSCLC cells. Mechanistically, SGLT1 protein was stabilized through the interaction with PKCδ-phosphorylated (Thr678) EGFR in the TKI-resistant cells. Our findings revealed that PKCδ/EGFR axis-dependent SGLT1 upregulation was a critical mechanism underlying the acquired resistance to EGFR TKIs. We suggest co-targeting PKCδ/SGLT1 as a potential strategy to improve the therapeutic efficacy of EGFR TKIs in NSCLC patients.

Introduction

The epidermal growth factor receptor (EGFR), a membrane-bound tyrosine kinase receptor, has been found to be a critical oncogene in promoting the tumorigenesis, mitogenesis, and tumor progression of various cancer types, including non-small cell lung cancer (NSCLC)[1, 2]. Overexpression or somatic mutation of EGFR causes the aberrant activation of its tyrosine kinase and the dysregulation of its downstream signals that contribute to the tumor growth and progression and the poor prognosis of NSCLC patients[3]. EGFR is therefore a rational and feasible therapeutic target for this disease.

Small molecule tyrosine kinase inhibitors (TKIs) targeting the ATP-binding pocket of the EGFR kinase domain were developed and approved for NSCLCs[4]. Gefitinib (ZD1839,

Iressa) and erlotinib (OSI-774, Tarceva) are two approved first-generation EGFR TKIs for NSCLC. However, these drugs fail to achieve maximum therapeutic efficacy, with response rates of typically 10%–20% across a variety of malignancies[4]. Gefitinib and erlotinib particularly benefit Asian NSCLC patients who are female, never-smokers, and have an adenocarcinoma histology. Importantly, the high prevalence of activating EGFR mutations, including the exon 19 (L746-A750) deletion and L858R point mutation, were found in these patients[5]. These activating mutations alter the protein structure of EGFR at its ATP-binding site and increase the binding affinity and vulnerability to TKIs[6]. However, a frequent substitution of threonine residue to methionine at codon 790 (T790M) of EGFR exon 20 has been found to reduce the binding affinity with gefitinib or erlotinib, and thereby contributes to the development of acquired resistance[1]. The second-generation irreversible TKI, afatinib (BIBW2992, Gilotrif), was developed to target the activating EGFR mutant with less likelihood of the EGFR T790M point mutation[7]. The third-generation TKI, osimertinib (AZD9291, Tagrisso), was further designed to target the EGFR T790M mutation[8, 9]. The secondary EGFR mutations[10] and activations of alternative RTKs creating a bypass track[11, 12] have been proposed as reasons for the failed responses to EGFR TKIs, yet fail to fully account for the development of acquired resistance to these drugs in NSCLC patients.

Several studies have shown that, in addition to delivering the classic proliferation and survival signals, activated EGFR also facilitates glucose utility and metabolic pathways through the stabilization of glucose transporters and dysregulation of glycolytic enzymes hexokinases and pyruvate kinase M2 (PKM2) that promote tumor growth, epithelial-mesenchymal transition (EMT), cancer stemness, and even immune evasion[13-17]. Recently, tyrosine kinase activation of EGFR was shown to enhance the activity of 6-phosphofructo-2-kinase/fructose-2,6-bisphosphatase-3 (PFKFB3), an essential

glycolytic activator for the synthesis and degradation of fructose-2,6-bisphosphate (F26BP) that contributes to the survival of NSCLC cells[18]. EGFR signaling also links glycolysis with serine synthesis to support for nucleotide biosynthesis and redox homeostasis[19]. Mounting evidence has proved that EGFR impacts on the rewiring of the glucose metabolic network to promote tumor progression in NSCLC[20].

Clinically, the decrease in glucose metabolism measured by the uptake of 2-[^{18}F]-fluoro-2-deoxy-D-glucose ([^{18}F]-FDG), the radiolabeled glucose analog, with positron emission tomography (PET) analysis appears within days of initiating EGFR TKI therapy in NSCLC patients[21]. [^{18}F]-FDG uptake is significantly decreased by erlotinib treatment in sensitive, not insensitive, human NSCLC-xenograft mouse tumors[22, 23]. Changes in tumor glucose metabolism precede decreases in tumor size in response to EGFR TKIs[22, 24]. These findings suggest that reduction of EGFR-mediated glycolysis may be involved in the anti-tumor activity of EGFR TKIs, and thus monitoring [^{18}F]-FDG-PET uptake has been used to predict therapeutic responses to EGFR TKIs in lung cancer patients[25-27]. Moreover, suppression of facilitative glucose transporter Glut was found to mediate the anti-cancer activity of TKIs in NSCLC cell lines bearing wild-type (wt) or mutant EGFR[28]. These studies suggested that the suppression of glucose uptake and metabolism may be essential to achieve the therapeutic response of EGFR TKIs in NSCLC patients. However, elevated lactate secretion and glycolysis were found in long-term TKI treatment of NSCLC cells and in prostate cancer cells[29-31], raising the possibility that glucose metabolic re-wiring may contribute to the development of acquired resistance of NSCLC to EGFR TKIs.

In this study, our data showed that NSCLC cells with acquired EGFR TKI resistance are more tolerant to low glucose-induced autophagy following a metabolic shift to higher glucose uptake and glycolysis activity due to upregulation of active glucose transporter

SGLT1 by Thr678-phosphorylated EGFR, in a PKCδ-dependent manner. Higher SGLT1 expression correlated with poorer clinical outcomes of EGFR TKI-treated NSCLC patients, while targeting SGLT1 with pharmacological inhibitors suppressed enhancements in glucose metabolism and lowered acquisition of EGFR TKI resistance in NSCLC xenograft-bearing mice. Our results not only elucidate the metabolic mechanism underlying the development of acquired resistance to EGFR TKIs, but also indicate that targeting PKCδ/SGLT1 in combination with EGFR TKIs may benefit NSCLC patients.

Results

TKI-resistant cells are tolerant to autophagic cell death induced by glucose deprivation

To determine whether alternation of glucose metabolism plays a role in the development of acquired resistance to EGFR TKIs, we first established erlotinib-resistant (ER) clones from wt EGFR-expressing NSCLC lines NCI-H322 (H322) and NCI-H292 (H292) and from an activating EGFR mutant-expressing HCC827 lung adenocarcinoma cell line by culturing the cells in increasing concentrations of erlotinib (by 2.5 μM every 2–3 weeks, up to a maintenance concentration of 10 μM for 3 months). Their resistance to erlotinib was validated in WST-1 assays (Supplementary Figs S1a-S1c). Interestingly, the viability of the parental cell lines, but not their corresponding ER clones, was dramatically and dose-dependently decreased by reducing glucose concentrations from 4.5 to 0.1 g/L in the culture medium in WST1 (Fig 1a and Supplementary Fig S1d) and cell counting assays (Fig 1b). Similarly, ER clones of H322 and HCC827 cells were also more tolerant to glucose deprivation in clonogenic formation assays (Fig 1c). Flow cytometric analysis further showed that glucose deprivation increased the sub-G1 population of parental H322 and HCC827 cells, but not their corresponding ER clones (Fig 1d).

Nutrition and energy deprivation trigger autophagy in a variety of cells[32], but the roles of autophagy in determining the sensitivity to EGFR TKIs in NSCLC remain controversial[11, 33-36]. Pretreatment of H322 and HCC827 cells with 3-methyladenine (3-MA) and chloroquine (CQ), which suppress autophagic flux by targeting PtdIns3Ks[37] and autophagosome-lysosome fusion[38] respectively, prevented the suppression of viability induced by glucose starvation (Supplementary Fig S1e), suggesting that autophagy contributes to glucose deprivation-induced cell death of these cell lines. In support of this finding, the reduction of glucose concentration induced the expression of autophagic marker (LC3β) and apoptotic markers (PARP or caspase 3 cleavage) in H322 (Fig 1e) and HCC827 (Fig 1f) cells, but not their corresponding ER clones. Consistently, the results from Cyto-ID® Autophagy dye staining showed that glucose deprivation enhanced the numbers (Fig 1g) and levels (Fig 1h) of autophagosome-positive cells in the parental H322 cells, but not their ER clones. All of these findings indicated that erlotinib-resistant NSCLC cells are more tolerant to glucose deprivation-induced autophagic cell death.

Erlotinib-resistant lung cancer cells exhibit higher glucose uptake through SGLT1 upregulation

Although TKI-resistant cells were more tolerant to glucose deprivation-induced cell death, inhibition of glycolysis with hexokinase inhibitor 2-deoxy-D-glucose (2-DG) still suppressed the colony formation of the corresponding ER clones of H322 and HCC827 cells (Supplementary Fig S2), suggesting that glucose remains the critical energy source to generate ATP and cell building blocks through glycolysis for cell proliferation in these clones. The elevation in the extracellular acidification rate (ECAR), an indicator of glycolysis, in the corresponding ER clones was higher than that in the parental H322 (Fig 2a) and HCC827 (Supplementary Fig S3a) cells. By monitoring the engulfment of the fluorescent-labeled

deoxyglucose analog 2-NBDG, the glucose uptake ability of these cells was examined. The 2-NBDG uptake was suppressed by erlotinib in H322 (Fig 2b) and HCC827 (Supplementary Figs S3b) cells, but was higher in H322/ER and HCC827/ER clones in the presence of TKI. Interestingly, the ER#2 clone, but not its parental HCC827 cells, elicited higher ECAR under the low (0.1g/L) glucose condition (Supplementary Fig S3c). Increases in 2-NBDG uptake in the corresponding ER clones of H322 cells were more obvious under low glucose culture conditions than under normal glucose conditions (Fig 2c). Active glucose transporters SGLTs are associated with 2-NBDG uptake in SGLT1-overexpressing HEK-293T cells (Supplementary Fig S3d) consistent with previous studies[39, 40], but compared with glucose, show a much lower binding affinity with 2-DG derivatives [41]. These findings imply the involvement of SGLTs in the higher glucose uptake in these TKI-resistant clones. Indeed, the ability to increase the uptake of α-methyl-D-glucopyranoside (α-MDG), a specific substrate for SGLTs, was apparent with H322/ER (Fig 2d) and HCC827/ER (Supplementary Fig S3e) cells compared with their parental cells. These findings support the contention that erlotinib-resistant cells express active glucose transporters that have greater ability for glucose uptake.

Among cancer-related glucose transporters[42, 43], only the expression of SGLT1, not Glut1, Glut3, or SGLT2, was significantly increased in different ER clones of H322 (Fig 2e) and HCC827 (Supplementary Fig S3f) cells. In support of this finding, higher expression of SGLT1 in H292/ER clones than in parental cells (Supplementary Fig S3g) was also detected by the validated anti-SGLT1 antibody (Supplementary Fig S3h) in the xenograft tumor tissues. These data suggest that increased levels of SGLT1 may enhance glucose uptake in erlotinib-resistant cells. Indeed, treatments with SGLT inhibitors phlorizin and LX4211 (sotagliflozin, approved in the European Union for type 1 diabetes mellitus) reduced the 2-NBDG uptake in H322/ER and HCC827/ER clones under low glucose culture conditions

(Fig 2f and Supplementary Fig S3i) without affecting GLUT3 activity (Supplementary Fig S3j). Similar suppressive effects of SGLT1 shRNA on α-MDG uptake were also found in different H322/ER (Fig 2g) and HCC827/ER (Supplementary Fig S3k) clones. SGLT1 shRNA also reduced the glucose consumption of H322/ER#1 cells (Supplementary Fig S3l). These results suggest that upregulation of SGLT1 mediates glucose uptake and thereby supports the viability of acquired EGFR TKI-resistant cells.

Targeting SGLT1 reduced EGFR TKI resistance in vitro and in vivo

We next examined the role of SGLT1 in conferring drug resistance to EGFR TKIs through increasing glucose uptake. Treatments with phlorizin or LX4211 decreased the proliferation rate of ER clones of H322 (Fig 3a) and HCC827 (Supplementary Fig S4a) cells and their viability under low glucose culture conditions (Fig 3b and Supplementary Fig S4b). Consistently, shRNA-mediated depletion of SGLT1 limited the cell growth of different H322/ER (Fig 3c) and HCC827/ER clones (Supplementary Fig S4c), and re-sensitized these ER clones to cell death induced by glucose deprivation (Fig 3d and Supplementary Fig S4d). Treatments with SGLT1 inhibitors phlorizin or LX4211 (Fig 3e, Supplementary Fig S4e) or shRNA (Fig 3f and Supplementary Fig S4f) also enhanced the glucose deprivation-induced caspase 3 or PARP cleavage and LC3β in H322/ER#2 and HCC827/ER#2 cells, but not in the parental H322 cells (Supplementary Fig S4g). Conversely, overexpression of SGLT1 was not only associated with higher α-MDG uptake (Supplementary Fig S4h) and lower levels of apoptotic markers (Supplementary Fig S4i) and cell death (Supplementary Fig S4j) in response to glucose deprivation in H322 cells, but SLGT1 overexpression also attenuated erlotinib-induced PARP and caspase 3 cleavages in parental H322 cells (Fig 3g) and HCC827 cells (Supplementary Fig S4k) and consequently restored the TKI-suppressed viability (Fig 3h and Supplementary Fig S4l). These results support the contention that increased SGLT1

expression enhances glucose uptake and thereby reduces the sensitivity of NSCLC cells to EGFR TKIs.

Next, we addressed whether SGLT1 inhibitors can enhance the therapeutic efficacy of EGFR TKIs in tumor xenograft mouse models. First, SCID mice bearing H292 subcutaneous xenografts were treated with erlotinib (50 mg/kg), phlorizin (20 mg/kg), LX4211 (60 mg/kg) alone, or the combination of erlotinib with either phlorizin or LX4211. Treatments with erlotinib, phlorizin, or LX4211 alone did not significantly reduce tumor growth, but the combination of erlotinib with either phlorizin (Fig 4a) or LX4211 (Supplementary Fig S5a) significantly suppressed the tumor growth. After treatment with erlotinib for 29 days, levels of EGFR and SGLT1 expression were elevated in the xenograft tumor tissues in IHC staining analysis. The combination treatments also enhanced the reduction of the proliferation marker Ki67 and the induction of apoptosis marker PARP cleavage and ATG7, which is induced to mediate autophagy under glucose deprivation [44], in the xenograft tumor tissues (Fig 4b and Supplementary Fig S5b). To examine whether SGLT1 also plays a role in conferring intrinsic resistance to EGFR TKIs, the experimental metastatic NSCLC xenograft model was established by tail vein injection of SGLT1-positive and TKI-insensitive A549 cells transfected with the luciferase gene. Co-treatment with erlotinib and phlorizin reduced the tumor size (Fig 4c) and the number of tumor nodules (Fig 4d). Remarkable reductions in Ki67 expression, as well as increases in ATG7 expression and PARP cleavage, were also found in the lung tumor tissues after co-treatment with erlotinib and phlorizin (Fig 4e). Together, these findings support the therapeutic potential of SGLT1 inhibitors for reducing the development of acquired EGFR TKI resistance in NSCLC patients.

SGLT1 is upregulated in recurrent tumor tissues after the failure of EGFR TKI treatment and is associated with poor prognosis of NSCLC

In the Kaplan-Meier survival analysis of records from the public transcriptomic database[45], higher SGLT1 mRNA expression correlated with an increasingly worse overall survival rate in lung adenocarcinoma patients (Supplementary Fig S6a), which was reflected in both smoker and non-smoker populations (Supplementary Figs S6b and S6c). We next analyzed the clinical correlation of SGLT1 expression with prognosis in 72 NSCLC patients who carried either wt or mutant EGFR and received erlotinib or gefitinib treatments. SGLT1 expression was associated with gender and age, but not smoking behavior, *EGFR* mutation status, tumor size, lymph node metastasis, pathological stage, or immediate response to EGFR TKIs, with higher SGLT1 expression detected in NSCLC tumors of males aged over 55 years (Supplementary Table S1 and Supplementary Figs S6d and S6e). EGFR TKI-treated NSCLC patients with the higher SGLT1-expressing tumors showed a lower overall survival rate with statistical significance (Fig 5a) and a more unfavorable progression-free survival rate with marginal significance (Fig 5b). The negative correlations of SGLT1 expression with overall and progression-free survival rates were also observed in both NSCLC subpopulations; in patients with wt EGFR tumors (Figs 5c and 5d) and those with EGFR mutations (Figs 5e and 5f), respectively.

We then examined the change in SGLT1 expression in human NSCLC tumor tissues after the development of acquired resistance to EGFR TKIs. Treatment-naïve primary tumor tissues paired with the acquired EGFR TKI-resistant tumor tissues were collected from 9 NSCLC patients and were subjected to IHC staining with an anti-SGLT1 antibody. In response to acquired EGFR TKI resistance, recurrent tumor tissues from 6 of 9 patients demonstrated upregulated SGLT1 expression (Fig 5g). Interestingly, SGLT1 expression was increased in all 5 male patients but was decreased in 3 of the 4 female patients (Fig 5h). These results suggest that SGLT1 upregulation may contribute to the acquired resistance to EGFR TKIs in NSCLC patients, especially in males. It is not yet clear whether hormone

receptors are involved in the regulation of SGLT1 expression in lung cancer tissues and would be worthy of further investigation.

Elevated EGFR expression stabilizes SGLT1 expression to support the survival of TKI-resistant cells

EGFR reportedly stabilizes SGLT1 expression, independent of its tyrosine kinase activity[46]. We observed elevations in EGFR expression after treatment with erlotinib (Fig 4b and Supplementary Fig S5b). Thus, we sought to determine whether the upregulation of SGLT1 in TKI-resistant cells depends upon EGFR. We observed increases in both SGLT1 expression and EGFR protein levels, but also a decrease in EGFR Y1068 phosphorylation, a marker for EGFR tyrosine kinase activity, in the TKI-resistant H322 clones in the presence of erlotinib (Fig 6a). Similarly, EGFR upregulation was also observed in the H292/ER xenograft tumor tissues compared to that of their parental cells in SCID mice (Supplementary Fig S7a). Silencing EGFR expression with specific siRNAs reduced the uptake of α-MDG (Fig 6b and 6c) and 2-NBDG (Supplementary Fig S7b) in erlotinib-resistant clones. Similarly, downregulation of EGFR by treatment with cetuximab, the EGFR monoclonal antibody, suppressed α-MDG (Fig 6d) and 2-NBDG (Supplementary Fig S7c) uptake in ER clones. Treatments with EGFR siRNAs (Fig 6e and Supplementary Fig S7d) or cetuximab (Fig 6f and Supplementary Fig S7e) also reduced the cell growth of H322/ER and HCC827/ER clones in colony formation assays. Moreover, downregulation of EGFR by siRNA administration (Fig 6g and Supplementary Fig S7f) or cetuximab (Fig 6h and Supplementary Fig S7g) reduced both EGFR and SGLT1 protein levels, and also increased PARP and caspase 3 cleavages in H322/ER and HCC827/ER clones. In contrast, overexpression of SGLT1 attenuated cetuximab-induced cell death (Fig 6i and Supplementary Fig S7h), PARP and caspase 3 cleavage, and AMPK activation (Fig 6j) in parental NSCLC cells. These results

support the notion that EGFR, in the presence of TKIs, upregulates SGLT1 expression to support cell growth and survival in cells with acquired EGFR TKI resistance.

Phosphorylation of EGFR T678 by PKCδ mediates SGLT1 protein stabilization by enhancing the interaction between EGFR and SGLT1

We next investigated how EGFR stabilizes SGLT1 in TKI-resistant cells independent of its tyrosine kinase activity. Despite tyrosine autophosphorylation, serine or threonine phosphorylation in members of the ErbB family has been found to regulate their kinase activity, protein stability, or endocytosis[47, 48]. Interestingly, we observed that EGFR phosphorylations at T678 and Ser1046/1047, but not T669, all of which are mediated by different Ser/Thr kinases[49-52], were increased in H322/ER clones while Y1068 phosphorylation was suppressed by erlotinib (Fig 7a and Supplementary Fig S8a). The upregulation of EGFR T678 phosphorylation was also observed in the xenograft tumor tissue of parental H292 cells after 1 month of erlotinib treatment (Fig 7b), in the xenograft tissues of H292/ER clones (Supplementary Fig S8b) and in human NSCLC tumors with acquired TKI resistance (Fig 7c), compared with their parental counterparts. Mutation of T678, but not S1046/1047, to Ala abolished EGFR-enhanced SGLT1 expression, and this effect was reversed by treatment with proteasome inhibitor MG132 in HEK-293T cells (Fig 7d). Mutation of T678A also reduced the interaction between EGFR and SGLT1 (Fig 7e). These results suggest that increased T678 phosphorylation of EGFR mediates SGLT1 protein stabilization through a protein-protein interaction.

PKC has been reported to phosphorylate EGFR at T678 to protect EGFR from degradation[49, 50]. Protein kinase Cδ has been found to contribute to the acquired resistance of NSCLCs to EGFR TKIs[12], but the underlying mechanisms remain unclear. Therefore, we next asked whether PKCδ is involved in SGLT1-mediated TKI resistance through EGFR

T678 phosphorylation. The viabilities of H322/ER#2 (Fig 7f) and HCC827/ER#2 (Supplementary Fig S8c) cells were decreased by treatment with the pan-PKC inhibitors GO6983, staurosporine, and sotrasturin, in a dose-dependent manner. GO6983 also suppressed basal and glucose-induced ECAR (Supplementary Figs. S8d and S8e) and glucose uptake (Fig 7g and Supplementary Fig S8f) in H322/ER#2 and HCC827/ER#2 cells. These PKC inhibitors also suppressed EGFR T678 phosphorylation and EGFR and SGLT1 protein levels (Fig 7h and Supplementary Fig S8g). Overexpression of PKCδ induced increases in EGFR levels, EGFR T678 phosphorylation and SGLT1 protein levels in H322 cells (Supplementary Fig S8h), and further enhanced EGFR-mediated SGLT1 upregulation, which was abolished by the mutation of *EGFR* T678A (Fig 7i). These findings indicate that PKCδ, in addition to its nuclear functions[12], confers EGFR TKI resistance by regulating formation of the EGFR/SGLT1 complex in the cytoplasm.

Interestingly, PKCδ S643/676 phosphorylation, which is mediated by mTORC2, but not T505 phosphorylation, was observed in the H322/ER and HCC827/ER clones (Fig 7j and Supplementary Fig S8i) and in the xenograft tumor tissues of parental H292 cells after 1 month of erlotinib treatment (Fig 7k). Since mTORC2 is inactivated by S6K in response to signaling of EGFR/mTORC1 axis[53], the mTORC2/PKCδ axis may be activated and mediate EGFR T678 phosphorylation for SGLT1 protein stabilization, when EGFR tyrosine kinase activity was suppressed by TKIs. In support of this notion, the mTORC1/2 inhibitor everolimus suppressed not only PKCδ S643/676 phosphorylation, but also EGFR T678 phosphorylation and SGLT1 levels (Supplementary Fig S8j).

In conclusion, TKIs suppressed EGFR and its downstream Akt and ERK signaling pathways, as well as the membrane levels of GLUT and glucose uptake in the sensitive cells. Reduced glucose uptake led to a subsequent reduction in ATP production, an increase in the intracellular AMP/ATP ratio, and activation of AMPK for the suppression of mTORC1 and

tumor growth (Fig 8, left). However, while EGFR tyrosine kinase activity was suppressed by long-term TKI treatment, mTORC2 was activated from the EGFR/mTORC1/S6K axis to phosphorylate PKCδ for subsequent EGFR T678 phosphorylation and SGLT1 protein stabilization. Even in an environment of low glucose, higher SGLT1 expression engulfs more glucose to maintain intracellular glucose levels, leading to acquired EGFR TKI resistance and maintenance of ATP production for cell viability (Fig 8, right). Thus, co-treatment with SGLT1 inhibitors may avoid the development of acquired resistance to EGFR TKIs.

Discussion

In addition to the inhibition of EGFR downstream PI3K/Akt and MAPK survival pathways, reductions in glucose uptake and glycolysis have been detected in gefitinib-treated lung cancer cells that precede cell cycle suppression and apoptosis induction[22], suggesting that glucose metabolic activity closely reflects the intrinsic response to EGFR TKI-based therapy. However, it remains unclear as to whether the development of acquired resistance to EGFR TKIs involves the reprogramming of glucose metabolism in NSCLC cells. In this study, our results showed that protein stability of the active glucose transporter SGLT1 was dramatically enhanced by EGFR relying on PKCδ-mediated phosphorylation to support glucose uptake and viability of erlotinib-resistant lung cancer cells.

Cancer cells support their growth by expressing glucose transporters that increase glucose uptake from the extracellular environment. Treatment with TKIs decreases glucose consumption and lactate production by inhibiting the translocation of the Glut3 transporter from the cytosol to the plasma membrane in lung adenocarcinoma[24]. The downregulation of Glut1 and Glut3 protein levels also accounts for the anticancer activity of EGFR TKIs in NSCLC cell lines and xenograft tumor tissues[24, 25]. EGFR expression and downstream signaling pathways have shown positive correlations with Glut1 expression and membrane

localization in lung cancer[54], pancreatic cancer tissue[55, 56] and triple-negative breast cancer (TNBC)[57], suggesting that TKI-sensitive cancer cells employ passive glucose transporters to engulf glucose and that downregulation of these transporters may account for the anticancer activity of TKIs. Under adaptation to long-term TKI treatment, however, SGLT1 upregulation compensated for glucose uptake in TKI-resistant cells in our study.

SGLT1 is generally expressed in the normal epithelial cells of the small intestine to transport glucose and galactose across the luminal side of enterocytes, but its overexpression in prostate cancer[58] and colorectal cancer[59] is associated with poor prognosis. Although SGLT2, typically expressed in the renal proximal tubule, has also been reported to play a critical role in the development of pancreatic or breast cancer[60, 61], our data showed that SGLT1, but not SGLT2, is upregulated in response to EGFR TKI treatment, which supports glucose uptake and cellular viability in NSCLC cells with acquired TKI resistance. Although the EGF-activated PI3K/Akt/CREB signaling axis upregulates SGLT1 expression and enhances glucose uptake in intestine epithelial cells[62], the tyrosine kinase activity of EGFR or IGF1R and Akt signals are not needed for SGLT1 upregulation in cancer cells[46, 63]. In this study, our data showed that enhanced SGLT1 protein expression and glucose uptake in TKI-resistant cells were mediated by kinase-inactive EGFR (Fig 6). Downregulation of EGFR expression involves the direct targeting of its 3'UTR activity by microRNA-7[64-67]. Interestingly, the kinase-dependent functioning of EGFR has been reported to induce miR-7 transcription[68], suggesting that miR-7 acts as a negative feedback regulator of EGFR expression. Indeed, EGFR expression without tyrosine kinase activity is increased in response to tyrosine kinase inhibitor treatment, which downregulates microRNA-7 and promotes the migration and invasion of TNBC cells[64, 69]. This negative-feedback regulation of EGFR may also contribute to the protein stabilization of SGLT1 in NSCLC cells with acquired EGFR TKI resistance.

Besides the elevation of EGFR protein levels, our data revealed that PKCδ-mediated EGFR T678 phosphorylation also enhanced the protein-protein interaction of EGFR with SGLT1 to stabilize SGLT1 protein levels in TKI-resistant cells (Fig 7). This conserved phosphorylation by PKC reduces endocytic trafficking of EGFR and ErbB3[70, 71], and the retention of these receptors on the plasma membrane may account for the higher interaction between EGFR and SGLT1 in TKI-resistant cells. Moreover, our data found that mTORC2-mediated PKCδ phosphorylation (Ser643 and Ser676) was notably increased in the cells with acquired resistance to erlotinib, and that mTORC1/2 inhibition suppressed PKCδ activation and EGFR/SGLT1 protein expression. PKCδ-mediated EGFR/SGLT1 stabilization may be involved in the mTORC2-mediated metabolic reprogramming in EGFR TKI-resistant NSCLC cells[72]. These findings also support targeting of mTORC2, which is activated due to the inhibition of EGFR/mTORC1/S6K signaling [53], as another therapeutic strategy to overcome EGFR TKI resistance in NSCLC cells [72].

Since SGLTs are functionally active in various cancer types, including pancreatic, prostate, and brain cancers[60], the use of new antidiabetic SGLT inhibitors for cancer therapy has also emerged as a possibility[73]. Four SGLT2 inhibitors, empagliflozin (Jardiance), dapagliflozin (Forxiga), canagliflozin (Invokana) and ertugliflozin (Stelagro) have recently been approved for the treatment of type 2 diabetes mellitus by the US Food and Drug Administration, and are associated with beneficial effects in the cardiovascular system and the kidney[74]. Randomized clinical trial data have not revealed any associations between treatment with these SGLT2 inhibitors and increased incidence rates of malignancies[75]. Our data show that co-targeting SGLT1 with LX4211 (sotagliflozin) enhanced the anticancer activity of EGFR TKIs in mouse model. LX4211 is an orally-delivered dual SGLT1/2 inhibitor approved for T1DM and exhibits a 20-fold higher potency for SGLT2 over SGLT1[76]; the involvement of SGLT2 inhibition in this synergism

cannot be ruled out. Moreover, this dual inhibitor improves severe glycemic and non-glycemic outcomes without severe gastrointestinal side effects[77], although its associated increased risk of diabetic ketoacidosis in patients with type 1 diabetes mellitus is of concern[78]. The possibility of this event should be evaluated during clinical testing of the synergistic effects of LX4211 on the anticancer activity of EGFR TKIs.

In conclusion, our results elucidate the role of PKCδ/EGFR-dependent SGLT1 expression in the rewiring of glucose uptake and metabolism that supports the expansion of cells with acquired TKI resistance (Fig 8). These findings indicate that SGLT1 is a potential target for avoiding acquired resistance to EGFR TKI therapy in NSCLC.

Availability of materials and methods

The materials and methods used in this study are available in the Supporting Information.

Acknowledgments

Experiments and data analysis were performed in part through the use of the Medical Research Core Facilities in the Office of Research & Development at China Medical University, Taichung, Taiwan. This research was funded in part by the following: Ministry of Science Technology, Taiwan (grant number: MOST 108-2314-B-039-032), China Medical University (grant number: CMU106-ASIA-18), and China Medical University Hospital (DMR-108-012, DMR-109-212, DMR-109-213). This work was also financially supported by the "Drug Development Center, China Medical University" from The Featured Areas Research Center Program within the framework of the Higher Education Sprout Project by the Ministry of Education (MOE) in Taiwan. Y. Wang was supported by Medical Research Council (MR/S025480/1). We would like to thank Iona J. MacDonald from China Medical University, Taichung, Taiwan, for her English language revision of this manuscript.

Author Contributions

C.-H. C. provided human tumor samples, performed the experiments and analyzed data. B.-W. W. and Y.-C. H. conceived the study, designed and performed the experiments, analyzed data, and wrote the manuscript. B.-W. W., C.-Y. W., F.-J. C., Y. W., Z.W., R.-H. C., C.-H. T., and Y.-L. W. performed the experiments, T.-C. H. and C.-Y. C. provided human tumor samples and performed the experiments. C.-Y. T. provided human tumor samples, performed the experiments and provided clinical information. W.-C. H. supervised the entire project and wrote the manuscript. M.-C. H. provided scientific input and wrote the manuscript.

Conflict of Interests

The authors declare no conflict of interest.

References

1 Skoulidis F, Heymach JV. Co-occurring genomic alterations in non-small-cell lung cancer biology and therapy. *Nat Rev Cancer* 2019; 19: 495-509.

2 Liu TC, Jin X, Wang Y, Wang K. Role of epidermal growth factor receptor in lung cancer and targeted therapies. *Am J Cancer Res* 2017; 7: 187-202.

3 Arteaga CL, Engelman JA. ERBB receptors: from oncogene discovery to basic science to mechanism-based cancer therapeutics. *Cancer Cell* 2014; 25: 282-303.

4 Recondo G, Facchinetti F, Olaussen KA, Besse B, Friboulet L. Making the first move in EGFR-driven or ALK-driven NSCLC: first-generation or next-generation TKI? *Nat Rev Clin Oncol* 2018; 15: 694-708.

5 Ke EE, Wu YL. EGFR as a Pharmacological Target in EGFR-Mutant Non-Small-Cell Lung Cancer: Where Do We Stand Now? *Trends Pharmacol Sci* 2016; 37: 887-903.

6 Carey KD, Garton AJ, Romero MS, Kahler J, Thomson S, Ross S *et al*. Kinetic analysis of epidermal growth factor receptor somatic mutant proteins shows increased sensitivity to the epidermal growth factor receptor tyrosine kinase inhibitor, erlotinib. *Cancer Res* 2006; 66: 8163-8171.

7 Wu SG, Shih JY. Management of acquired resistance to EGFR TKI-targeted therapy in advanced non-small cell lung cancer. *Mol Cancer* 2018; 17: 38.

8 Murtuza A, Bulbul A, Shen JP, Keshavarzian P, Woodward BD, Lopez-Diaz FJ *et al*. Novel Third-Generation EGFR Tyrosine Kinase Inhibitors and Strategies to Overcome Therapeutic Resistance in Lung Cancer. *Cancer Res* 2019; 79: 689-698.

9 Mok TS, Wu YL, Ahn MJ, Garassino MC, Kim HR, Ramalingam SS *et al*. Osimertinib or Platinum-Pemetrexed in EGFR T790M-Positive Lung Cancer. *N Engl J Med* 2017; 376: 629-640.

10 Jia Y, Yun CH, Park E, Ercan D, Manuia M, Juarez J *et al*. Overcoming EGFR(T790M) and EGFR(C797S) resistance with mutant-selective allosteric inhibitors. *Nature* 2016; 534: 129-132.

11 Husain H, Scur M, Murtuza A, Bui N, Woodward B, Kurzrock R. Strategies to Overcome Bypass Mechanisms Mediating Clinical Resistance to EGFR Tyrosine Kinase Inhibition in Lung Cancer. *Mol Cancer Ther* 2017; 16: 265-272.

12 Lee PC, Fang YF, Yamaguchi H, Wang WJ, Chen TC, Hong X *et al*. Targeting PKCdelta as a Therapeutic Strategy against Heterogeneous Mechanisms of EGFR Inhibitor Resistance in EGFR-Mutant Lung Cancer. *Cancer Cell* 2018; 34: 954-969 e954.

13 Nagarajan A MP, Wajapeyee N. Oncogene-Directed Alterations in Cancer Cell Metabolism. *Trends Cancer* 2016; 2: 365-377.

14 Xu Q, Zhang Q, Ishida Y, Hajjar S, Tang X, Shi H *et al*. EGF induces epithelial-mesenchymal transition and cancer stem-like cell properties in human oral cancer cells via promoting Warburg effect. *Oncotarget* 2017; 8: 9557-9571.

15 Yang W, Xia Y, Hawke D, Li X, Liang J, Xing D *et al*. PKM2 phosphorylates histone

H3 and promotes gene transcription and tumorigenesis. *Cell* 2012; 150: 685-696.

16 Yang W, Xia Y, Ji H, Zheng Y, Liang J, Huang W *et al*. Nuclear PKM2 regulates beta-catenin transactivation upon EGFR activation. *Nature* 2011; 480: 118-122.

17 Lim SO LC, Xia W, Lee HH, Chang SS, Shen J, Hsu JL, Raftery D, Djukovic D, Gu H, Chang WC, Wang HL, Chen ML, Huo L, Chen CH, Wu Y, Sahin A, Hanash SM, Hortobagyi GN, Hung MC. EGFR Signaling Enhances Aerobic Glycolysis in Triple-Negative Breast Cancer Cells to Promote Tumor Growth and Immune Escape. *Cancer Res* 2016; 76: 1284-1296.

18 Lypova N, Telang S, Chesney J, Imbert-Fernandez Y. Increased 6-phosphofructo-2-kinase/fructose-2,6-bisphosphatase-3 activity in response to EGFR signaling contributes to non-small cell lung cancer cell survival. *J Biol Chem* 2019; 294: 10530-10543.

19 Jin N, Bi A, Lan X, Xu J, Wang X, Liu Y *et al*. Identification of metabolic vulnerabilities of receptor tyrosine kinases-driven cancer. *Nat Commun* 2019; 10: 2701.

20 Kim JH, Nam B, Choi YJ, Kim SY, Lee JE, Sung KJ *et al*. Enhanced Glycolysis Supports Cell Survival in EGFR-Mutant Lung Adenocarcinoma by Inhibiting Autophagy-Mediated EGFR Degradation. *Cancer Res* 2018; 78: 4482-4496.

21 Hachemi M, Couturier O, Vervueren L, Fosse P, Lacoeuille F, Urban T *et al*. [(1)(8)F]FDG positron emission tomography within two weeks of starting erlotinib therapy can predict response in non-small cell lung cancer patients. *PLoS One* 2014; 9: e87629.

22 Su H, Bodenstein C, Dumont RA, Seimbille Y, Dubinett S, Phelps ME *et al*. Monitoring tumor glucose utilization by positron emission tomography for the prediction of treatment response to epidermal growth factor receptor kinase inhibitors. *Clin Cancer Res* 2006; 12: 5659-5667.

23 Momcilovic M, Bailey ST, Lee JT, Fishbein MC, Magyar C, Braas D *et al*. Targeted Inhibition of EGFR and Glutaminase Induces Metabolic Crisis in EGFR Mutant Lung Cancer. *Cell Rep* 2017; 18: 601-610.

24 Makinoshima H TM, Matsumoto S, Yagishita A, Owada S, Esumi H, Tsuchihara K. Epidermal growth factor receptor (EGFR) signaling regulates global metabolic pathways in EGFR-mutated lung adenocarcinoma. *J Biol Chem* 2014; 289: 20813-20823.

25 Zander T, Scheffler M, Nogova L, Kobe C, Engel-Riedel W, Hellmich M *et al*. Early prediction of nonprogression in advanced non-small-cell lung cancer treated with erlotinib by using [(18)F]fluorodeoxyglucose and [(18)F]fluorothymidine positron emission tomography. *J Clin Oncol* 2011; 29: 1701-1708.

26 Sunaga N, Oriuchi N, Kaira K, Yanagitani N, Tomizawa Y, Hisada T *et al*. Usefulness of FDG-PET for early prediction of the response to gefitinib in non-small cell lung cancer. *Lung Cancer* 2008; 59: 203-210.

27 Cheng FJ, Chen CH, Tsai WC, Wang BW, Yu MC, Hsia TC *et al*. Cigarette smoke-induced LKB1/AMPK pathway deficiency reduces EGFR TKI sensitivity in NSCLC. *Oncogene* 2021; 40: 1162-1175.

28 Suzuki S, Okada M, Takeda H, Kuramoto K, Sanomachi T, Togashi K *et al*. Involvement of GLUT1-mediated glucose transport and metabolism in gefitinib resistance of non-small-cell lung cancer cells. *Oncotarget* 2018; 9: 32667-32679.

29 Apicella M, Giannoni E, Fiore S, Ferrari KJ, Fernandez-Perez D, Isella C *et al*. Increased Lactate Secretion by Cancer Cells Sustains Non-cell-autonomous Adaptive Resistance to MET and EGFR Targeted Therapies. *Cell metabolism* 2018.

30 Kunimasa K, Nagano T, Shimono Y, Dokuni R, Kiriu T, Tokunaga S *et al*. Glucose metabolism-targeted therapy and withaferin A are effective for epidermal growth factor receptor tyrosine kinase inhibitor-induced drug-tolerant persisters. *Cancer science* 2017; 108: 1368-1377.

31 Zhang H, Du X, Sun TT, Wang CL, Li Y, Wu SZ. Lectin PCL inhibits the Warburg effect of PC3 cells by combining with EGFR and inhibiting HK2. *Oncology reports* 2017; 37: 1765-1771.

32 Moruno F, Perez-Jimenez E, Knecht E. Regulation of autophagy by glucose in Mammalian cells. *Cells* 2012; 1: 372-395.

33 Ma R, Li X, Liu H, Jiang R, Yang M, Zhang M *et al*. GATA6-upregulating autophagy promotes TKI resistance in nonsmall cell lung cancer. *Cancer Biol Ther* 2019; 20: 1206-1212.

34 Li L, Wang Y, Jiao L, Lin C, Lu C, Zhang K *et al*. Protective autophagy decreases osimertinib cytotoxicity through regulation of stem cell-like properties in lung cancer. *Cancer Lett* 2019; 452: 191-202.

35 Wang Z, Du T, Dong X, Li Z, Wu G, Zhang R. Autophagy inhibition facilitates erlotinib cytotoxicity in lung cancer cells through modulation of endoplasmic reticulum stress. *Int J Oncol* 2016; 48: 2558-2566.

36 Gorzalczany Y, Gilad Y, Amihai D, Hammel I, Sagi-Eisenberg R, Merimsky O. Combining an EGFR directed tyrosine kinase inhibitor with autophagy-inducing drugs: a beneficial strategy to combat non-small cell lung cancer. *Cancer Lett* 2011; 310: 207-215.

37 Miller S, Oleksy A, Perisic O, Williams RL. Finding a fitting shoe for Cinderella: searching for an autophagy inhibitor. *Autophagy* 2010; 6: 805-807.

38 Mauthe M, Orhon I, Rocchi C, Zhou X, Luhr M, Hijlkema KJ *et al*. Chloroquine inhibits autophagic flux by decreasing autophagosome-lysosome fusion. *Autophagy* 2018; 14: 1435-1455.

39 Kanwal A, Singh SP, Grover P, Banerjee SK. Development of a cell-based nonradioactive glucose uptake assay system for SGLT1 and SGLT2. *Anal Biochem* 2012; 429: 70-75.

40 Blodgett AB, Kothinti RK, Kamyshko I, Petering DH, Kumar S, Tabatabai NM. A fluorescence method for measurement of glucose transport in kidney cells. *Diabetes Technol Ther* 2011; 13: 743-751.

41 Barrio JR, Huang SC, Satyamurthy N, Scafoglio CS, Yu AS, Alavi A *et al*. Does 2-FDG PET Accurately Reflect Quantitative In Vivo Glucose Utilization? *J Nucl Med* 2020; 61: 931-937.

42 McCracken AN, Edinger AL. Nutrient transporters: the Achilles' heel of anabolism. *Trends Endocrinol Metab* 2013; 24: 200-208.

43 Ancey PB, Contat C, Meylan E. Glucose transporters in cancer - from tumor cells to the tumor microenvironment. *FEBS J* 2018; 285: 2926-2943.

44 Wang L, Shang Z, Zhou Y, Hu X, Chen Y, Fan Y *et al*. Autophagy mediates glucose starvation-induced glioblastoma cell quiescence and chemoresistance through coordinating cell metabolism, cell cycle, and survival. *Cell Death Dis* 2018; 9: 213.

45 Gyorffy B, Surowiak P, Budczies J, Lanczky A. Online survival analysis software to assess the prognostic value of biomarkers using transcriptomic data in non-small-cell lung cancer. *PLoS One* 2013; 8: e82241.

46 Weihua Z, Tsan R, Huang WC, Wu Q, Chiu CH, Fidler IJ *et al*. Survival of cancer cells is maintained by EGFR independent of its kinase activity. *Cancer Cell* 2008; 13: 385-393.

47 Chen CH, Hsia TC, Yeh MH, Chen TW, Chen YJ, Chen JT *et al*. MEK inhibitors induce Akt activation and drug resistance by suppressing negative feedback ERK-mediated HER2 phosphorylation at Thr701. *Mol Oncol* 2017; 11: 1273-1287.

48 Kluba M, Engelborghs Y, Hofkens J, Mizuno H. Inhibition of Receptor Dimerization as a Novel Negative Feedback Mechanism of EGFR Signaling. *PLoS One* 2015; 10: e0139971.

49 Hunter T, Ling N, Cooper JA. Protein kinase C phosphorylation of the EGF receptor at a threonine residue close to the cytoplasmic face of the plasma membrane. *Nature* 1984; 311: 480-483.

50 Liu M, Idkowiak-Baldys J, Roddy PL, Baldys A, Raymond J, Clarke CJ *et al*. Sustained activation of protein kinase C induces delayed phosphorylation and regulates the fate of epidermal growth factor receptor. *PLoS One* 2013; 8: e80721.

51 Feinmesser RL, Wicks SJ, Taverner CJ, Chantry A. Ca2+/calmodulin-dependent kinase II phosphorylates the epidermal growth factor receptor on multiple sites in the cytoplasmic tail and serine 744 within the kinase domain to regulate signal generation. *J Biol Chem* 1999; 274: 16168-16173.

52 Chen Y, Wei G, Xia H, Yu H, Tang Q, Bi F. Down regulation of lincRNA-p21

contributes to gastric cancer development through Hippo-independent activation of YAP. *Oncotarget* 2017; 8: 63813-63824.

53 Kim J, Guan KL. mTOR as a central hub of nutrient signalling and cell growth. *Nat Cell Biol* 2019; 21: 63-71.

54 Sasaki H, Shitara M, Yokota K, Hikosaka Y, Moriyama S, Yano M *et al*. Overexpression of GLUT1 correlates with Kras mutations in lung carcinomas. *Mol Med Rep* 2012; 5: 599-602.

55 Kaida H, Azuma K, Kawahara A, Yasunaga M, Kitasato Y, Hattori S *et al*. The correlation between FDG uptake and biological molecular markers in pancreatic cancer patients. *Eur J Radiol* 2016; 85: 1804-1810.

56 Hudson CD, Hagemann T, Mather SJ, Avril N. Resistance to the tyrosine kinase inhibitor axitinib is associated with increased glucose metabolism in pancreatic adenocarcinoma. *Cell Death Dis* 2014; 5: e1160.

57 Hussein YR, Bandyopadhyay S, Semaan A, Ahmed Q, Albashiti B, Jazaerly T *et al*. Glut-1 Expression Correlates with Basal-like Breast Cancer. *Transl Oncol* 2011; 4: 321-327.

58 Ren J, Bollu LR, Su F, Gao G, Xu L, Huang WC *et al*. EGFR-SGLT1 interaction does not respond to EGFR modulators, but inhibition of SGLT1 sensitizes prostate cancer cells to EGFR tyrosine kinase inhibitors. *Prostate* 2013; 73: 1453-1461.

59 Guo GF, Cai YC, Zhang B, Xu RH, Qiu HJ, Xia LP *et al*. Overexpression of SGLT1 and EGFR in colorectal cancer showing a correlation with the prognosis. *Medical oncology* 2011; 28 Suppl 1: S197-203.

60 Scafoglio C, Hirayama BA, Kepe V, Liu J, Ghezzi C, Satyamurthy N *et al*. Functional expression of sodium-glucose transporters in cancer. *Proceedings of the National Academy of Sciences of the United States of America* 2015; 112: E4111-4119.

61 Lin HW, Tseng CH. A Review on the Relationship between SGLT2 Inhibitors and Cancer. *International journal of endocrinology* 2014; 2014: 719578.

62 Wang CW, Chang WL, Huang YC, Chou FC, Chan FN, Su SC *et al*. An essential role

of cAMP response element-binding protein in epidermal growth factor-mediated induction of sodium/glucose cotransporter 1 gene expression and intestinal glucose uptake. *The international journal of biochemistry & cell biology* 2015; 64: 239-251.

63 Janku F, Huang HJ, Angelo LS, Kurzrock R. A kinase-independent biological activity for insulin growth factor-1 receptor (IGF-1R) : implications for inhibition of the IGF-1R signal. *Oncotarget* 2013; 4: 463-473.

64 Hsia TC, Tu CY, Chen YJ, Wei YL, Yu MC, Hsu SC *et al*. Lapatinib-mediated cyclooxygenase-2 expression via epidermal growth factor receptor/HuR interaction enhances the aggressiveness of triple-negative breast cancer cells. *Molecular pharmacology* 2013; 83: 857-869.

65 Tu CY, Chen CH, Hsia TC, Hsu MH, Wei YL, Yu MC *et al*. Trichostatin A suppresses EGFR expression through induction of microRNA-7 in an HDAC-independent manner in lapatinib-treated cells. *BioMed research international* 2014; 2014: 168949.

66 Chen YJ, Chien PH, Chen WS, Chien YF, Hsu YY, Wang LY *et al*. Hepatitis B Virus-Encoded X Protein Downregulates EGFR Expression via Inducing MicroRNA-7 in Hepatocellular Carcinoma Cells. *Evidence-based complementary and alternative medicine : eCAM* 2013; 2013: 682380.

67 Chen WS, Yen CJ, Chen YJ, Chen JY, Wang LY, Chiu SJ *et al*. miRNA-7/21/107 contribute to HBx-induced hepatocellular carcinoma progression through suppression of maspin. *Oncotarget* 2015; 6: 25962-25974.

68 Chou YT, Lin HH, Lien YC, Wang YH, Hong CF, Kao YR *et al*. EGFR promotes lung tumorigenesis by activating miR-7 through a Ras/ERK/Myc pathway that targets the Ets2 transcriptional repressor ERF. *Cancer Res* 2010; 70: 8822-8831.

69 Hsiao YC, Yeh MH, Chen YJ, Liu JF, Tang CH, Huang WC. Lapatinib increases motility of triple-negative breast cancer cells by decreasing miRNA-7 and inducing Raf-1/MAPK-dependent interleukin-6. *Oncotarget* 2015; 6: 37965-37978.

70 Llado A, Tebar F, Calvo M, Moreto J, Sorkin A, Enrich C. Protein kinaseCdelta-calmodulin crosstalk regulates epidermal growth factor receptor exit from early endosomes. *Mol Biol Cell* 2004; 15: 4877-4891.

71 Dietrich M, Malik MS, Skeie M, Bertelsen V, Stang E. Protein kinase C regulates ErbB3 turnover. *Exp Cell Res* 2019; 382: 111473.

72 Khuong HT, Midha R. Advances in nerve repair. *Curr Neurol Neurosci Rep* 2013; 13: 322.

73 Yamazaki Y, Harada S, Tokuyama S. Sodium-glucose transporter as a novel therapeutic target in disease. *Eur J Pharmacol* 2018; 822: 25-31.

74 Rieg T, Vallon V. Development of SGLT1 and SGLT2 inhibitors. *Diabetologia* 2018; 61: 2079-2086.

75 Dicembrini I, Nreu B, Mannucci E, Monami M. Sodium-glucose co-transporter-2 (SGLT-2) inhibitors and cancer: A meta-analysis of randomized controlled trials. *Diabetes Obes Metab* 2019; 21: 1871-1877.

76 Lapuerta P, Zambrowicz B, Strumph P, Sands A. Development of sotagliflozin, a dual sodium-dependent glucose transporter 1/2 inhibitor. *Diab Vasc Dis Res* 2015; 12: 101-110.

77 Zambrowicz B, Freiman J, Brown PM, Frazier KS, Turnage A, Bronner J *et al*. LX4211, a dual SGLT1/SGLT2 inhibitor, improved glycemic control in patients with type 2 diabetes in a randomized, placebo-controlled trial. *Clin Pharmacol Ther* 2012; 92: 158-169.

78 Musso G, Gambino R, Cassader M, Paschetta E. Efficacy and safety of dual SGLT 1/2 inhibitor sotagliflozin in type 1 diabetes: meta-analysis of randomised controlled trials. *BMJ* 2019; 365: l1328.

Fig Legends

Fig 1. The acquired erlotinib-resistant NSCLC cells were more tolerant to glucose deprivation. H322, HCC827 and their erlotinib-resistant (ER) cells were cultured in different concentrations of glucose. **a–c**, The cell viability was measured in WST-1 (a), cell counting (b), and clonogenic (c) assays. **d,** The changes in sub-G1 population of the indicated cells in response to different concentrations of glucose were measured with PI staining in FACS

analysis. **e** and **f**, The levels of LC3β and caspase 3 cleavage in H322, HCC827 cells and their ER clones in response to glucose deprivation were analyzed by WB. **g**, The low glucose concentration-induced autophagosome accumulation was detected by staining with Cyto-ID® Green autophagy dye in fluorescence analysis was shown in upper panel, and the number of autophagosome-positive cells was quantitated in lower panel. **h**, The effects of glucose deprivation on autophagosome formation in H322 and their ER cells were determined by FACS analysis (upper panel) and quantitated (lower panel). Data in (a-b), (d), and (g-h) represent mean ± s.d. from three independent experiments. *$P < 0.05$; ***$P < 0.001$ vs. control group, Student's t-test. Data in (c), (e), and (f) are representative of three experiments.

Fig 2. The upregulated SGLT1 mediated the glucose uptake of the acquired erlotinib-resistant cells. a, The changes in ECAR of H322 cells and their ER clones were measured by using the XF-24 Seahorse extracellular flux analyzer. **b**, 2-NBDG uptake ability of H322 cells and their ER clone was detected following EGFR-TKI-treatment. **c** and **d**, 2-NBDG (c) and α-MDG (d) uptake ability of H322 cells and their ER clones were detected by FACS and Beckman LS6000 Scintillation Counter, respectively. **e**, The protein levels of various glucose transporters in H322 cells and their ER clones were detected in WB with the indicated antibodies. **f**, The effects of 100 μM phlorizin or 1 μM LX4211 on glucose uptake in the H322/ER#2 clone were measured under a low glucose concentration condition in 2-NBDG assay. **g**, The effects of SGLT1 shRNA on α-MDG uptake in the H322/ER#2 clone were measured under low glucose conditions by using the Beckman LS6000 Scintillation Counter. Data in (b), (c), (d), (f), and (g) represent mean ± s.d. from three independent experiments. *$p < 0.05$; **$p < 0.01$; ***$p < 0.001$ vs. control, Student's t-test. Data in (a) and (e) are representative of three experiments.

Fig 3. The upregulated SGLT1 supported the cell viability of the acquired TKI-resistant cells. **a**, The cell proliferation of H322/ER clones in response to erlotinib, phlorizin, or LX4211 was determined in WST-1 analysis. **b**, The effects of phlorizin or LX4211 on cell viability of H322/ER clones under low glucose concentration were measured in WST-1 analysis. **c** and **d**, The effects of SGLT1 shRNA on cell proliferation (c) and viability (d) of H322/ER clones under low glucose concentration were determined by cell counting and WST-1 analyses, respectively. **e** and **f**, The effects of SGLT1 inhibitors (e) and shRNA (f) on caspase 3 or PARP cleavages or LC3β in H322/ER clones were analyzed by WB. **g** and **h**, The effects of SGLT1 overexpression on the erlotinib-induced PARP and caspase 3 cleavages (g) and cell death (h) in H322 cells were examined in WB and WST-1 analyses, respectively. Data in (a–d), and (h) represent mean and s.d. from three independent experiments. *$p < 0.05$; **$p < 0.01$; ***$p< 0.001$ vs. control, Student's t-test. Data in (e-g) are representative of three experiments.

Fig 4. Targeting SGLT1 reduced the development of acquired resistance to EGFR TKI *in vivo*. **a**, The growth rate of xenograft tumors of H292 cells in response to treatments with erlotinib, phlorizin, or the combination was determined by measuring tumor size. **b**, The representative IHC staining of tumor sections from (a) were shown (left) and the results from five independent sections for all groups were quantitated with H-score (Right). Scale bar, 50 μm. **c–e**, SCID mice injected with A549-Luc cells were treated with erlotinib, phlorizin, or the combination. The tumor volumes were measured by detecting luminescent signals in the Lumina LT *In Vivo* Imaging System (upper in c) and the luciferase activity was quantitated (lower in c). After treatment for 3 weeks, the lungs of A549 cell-xenograft SCID mice were harvested and the numbers of lung tumor nodules were quantitated. (e) The representative IHC staining of tumor sections from (d) were shown (left) and the results from five

832 independent sections for all groups were quantitated with H-score (Right). Scale bar, 50μm.
833 Data represent mean ± s.d. *$p < 0.05$ and **$p < 0.01$ vs. control, Student's t-test.
834
835 **Fig 5. SGLT1 expression negatively correlates with the clinical benefits of EGFR TKI in**
836 **NSCLC patients. a** and **b**, Tumor tissues from total NSCLC patients ever treated with EGFR
837 TKIs were subjected to IHC staining with anti-SGLT1 antibody (a, upper). Scale bar, 50μm.
838 The clinical correlation of SGLT1 expression with overall survival (a) and progression-free
839 survival (PFS) (b) rates were analyzed in Kaplan-Meier analysis. **c**-**f**, The EGFR TKI-treated
840 NSCLC patients in (a and b) were further classified into wt EGFR (c and d) and mutant
841 EGFR (e and f) groups for Kaplan-Meier overall survival and progression-free survival
842 analysis. **g** and **h**, SGLT1 protein levels in the paired tissues from treatment-naïve tumors and
843 acquired TKI-resistant tumors of 9 lung cancer patients were examined by IHC staining
844 (upper in g) and quantitated (lower in g). The results from (g) were further divided into to two
845 groups according to the genders of patients (h). Scale bar, 50 μm.
846
847 **Fig 6. The increased EGFR mediated glucose uptake and viability of the acquired**
848 **erlotinib-resistant cells through SGLT1 upregulation. a**, The protein expressions of ErbB
849 family and SGLT1 in H322 cells and their ER clones were analyzed in WB analysis. **b**-**h**, The
850 effects of EGFR siRNA or monoclonal antibody cetuximab on α-MDG uptake (b-d), colony
851 formation (e and f), and caspase and PARP cleavages (g and h) of H322/ER#2 and
852 HCC827/ER#2 cells were examined, respectively. **i** and **j**, The effects of SGLT1
853 overexpression on the cetuximab-induced viability inhibition (i) or PARP and caspase 3
854 cleavages (j) of H322 cells were examined in WST-1 analysis and WB, respectively. Data in
855 (c-d) and (i) represent as mean ± s.d. from three independent experiments. *$p< 0.05$; ***$p <$

0.001 vs. control, Student's t-test. Data in (a), (e-h) and (j) are representative of three experiments.

Fig 7. EGFR Thr678 phosphorylation by PKC delta mediated the SGLT1/EGFR interaction for SGLT1 protein stabilization. a, EGFR phosphorylations in H322 cells and their ER clones were examined in WB with the indicated antibodies. **b**, EGFR pT678 phosphorylation in expression of IHC pictures in lung sections (left) and the H-score of protein expression was shown (right). Scale bar, 50 μm. **c**, EGFR T678 phosphorylation and EGFR protein level in the paired treatment-naïve and acquired TKI-resistant tumor tissues of lung cancer patients was determined by IHC staining. Scale bar, 50 μm. **d** and **e**, The indicated protein expression in HEK-293T cells co-transfected with EGFR mutants and SGLT1 in the presence or absence of MG-132 was analyzed by WB (d) and IP/WB (e). **f**, The effects of GO6983, staurosporine, or sotrasturin on cell viability were determined in WST-1 assay. **g**, Glucose uptake in H322/ER cells in response to GO6983 treatment was analyzed with the 2-NBDG uptake assay. Scale bar, 330μm. **h-j,** The total lysates from H322/ER#2 cells treated with various PKC inhibitors (h), HEK-293T cells co-transfected with EGFR mutants and PKCδ (i), and H322 cells and ER clones (h) were subjected to WB with the indicated antibodies. **k**, PKCδ pS643/676 and PKCδ expression in the H292 cells-xenograft tumor tissues in response to erlotinib treatment were examined in IHC analysis (left panel), and the H-score of protein expression were shown (right). Scale bar, 50μm. Data shown in (a) and (d–j) represent mean and s.d. from three experiments. Data in (b) and (k) are representative of five experiments and shown as mean ± s.d. *$p < 0.05$; **$p < 0.01$; ***$p < 0.001$ vs. control group, Student's t-test.

Fig 8. A proposed model illustrating the involvement of SGLT1-mediated metabolic reprograming in the development of acquired resistance to EGFR TKIs. In sensitive NSCLC cells, EGFR TKIs suppressed EGFR and its downstream Akt and ERK signaling pathways as well as the membrane level of GLUT and glucose uptake. Reduced glucose uptake leads to lower ATP production, an increase in the intracellular AMP/ATP ratio, and activation of AMPK for the suppression of mTORC1 and tumor growth. In the presence of TKIs, however, PKCδ is activated by mTORC2 to phosphorylate EGFR at T678 to stabilize SGLT1 protein in an EGFR tyrosine kinase-independent manner while EGFR/mTORC1/S6K axis was inhibited. Even under low glucose environment, the elevated SGLT1 engulfs more glucose to maintain intracellular glucose level and subsequently ATP production for cell survival, leading to the acquired EGFR TKI resistance. Co-treatment with SGLT1 inhibitors may avoid the development of acquired EGFR TKI resistance.

Figure 1

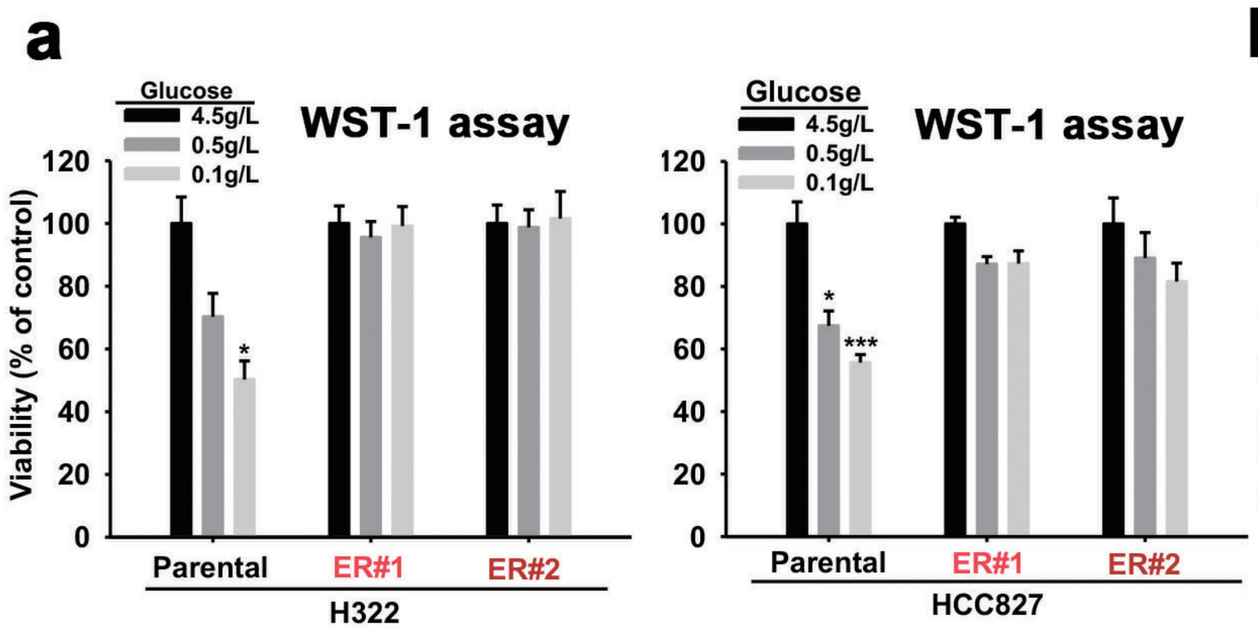
a
Glucose
4.5g/L
0.5g/L
0.1g/L
WST-1 assay
Viability (% of control)
Parental
ER#1
ER#2
H322
HCC827

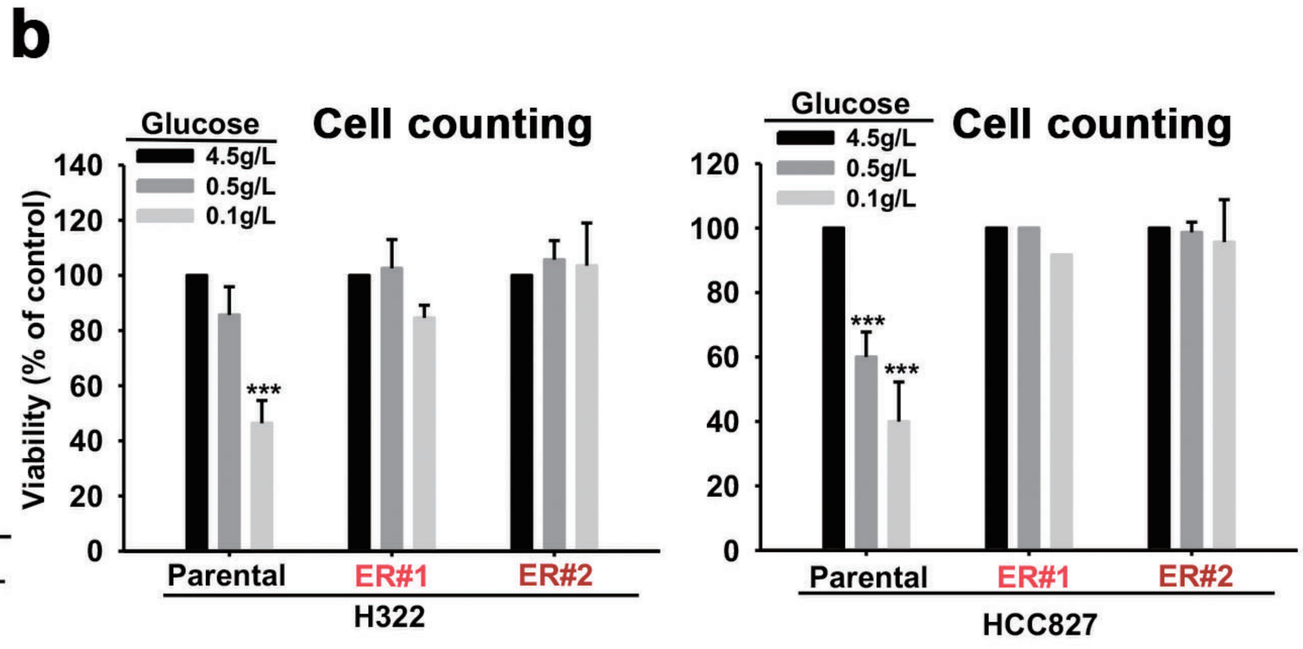
b
Glucose
4.5g/L
0.5g/L
0.1g/L
Cell counting
Viability (% of control)
Parental
ER#1
ER#2
H322
HCC827

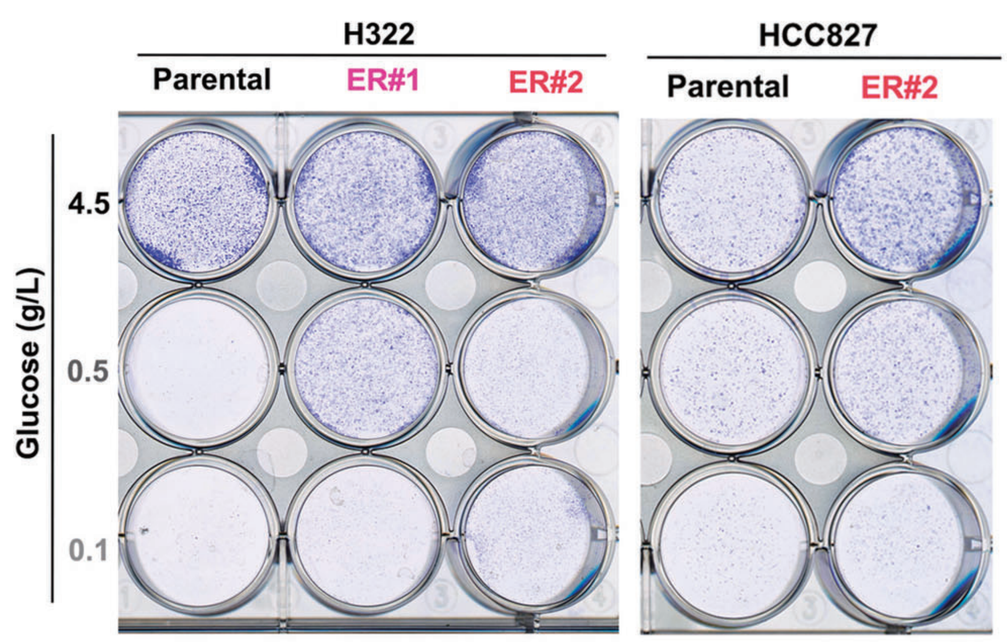
c
H322
HCC827
Parental
ER#1
ER#2
Glucose (g/L)
4.5
0.1

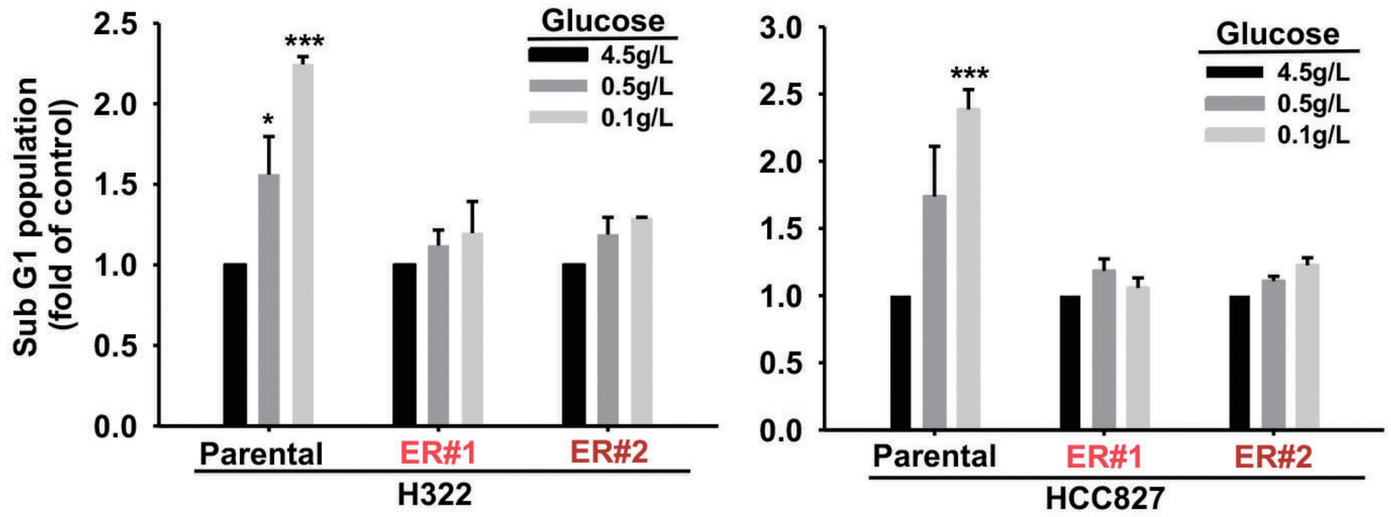
d
Glucose
4.5g/L
0.5g/L
0.1g/L
Sub G1 population
(fold of control)
Parental
ER#1
ER#2
H322
HCC827

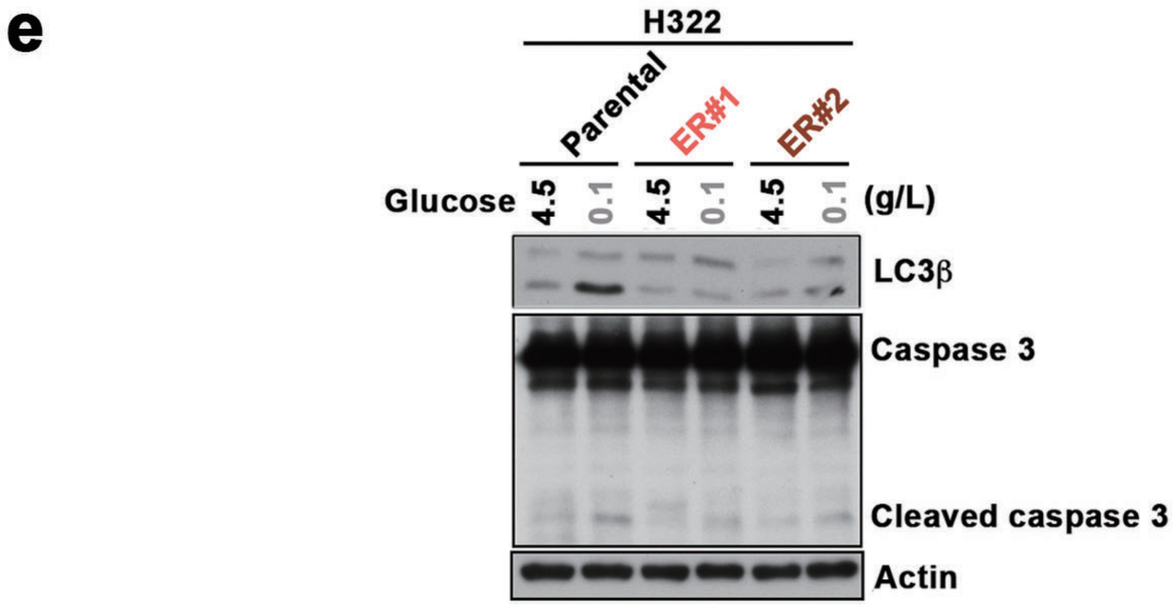
e
H322
Parental
ER#1
ER#2
Glucose
4.5
0.1
(g/L)
LC3β
Caspase 3
Cleaved caspase 3
Actin

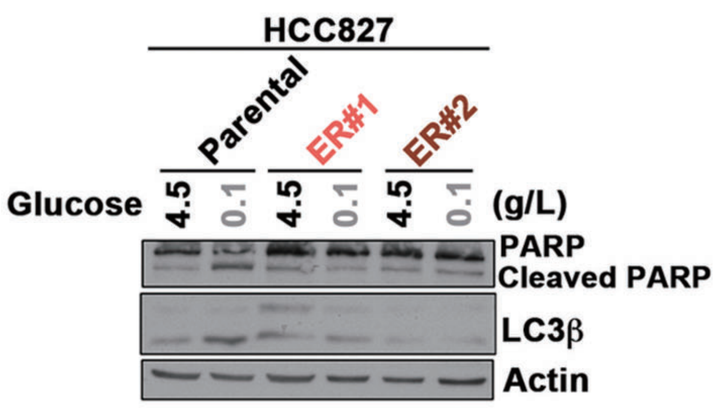
f
HCC827
Parental
ER#1
ER#2
Glucose
4.5
0.1
(g/L)
PARP
Cleaved PARP
LC3β
Actin

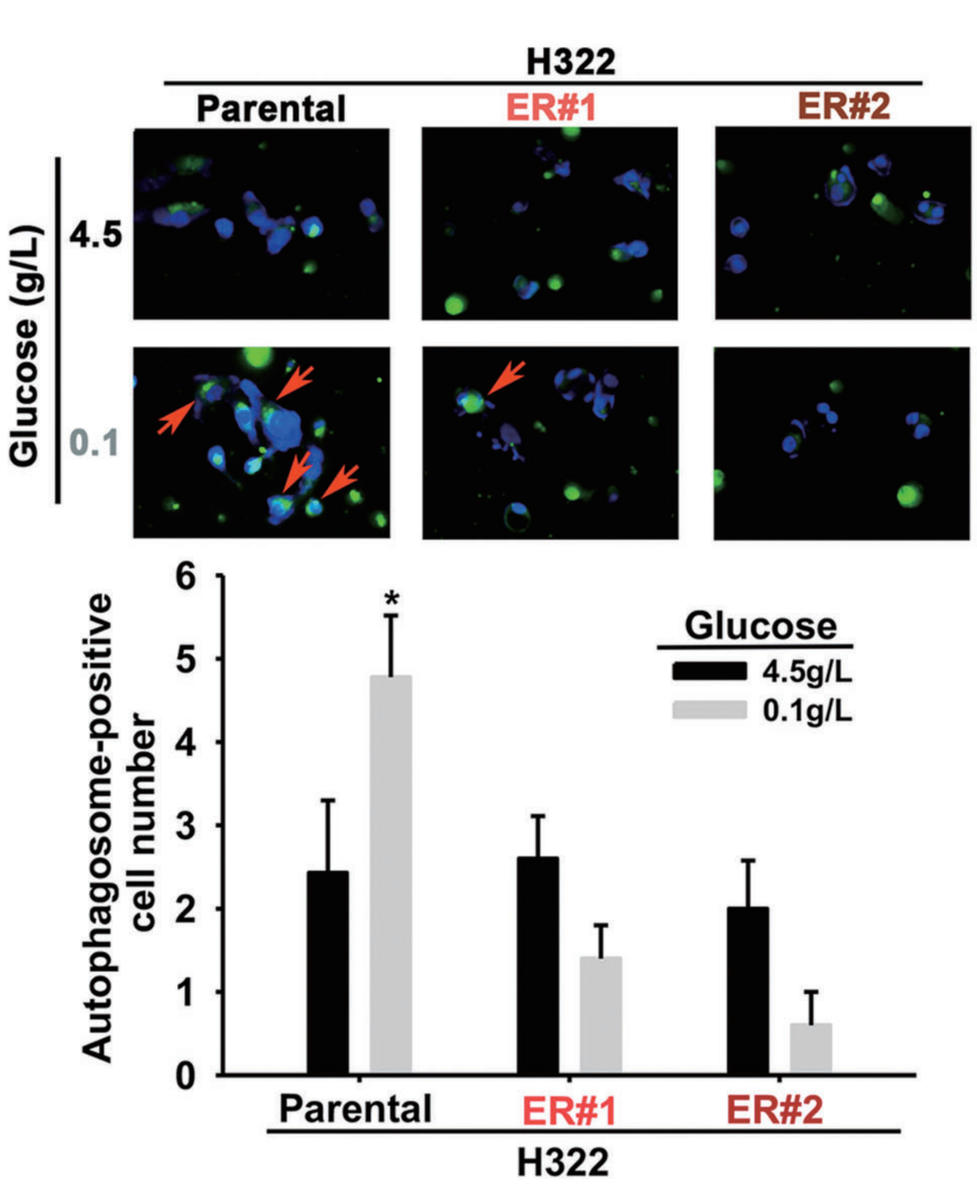
g
H322
Parental
ER#1
ER#2
Glucose (g/L)
4.5
0.1
Autophagosome-positive
cell number
Glucose
4.5g/L
0.1g/L
Parental
ER#1
ER#2
H322

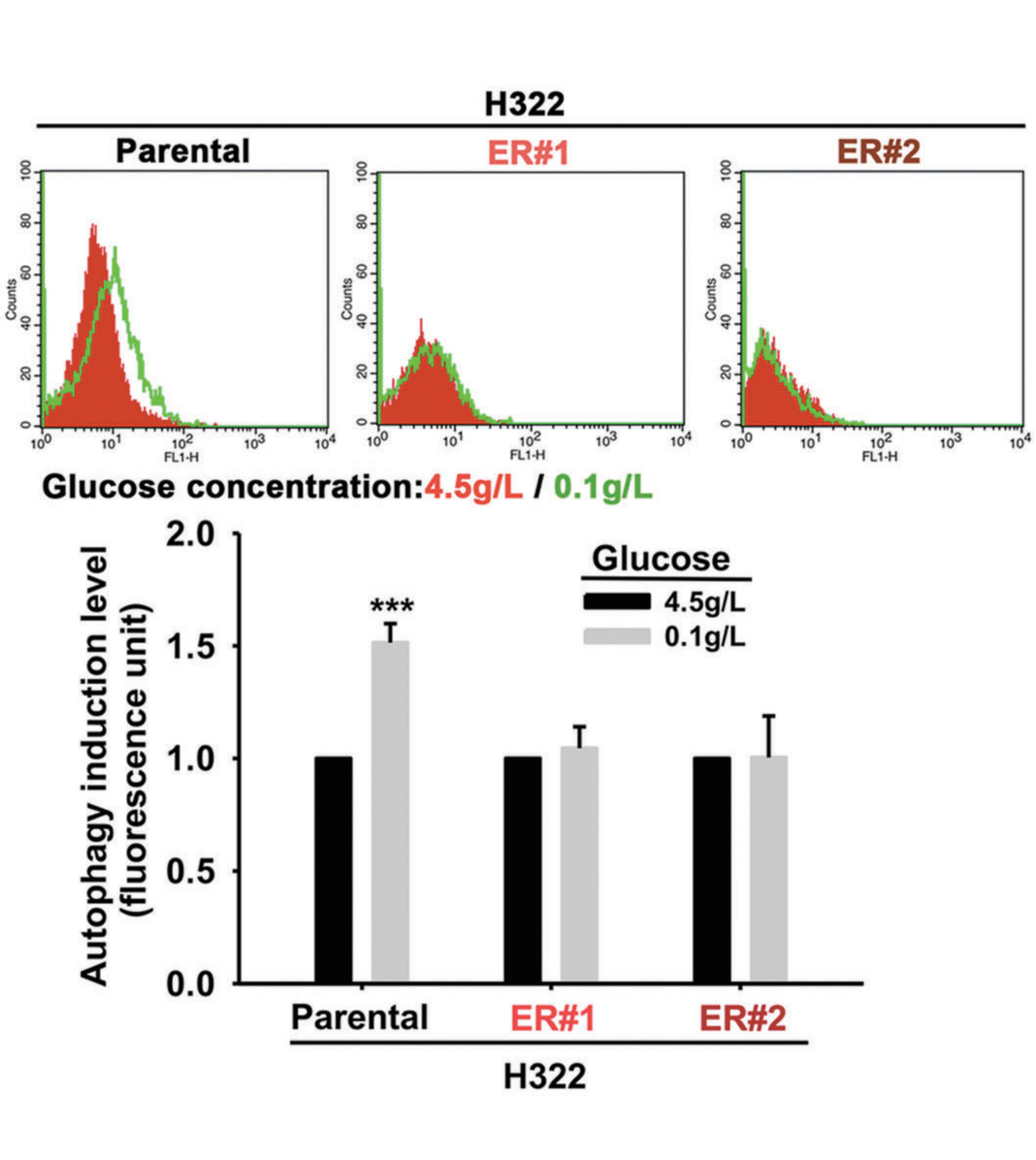
h
H322
Parental
ER#1
ER#2
Counts
FL1-H
Glucose concentration:4.5g/L / 0.1g/L
Autophagy induction level
(fluorescence unit)
Glucose
4.5g/L
0.1g/L
Parental
ER#1
ER#2
H322

Figure 2

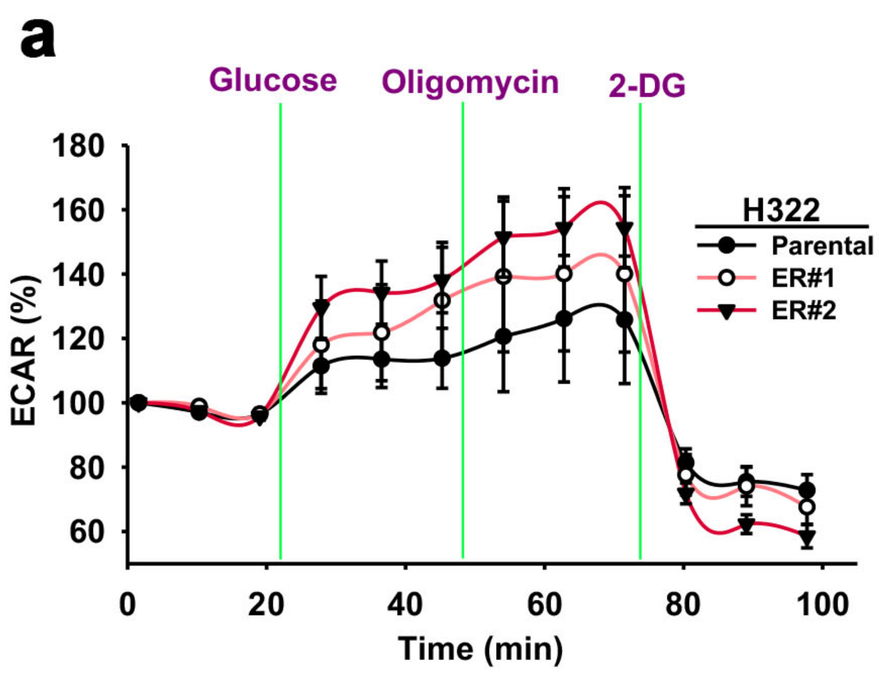
a
Glucose
Oligomycin
2-DG
ECAR (%)
Time (min)
H322
Parental
ER#1
ER#2

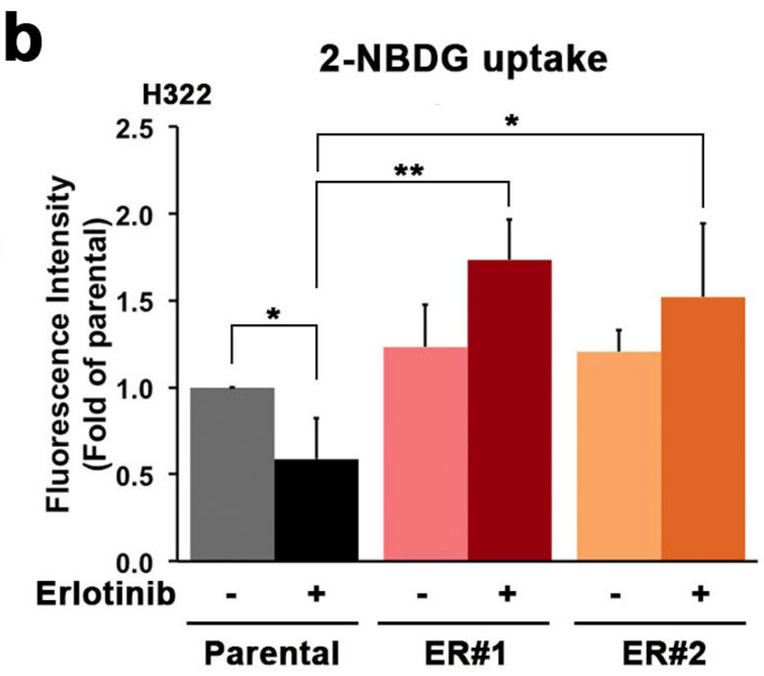
b
2-NBDG uptake
H322
Fluorescence Intensity (Fold of parental)
Erlotinib
Parental
ER#1
ER#2

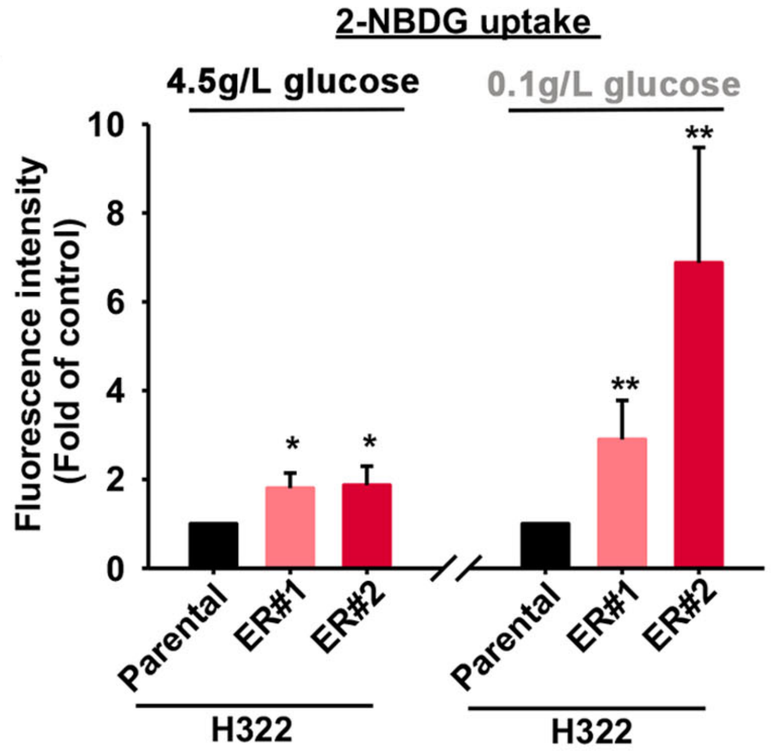
c
2-NBDG uptake
4.5g/L glucose
0.1g/L glucose
Fluorescence intensity (Fold of control)
Parental
ER#1
ER#2
H322

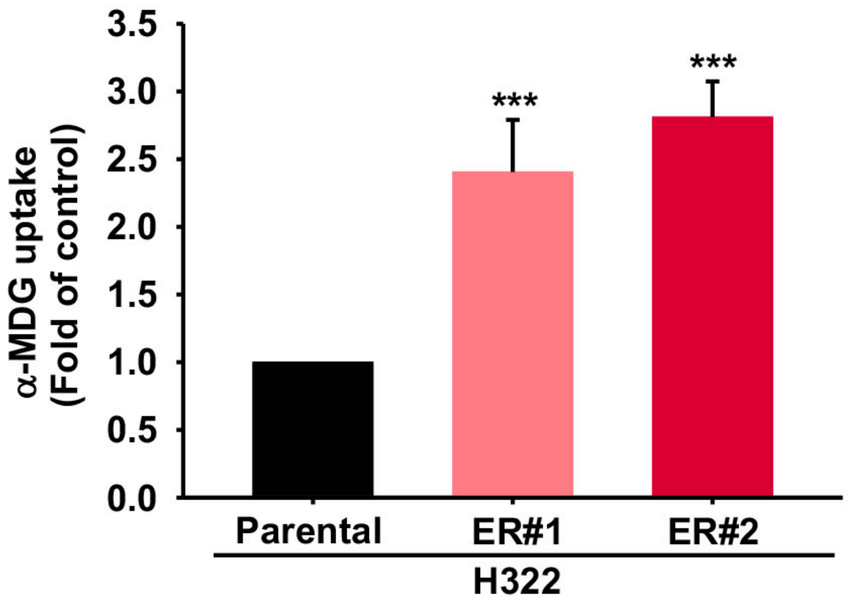
d
α-MDG uptake (Fold of control)
Parental
ER#1
ER#2
H322

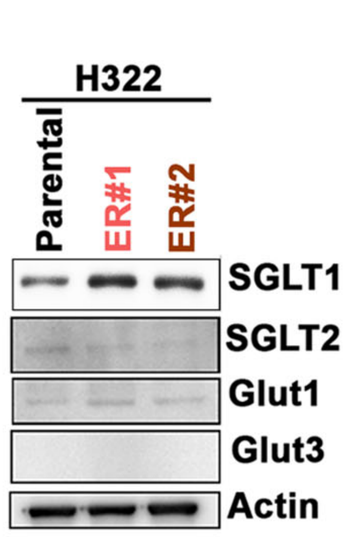
H322
Parental
ER#1
ER#2
SGLT1
SGLT2
Glut1
Glut3
Actin

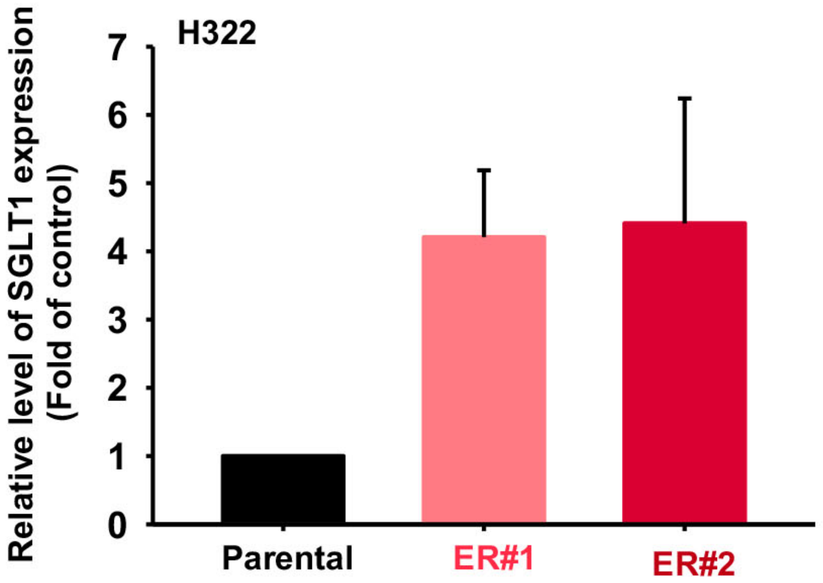
e
H322
Relative level of SGLT1 expression (Fold of control)
Parental
ER#1
ER#2

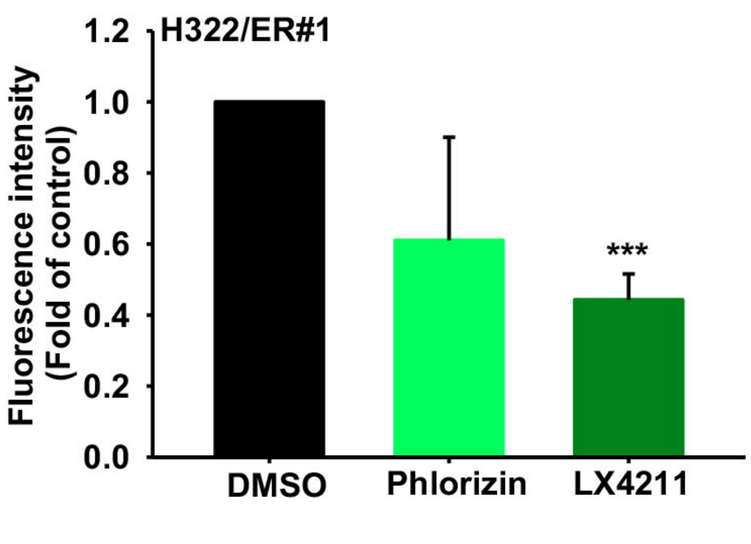
f
H322/ER#1
Fluorescence intensity (Fold of control)
DMSO
Phlorizin
LX4211

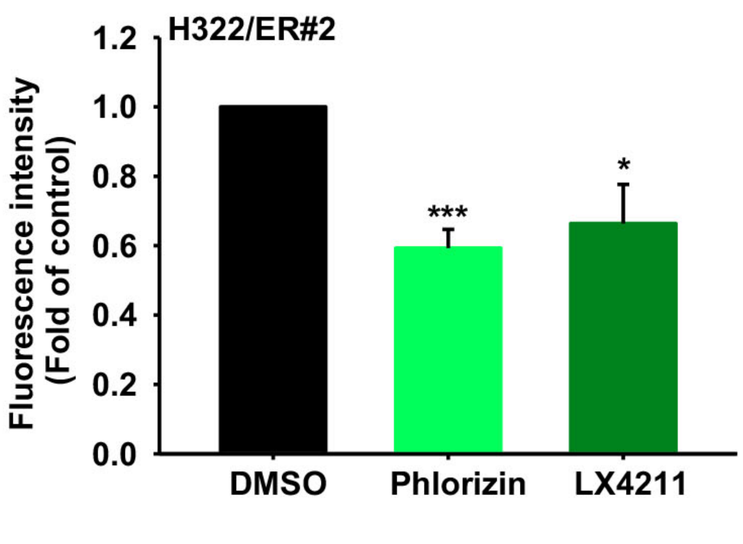
H322/ER#2
Fluorescence intensity (Fold of control)
DMSO
Phlorizin
LX4211

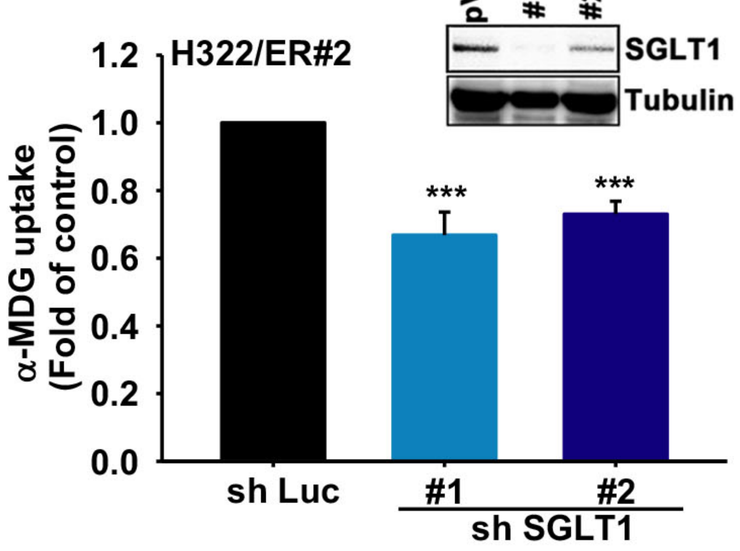
g
H322/ER#2
pVoid
sh SGLT1
#1
#2
SGLT1
Tubulin
α-MDG uptake (Fold of control)
sh Luc
#1
#2
sh SGLT1

Figure 3

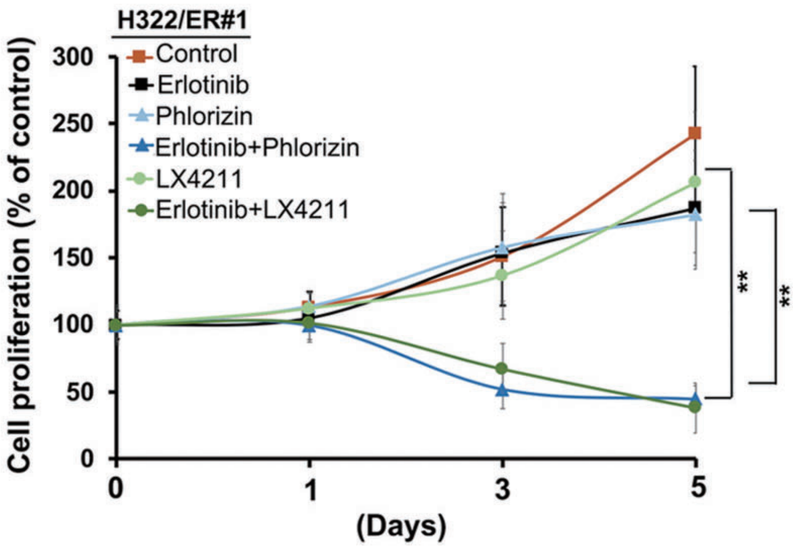
a
H322/ER#1
Control
Erlotinib
Phlorizin
Erlotinib+Phlorizin
LX4211
Erlotinib+LX4211
Cell proliferation (% of control)
(Days)
**
**

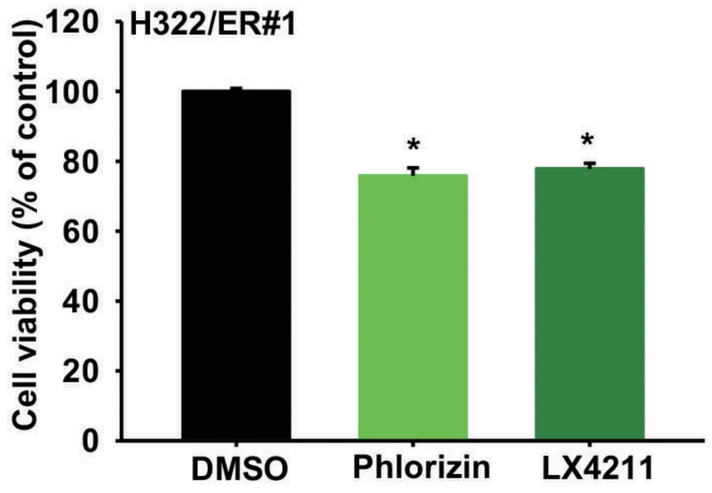
b
H322/ER#1
Cell viability (% of control)
DMSO
Phlorizin
LX4211
*
*

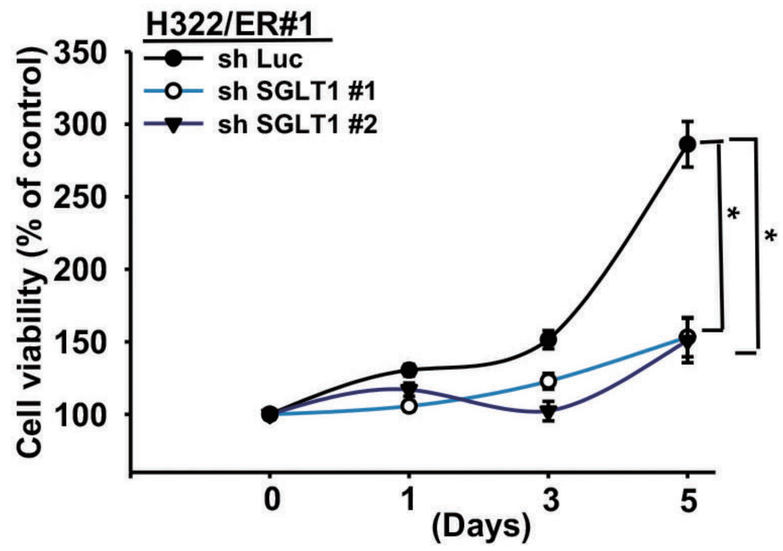
c
H322/ER#1
sh Luc
sh SGLT1 #1
sh SGLT1 #2
Cell viability (% of control)
(Days)
*
*

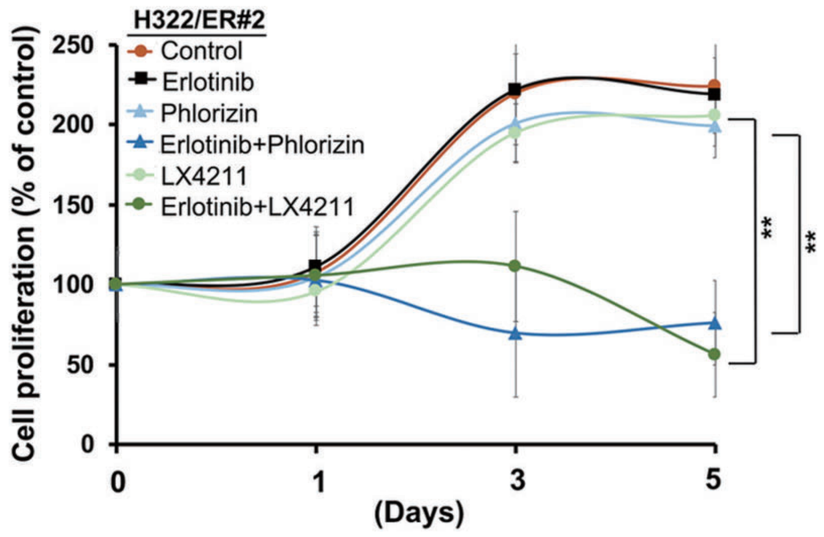
H322/ER#2
Control
Erlotinib
Phlorizin
Erlotinib+Phlorizin
LX4211
Erlotinib+LX4211
Cell proliferation (% of control)
(Days)
**
**

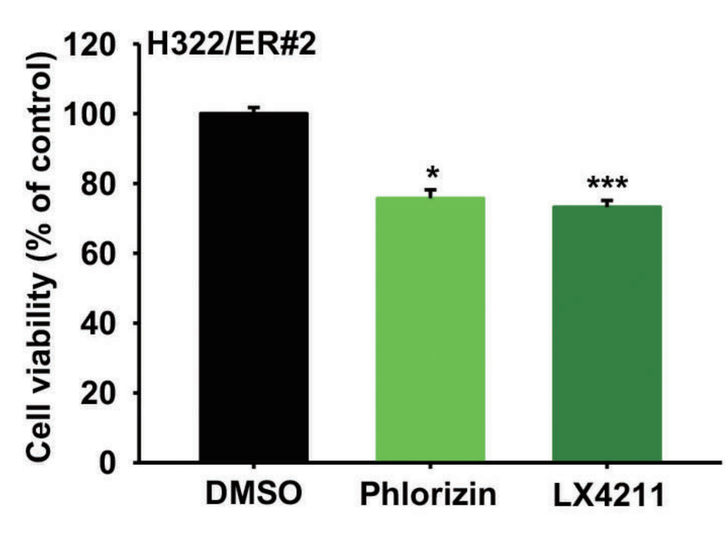
H322/ER#2
Cell viability (% of control)
DMSO
Phlorizin
LX4211
*
***

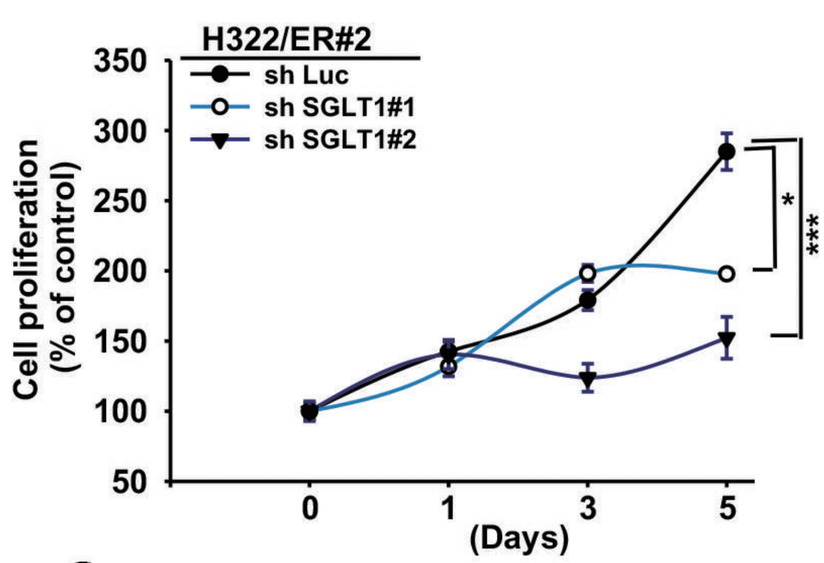
H322/ER#2
sh Luc
sh SGLT1#1
sh SGLT1#2
Cell proliferation (% of control)
(Days)
*
***

d
H322/ER#2
Cell survival (% of control)
sh Luc
#1
#2
sh SGLT1
*
*

e
H322/ER#2
Control
Phlorizin
LX4211
PARP
Cleaved PARP
Caspase3
Cleaved caspase3
Tubulin

f
H322/ER#2
pVoid
shSGLT1
#1
#2
SGLT1
Caspase 3
Cleaved caspase 3
LC3β
Actin

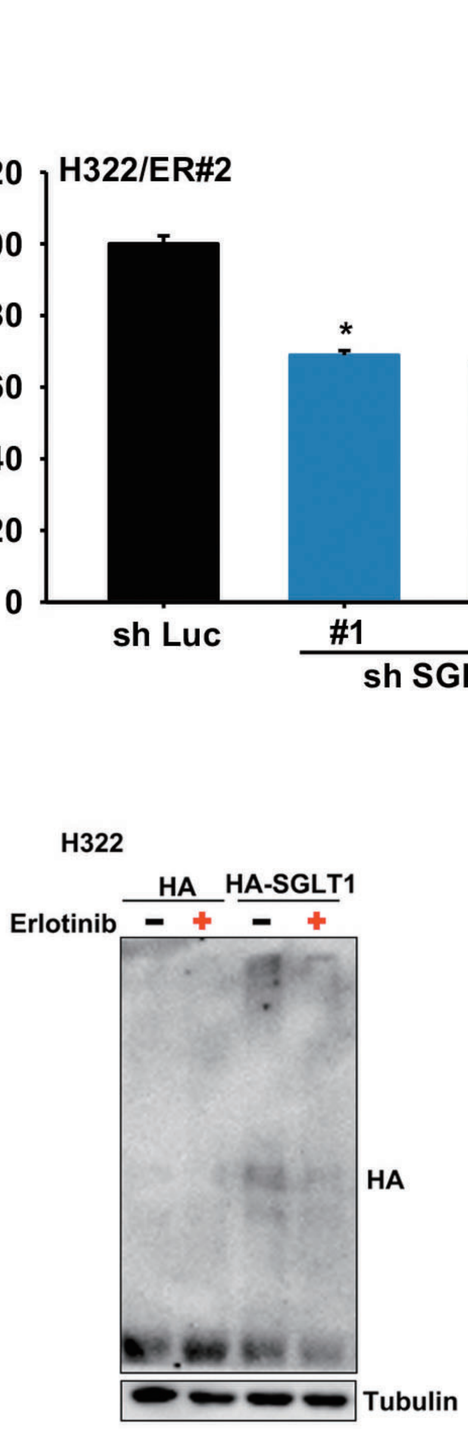
g
H322
HA
HA-SGLT1
Erlotinib
HA
Tubulin

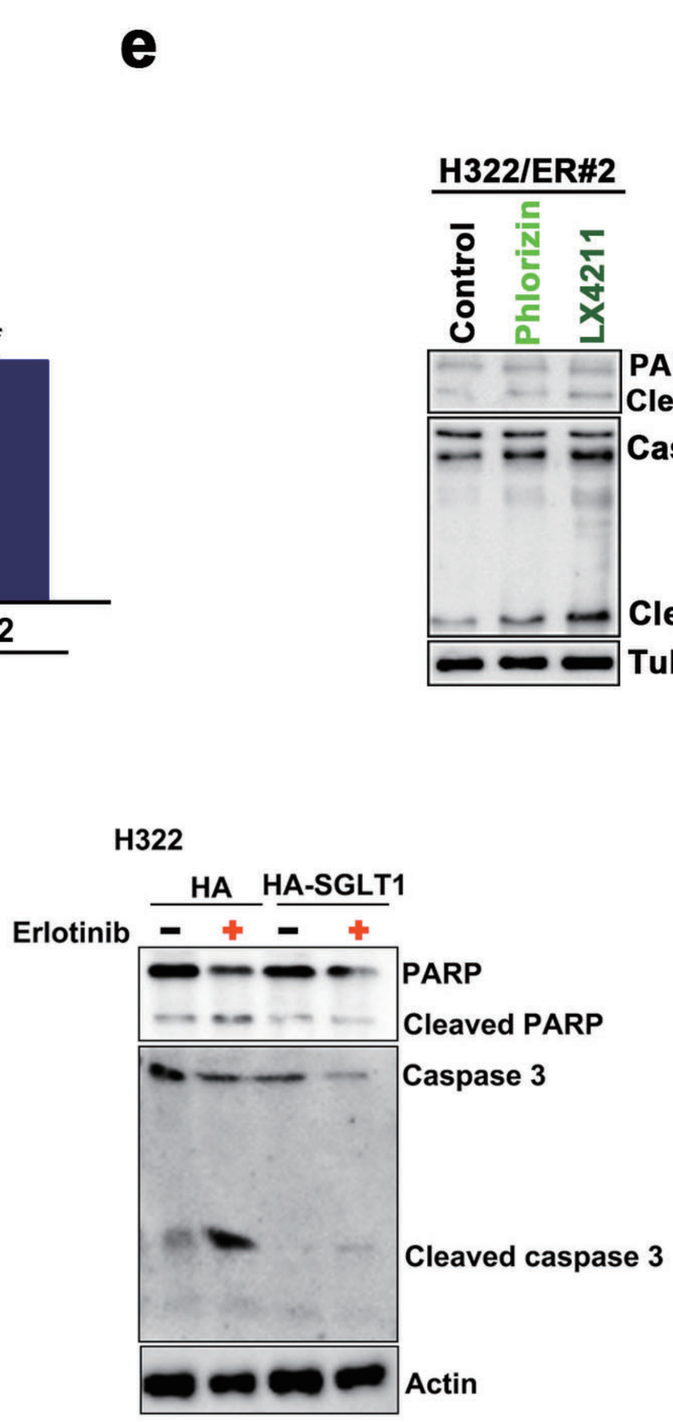
H322
HA
HA-SGLT1
Erlotinib
PARP
Cleaved PARP
Caspase 3
Cleaved caspase 3
Actin

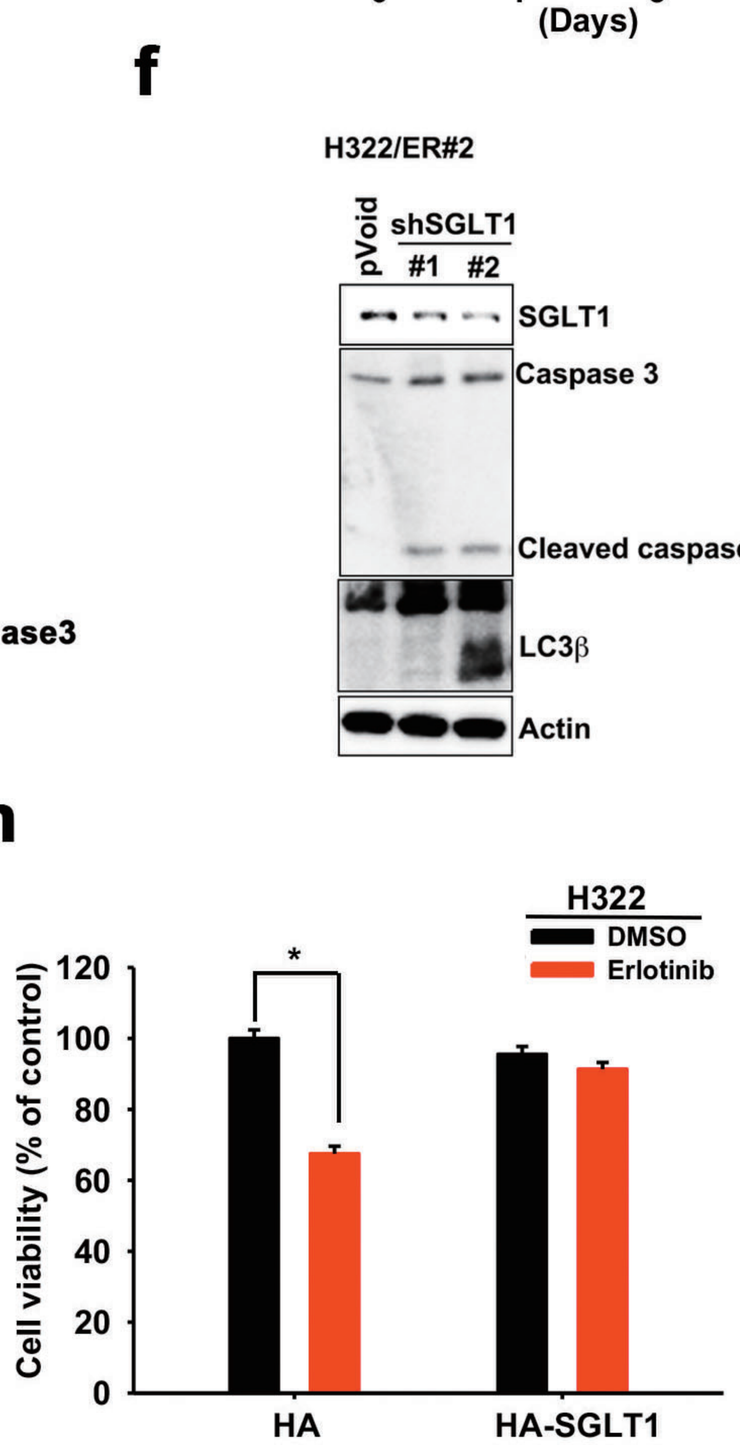
h
H322
DMSO
Erlotinib
Cell viability (% of control)
HA
HA-SGLT1
*

Figure 4

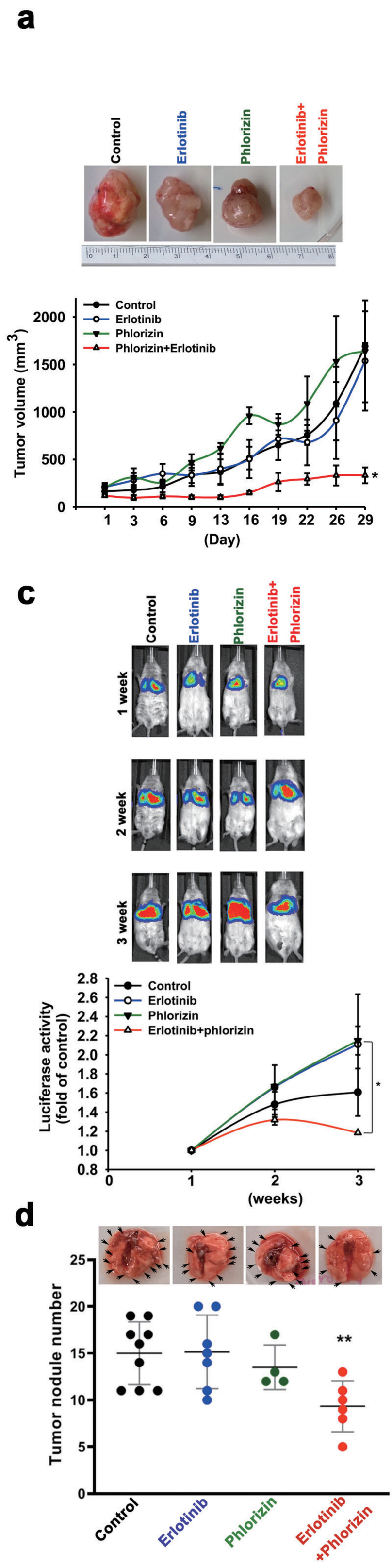
a
Control
Erlotinib
Phlorizin
Erlotinib+ Phlorizin
Tumor volume (mm3)
Control
Erlotinib
Phlorizin
Phlorizin+Erlotinib
(Day)
b
Control
Erlotinib
Phlorizin
Erlotinib+Phlorizin
EGFR
α-SGLT1
Ki67
ATG7
Cleaved PARP
H-score
c
1 week
2 week
3 week
Luciferase activity (fold of control)
(weeks)
d
Tumor nodule number
e
H&E
EGFR
α-SGLT1
Ki67
ATG7
Cleaved PARP
50 μm

Figure 5

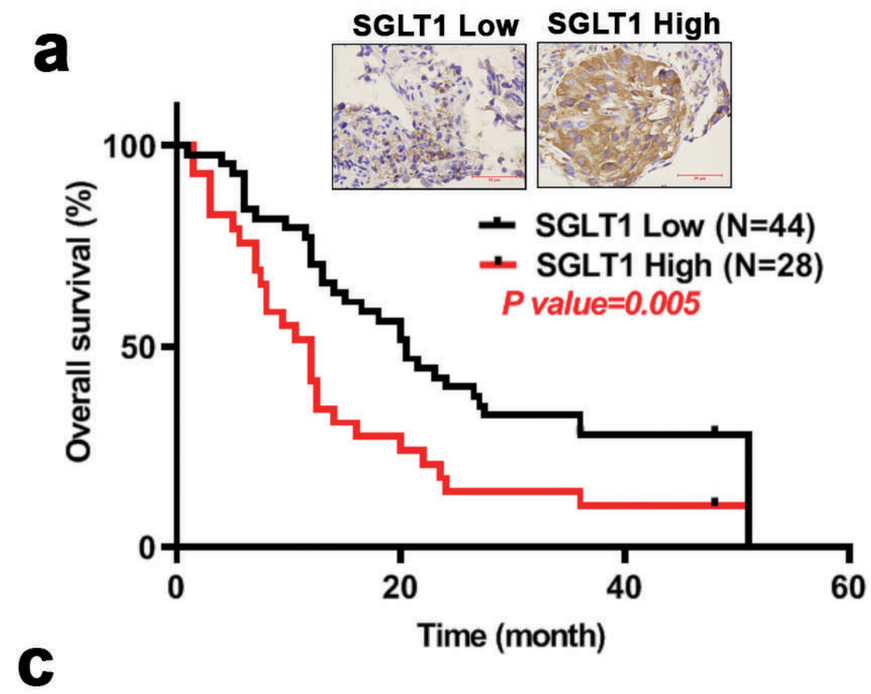
a
SGLT1 Low
SGLT1 High
Overall survival (%)
100
50
0
0
20
40
60
Time (month)
SGLT1 Low (N=44)
SGLT1 High (N=28)
P value=0.005

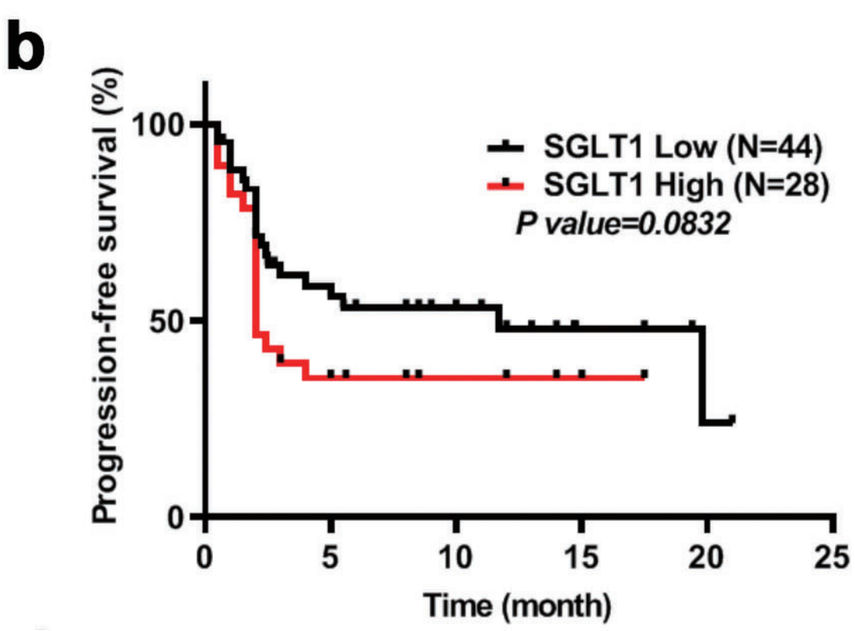
b
Progression-free survival (%)
100
50
0
0
5
10
15
20
25
Time (month)
SGLT1 Low (N=44)
SGLT1 High (N=28)
P value=0.0832

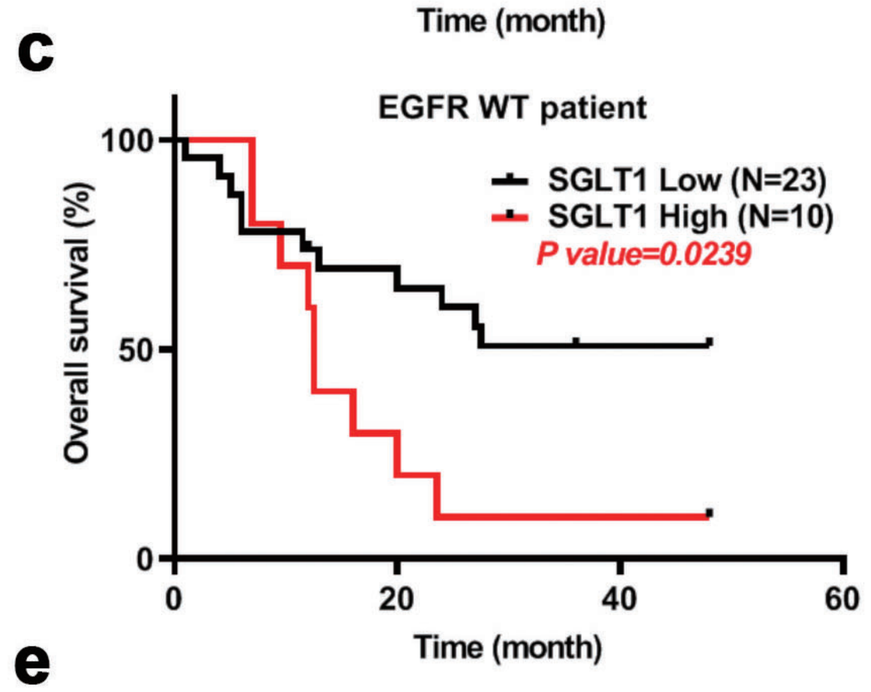
c
EGFR WT patient
Overall survival (%)
100
50
0
0
20
40
60
Time (month)
SGLT1 Low (N=23)
SGLT1 High (N=10)
P value=0.0239

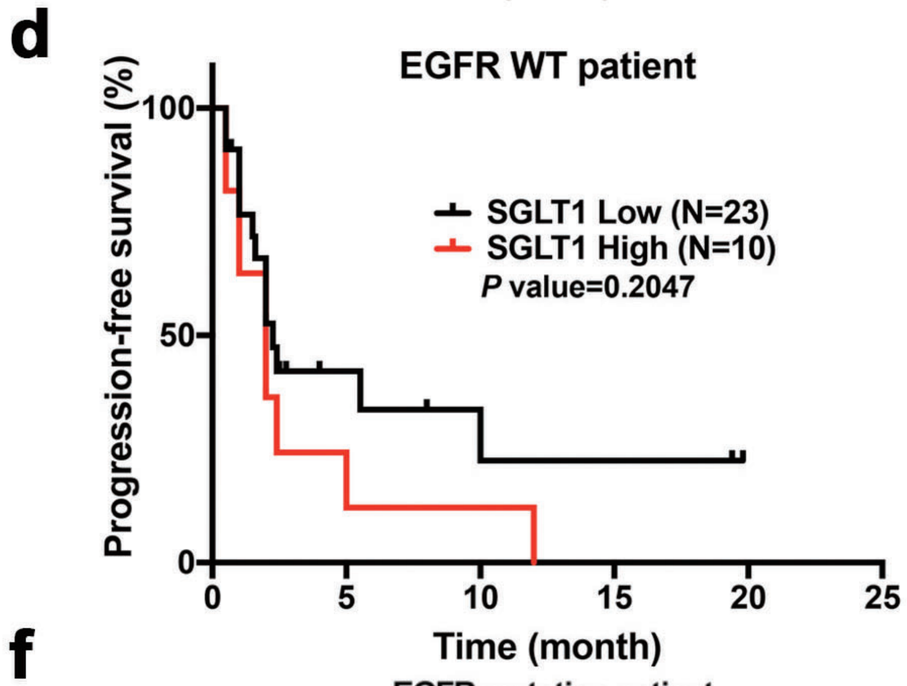
d
EGFR WT patient
Progression-free survival (%)
100
50
0
0
5
10
15
20
25
Time (month)
SGLT1 Low (N=23)
SGLT1 High (N=10)
P value=0.2047

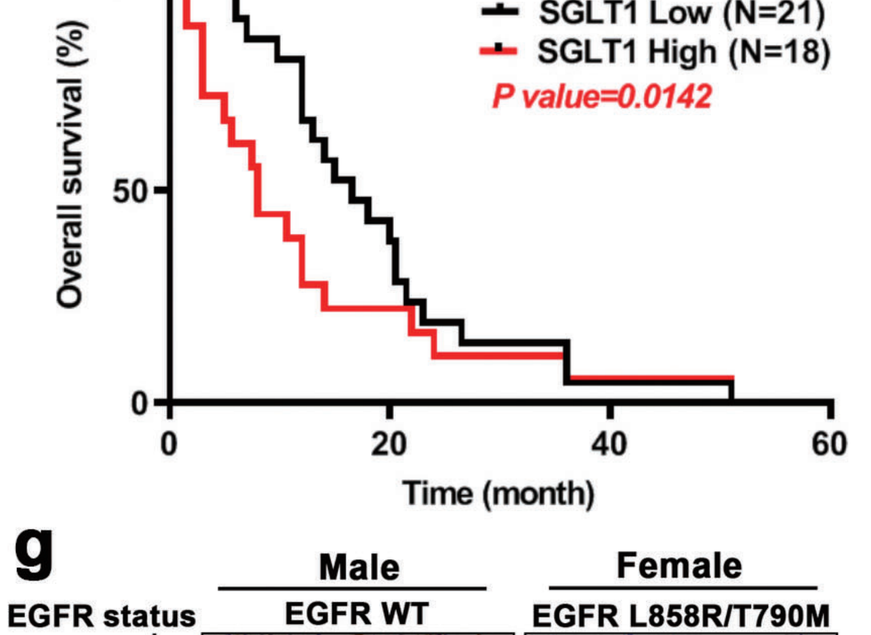
e
EGFR mutation patient
Overall survival (%)
100
50
0
0
20
40
60
Time (month)
SGLT1 Low (N=21)
SGLT1 High (N=18)
P value=0.0142

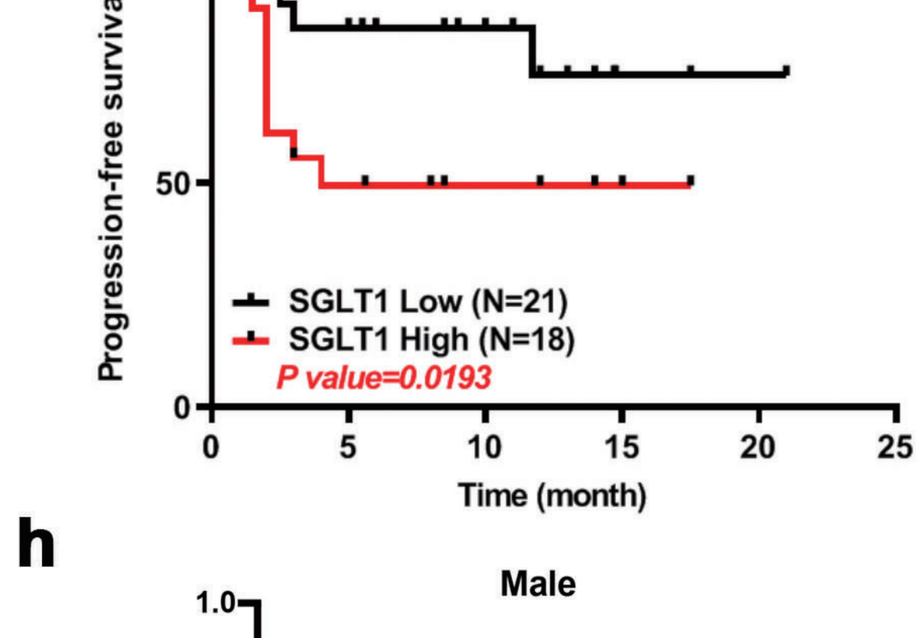
f
EGFR mutation patient
Progression-free survival (%)
100
50
0
0
5
10
15
20
25
Time (month)
SGLT1 Low (N=21)
SGLT1 High (N=18)
P value=0.0193

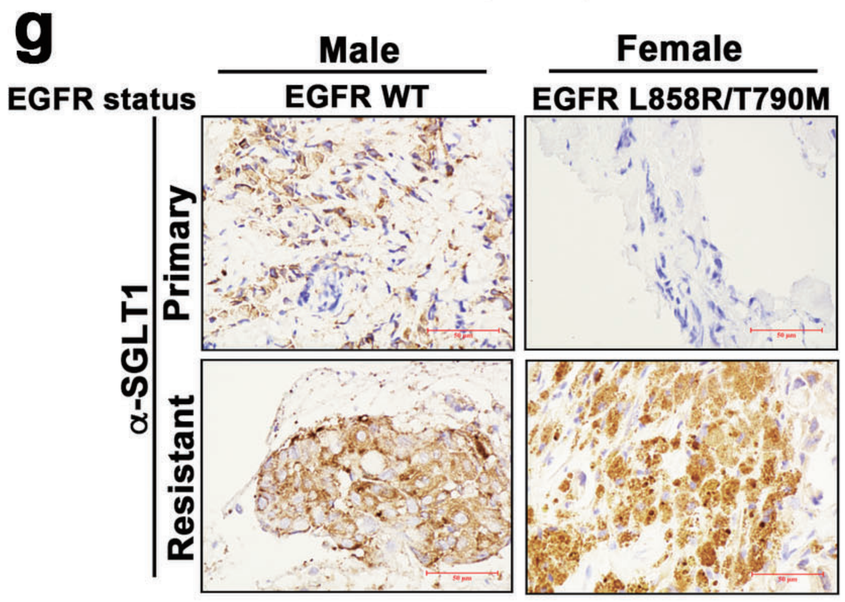
g
Male
Female
EGFR status
EGFR WT
EGFR L858R/T790M
α-SGLT1
Primary
Resistant

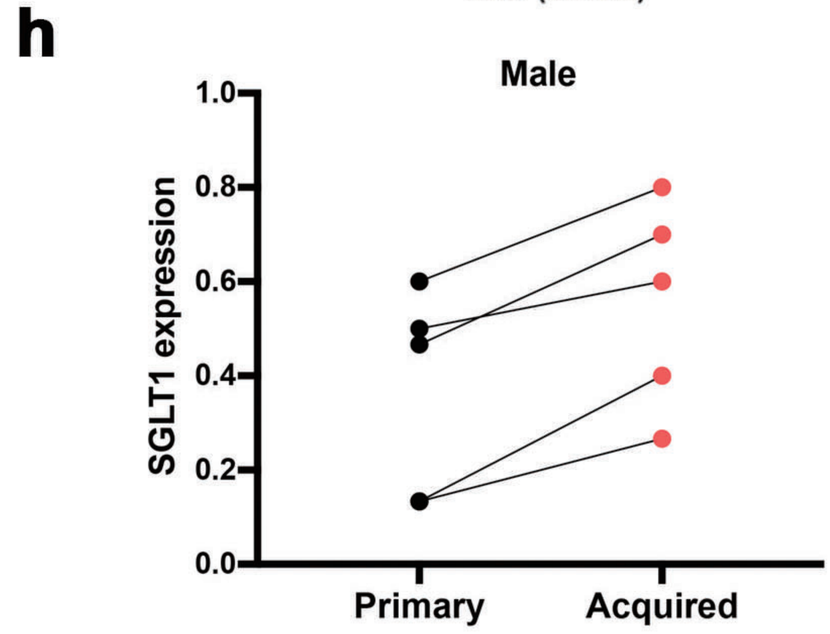
h
Male
SGLT1 expression
1.0
0.8
0.6
0.4
0.2
0.0
Primary
Acquired
Female
SGLT1 expression
1.0
0.8
0.6
0.4
0.2
0.0
Primary
Acquired

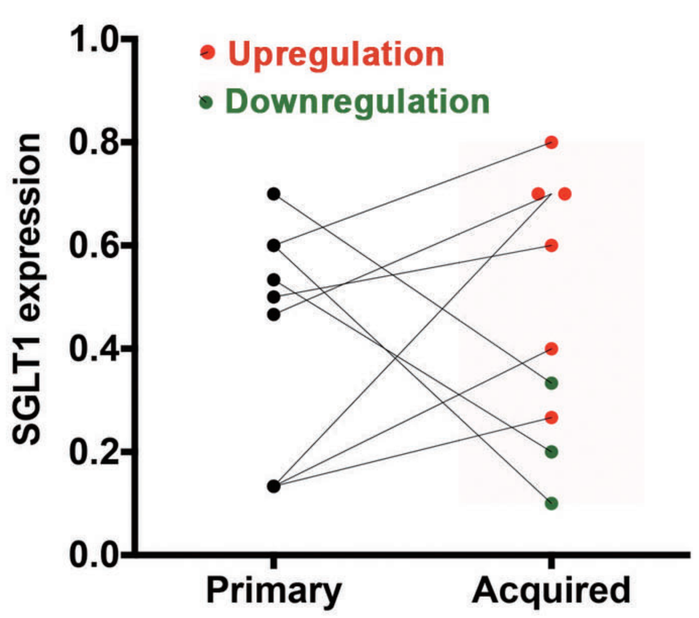
Upregulation
Downregulation
SGLT1 expression
1.0
0.8
0.6
0.4
0.2
0.0
Primary
Acquired

Figure 6

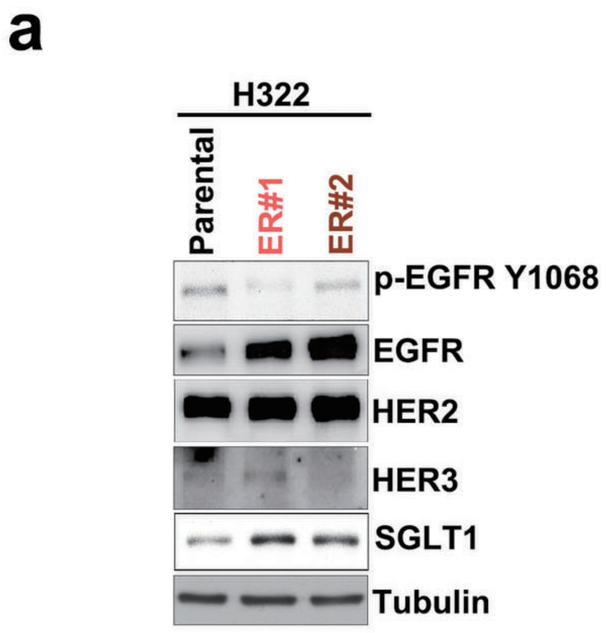
a
H322
Parental
ER#1
ER#2
p-EGFR Y1068
EGFR
HER2
HER3
SGLT1
Tubulin

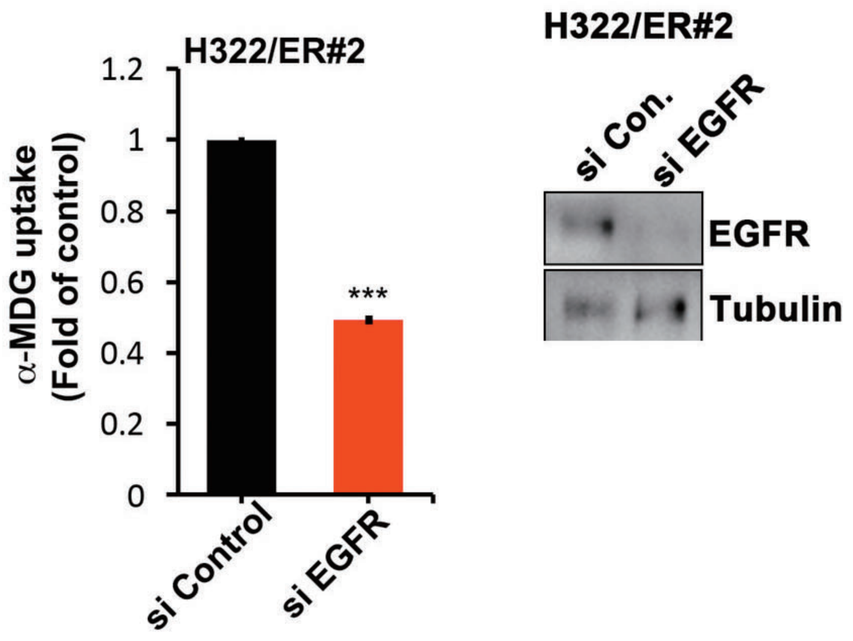
b
H322/ER#2
α-MDG uptake (Fold of control)
1.2
1
0.8
0.6
0.4
0.2
0
***
si Control
si EGFR
H322/ER#2
si Con.
si EGFR
EGFR
Tubulin

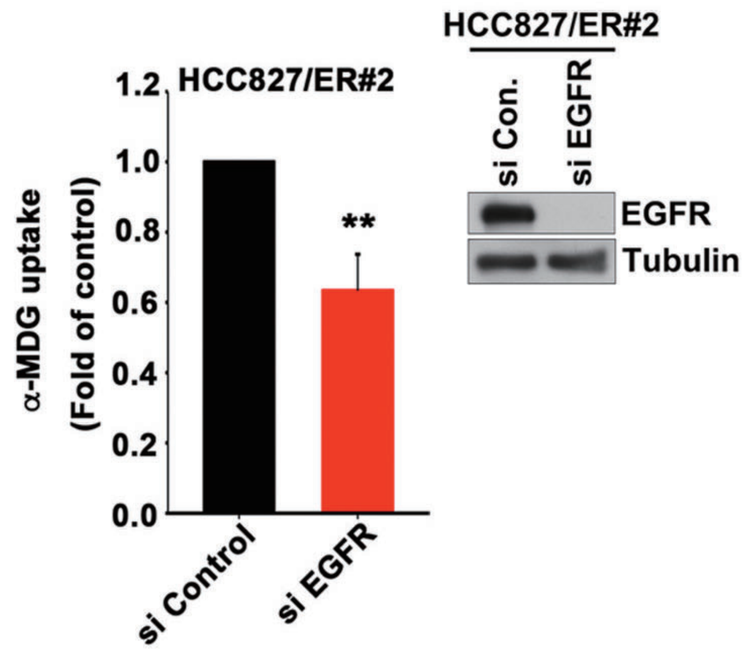
c
HCC827/ER#2
α-MDG uptake (Fold of control)
1.2
1.0
0.8
0.6
0.4
0.2
0.0
**
si Control
si EGFR
HCC827/ER#2
si Con.
si EGFR
EGFR
Tubulin

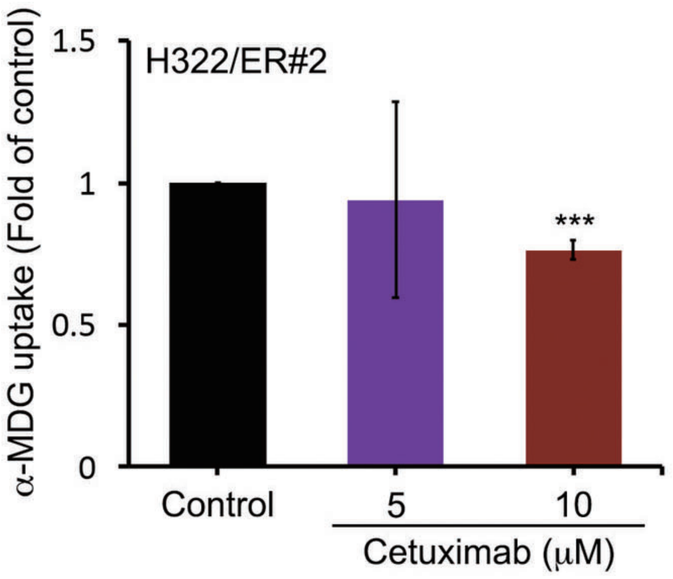
d
α-MDG uptake (Fold of control)
H322/ER#2
1.5
1
0.5
0
***
Control
5
10
Cetuximab (μM)

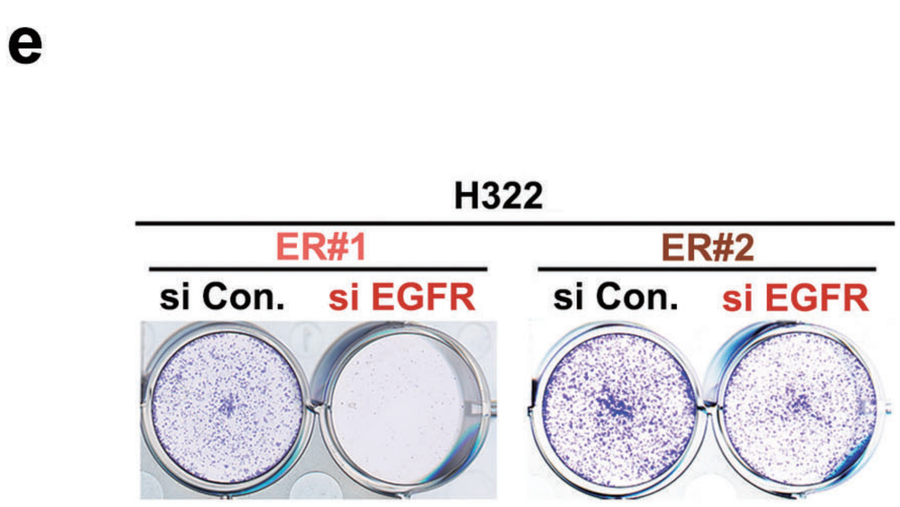
e
H322
ER#1
ER#2
si Con.
si EGFR
si Con.
si EGFR

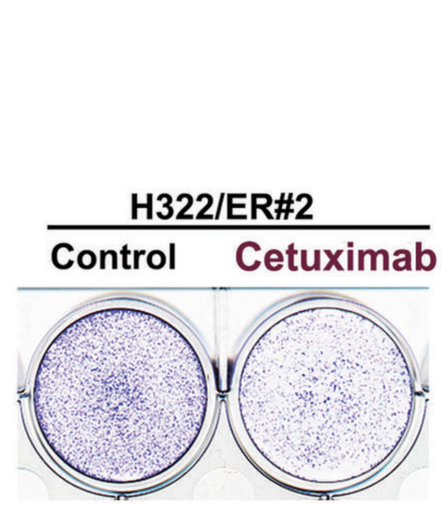
f
H322/ER#2
Control
Cetuximab

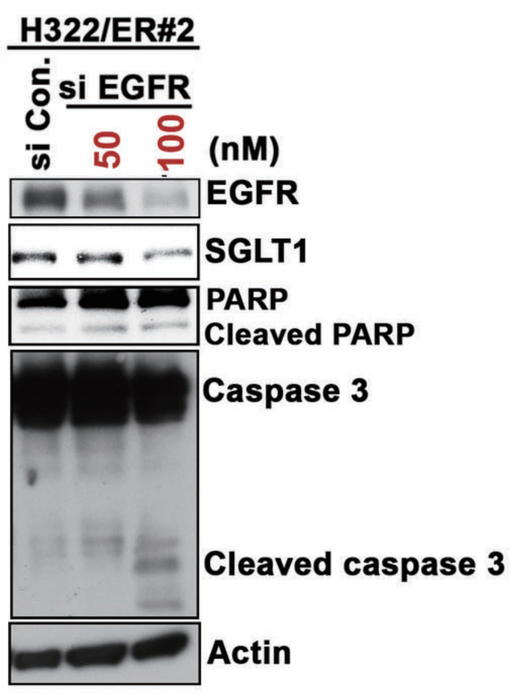
g
H322/ER#2
si Con.
si EGFR
50
100
(nM)
EGFR
SGLT1
PARP
Cleaved PARP
Caspase 3
Cleaved caspase 3
Actin

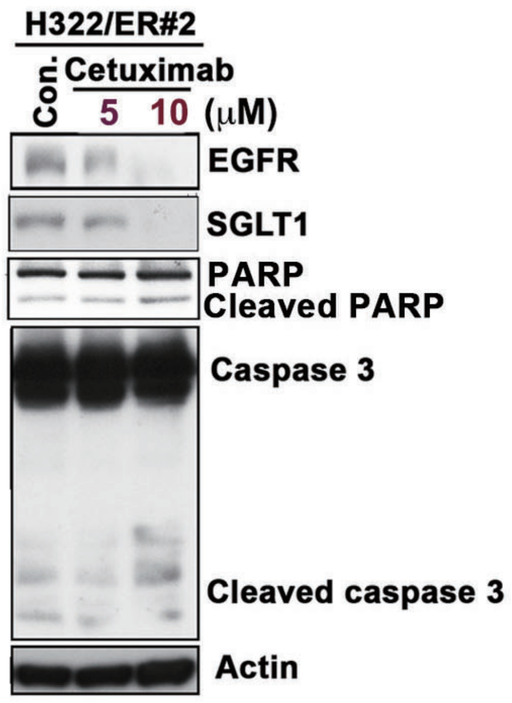
h
H322/ER#2
Con.
Cetuximab
5
10
(μM)
EGFR
SGLT1
PARP
Cleaved PARP
Caspase 3
Cleaved caspase 3
Actin

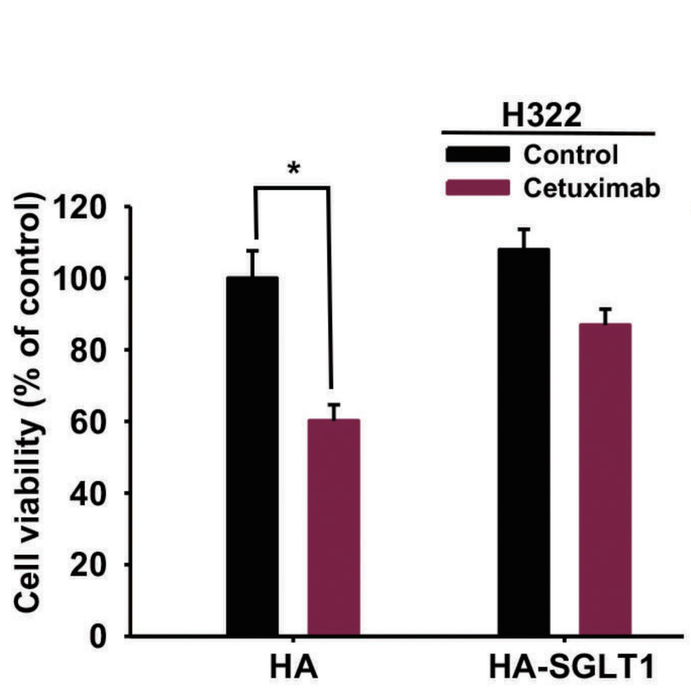
i
H322
Control
Cetuximab
Cell viability (% of control)
120
100
80
60
40
20
0
*
HA
HA-SGLT1

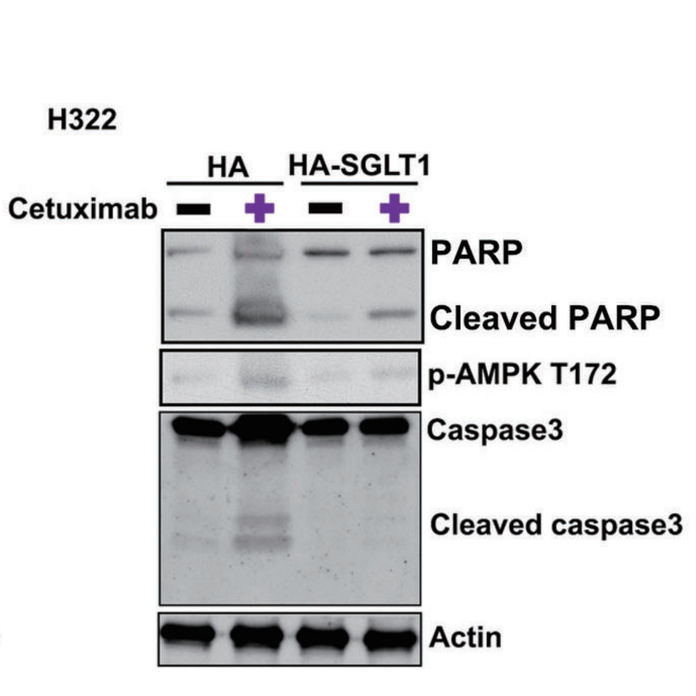
j
H322
HA
HA-SGLT1
Cetuximab
PARP
Cleaved PARP
p-AMPK T172
Caspase3
Cleaved caspase3
Actin

Figure 7

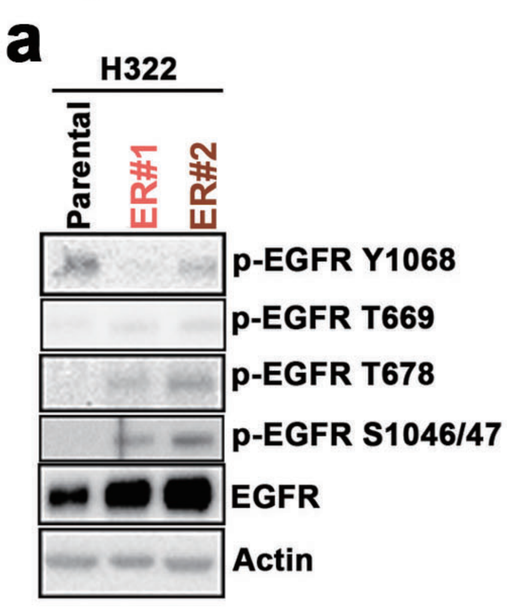
a
H322
Parental
ER#1
ER#2
p-EGFR Y1068
p-EGFR T669
p-EGFR T678
p-EGFR S1046/47
EGFR
Actin

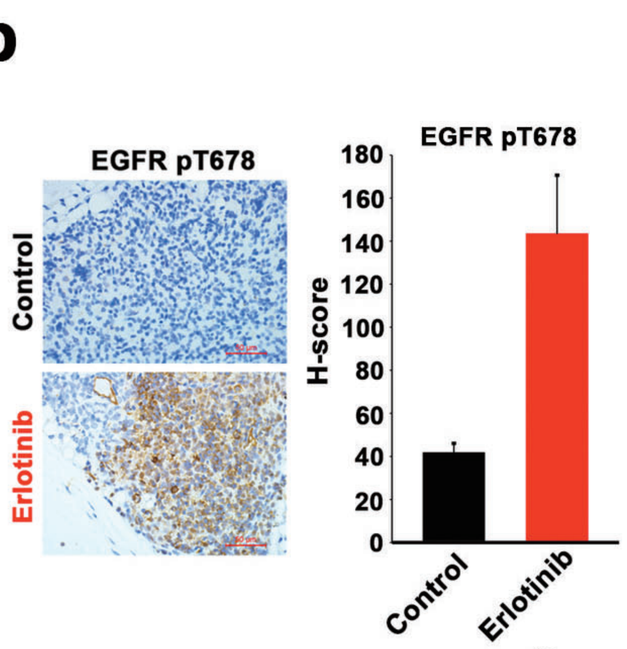
b
EGFR pT678
Control
Erlotinib
EGFR pT678
H-score
180
160
140
120
100
80
60
40
20
0
Control
Erlotinib

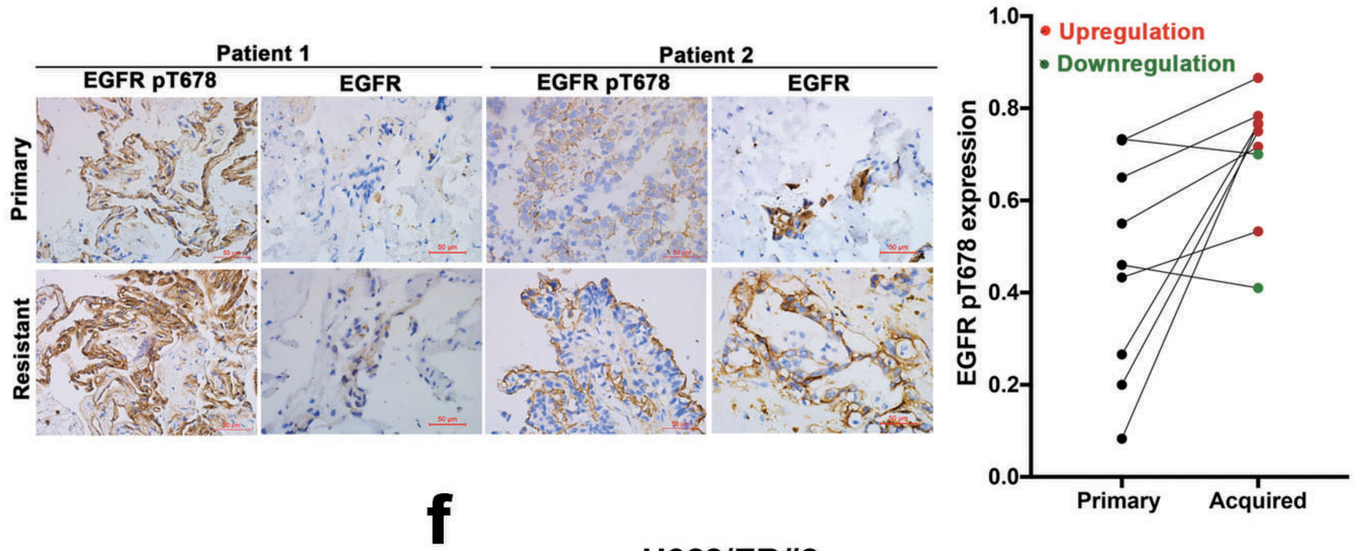
c
Patient 1
Patient 2
EGFR pT678
EGFR
EGFR pT678
EGFR
Primary
Resistant
Upregulation
Downregulation
EGFR pT678 expression
1.0
0.8
0.6
0.4
0.2
0.0
Primary
Acquired

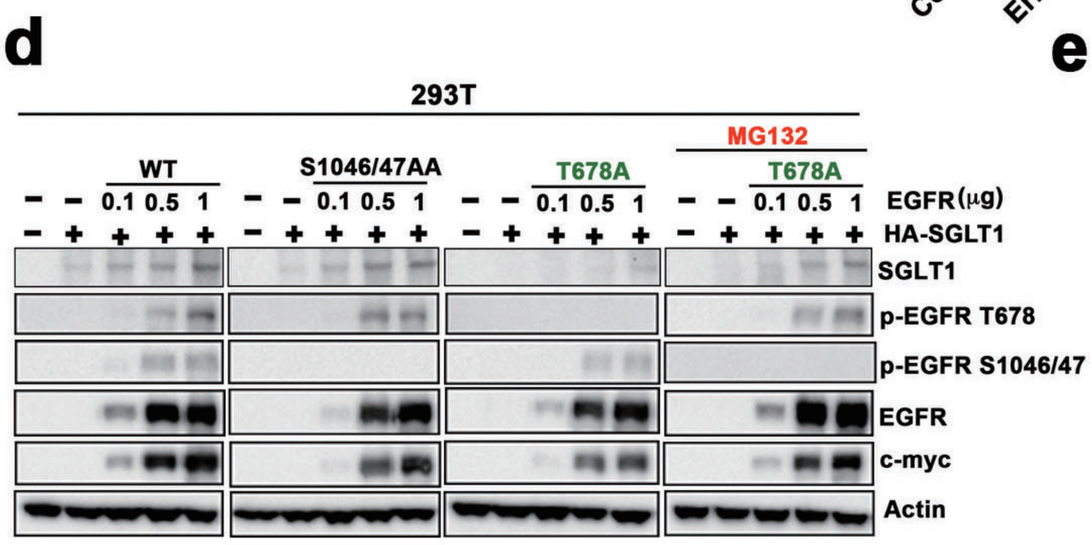
d
293T
MG132
WT
S1046/47AA
T678A
T678A
0.1 0.5 1
EGFR(μg)
HA-SGLT1
SGLT1
p-EGFR T678
p-EGFR S1046/47
EGFR
c-myc
Actin

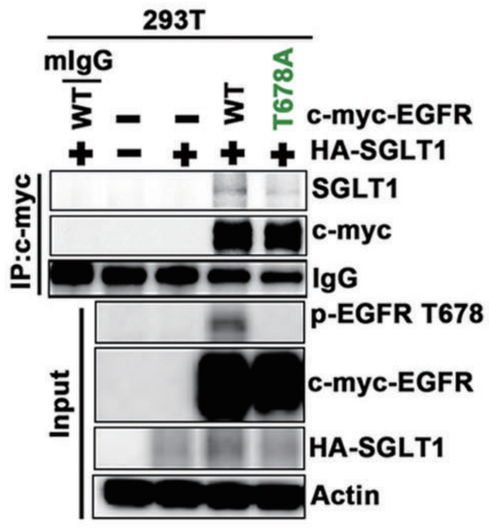
e
293T
mIgG
WT
WT
T678A
c-myc-EGFR
HA-SGLT1
IP:c-myc
SGLT1
c-myc
IgG
Input
p-EGFR T678
c-myc-EGFR
HA-SGLT1
Actin

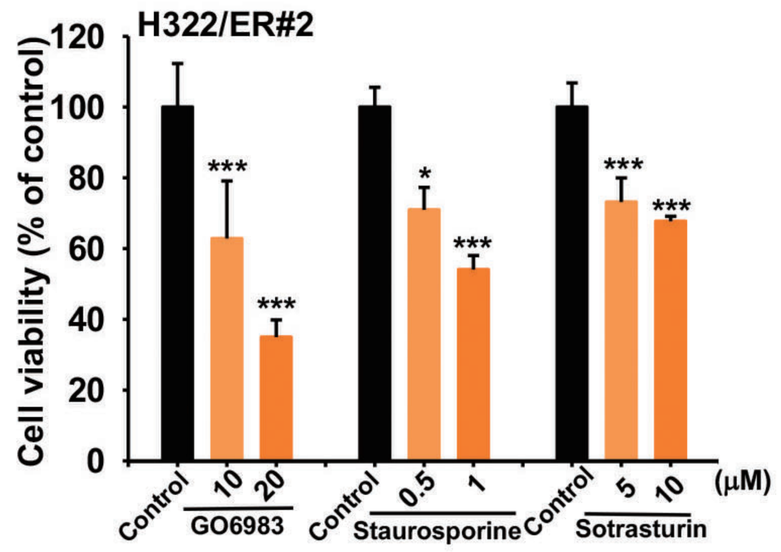
f
H322/ER#2
Cell viability (% of control)
120
100
80
60
40
20
0
***
*
***
***
***
***
Control
10
20
GO6983
Control
0.5
1
Staurosporine
Control
5
10
Sotrasturin
(μM)

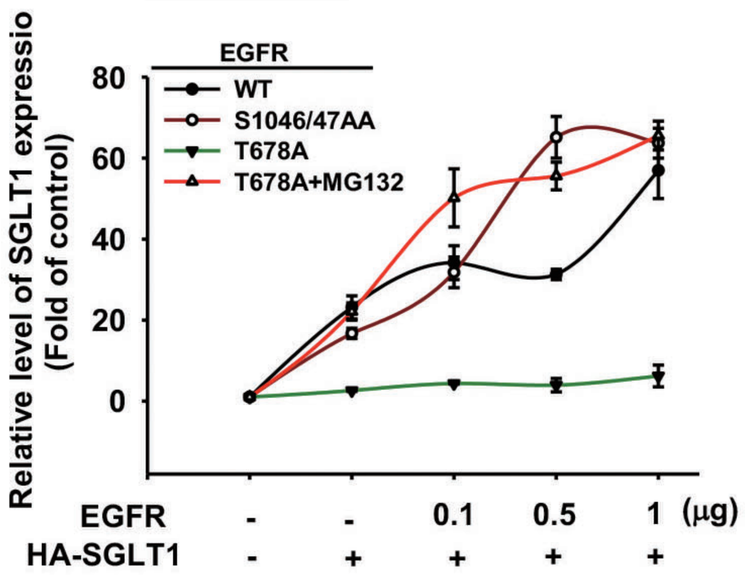
EGFR
WT
S1046/47AA
T678A
T678A+MG132
Relative level of SGLT1 expressio
(Fold of control)
80
60
40
20
0
EGFR - - 0.1 0.5 1 (μg)
HA-SGLT1 - + + + +

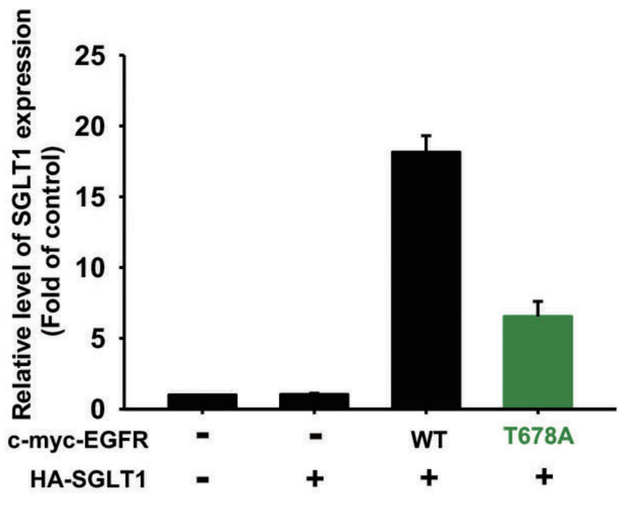
Relative level of SGLT1 expression
(Fold of control)
25
20
15
10
5
0
c-myc-EGFR - - WT T678A
HA-SGLT1 - + + +

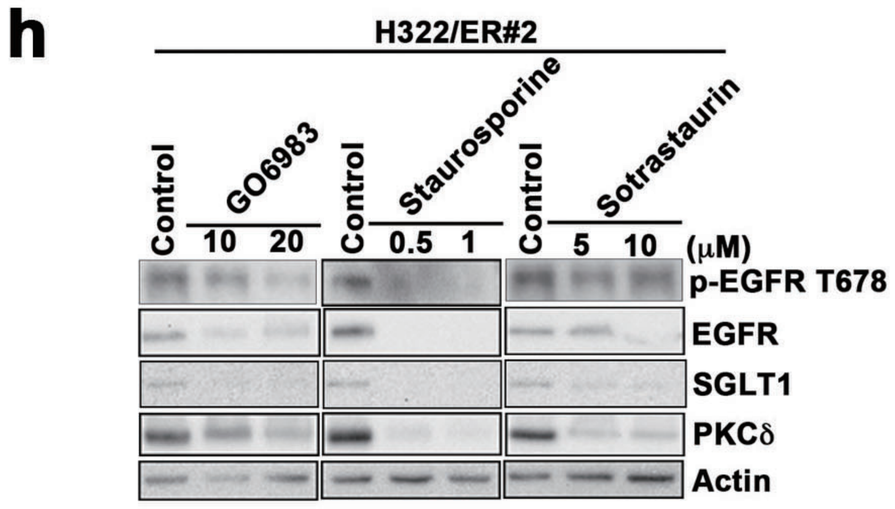
h
H322/ER#2
Control
GO6983
10 20
Control
Staurosporine
0.5 1
Control
Sotrastaurin
5 10
(μM)
p-EGFR T678
EGFR
SGLT1
PKCδ
Actin

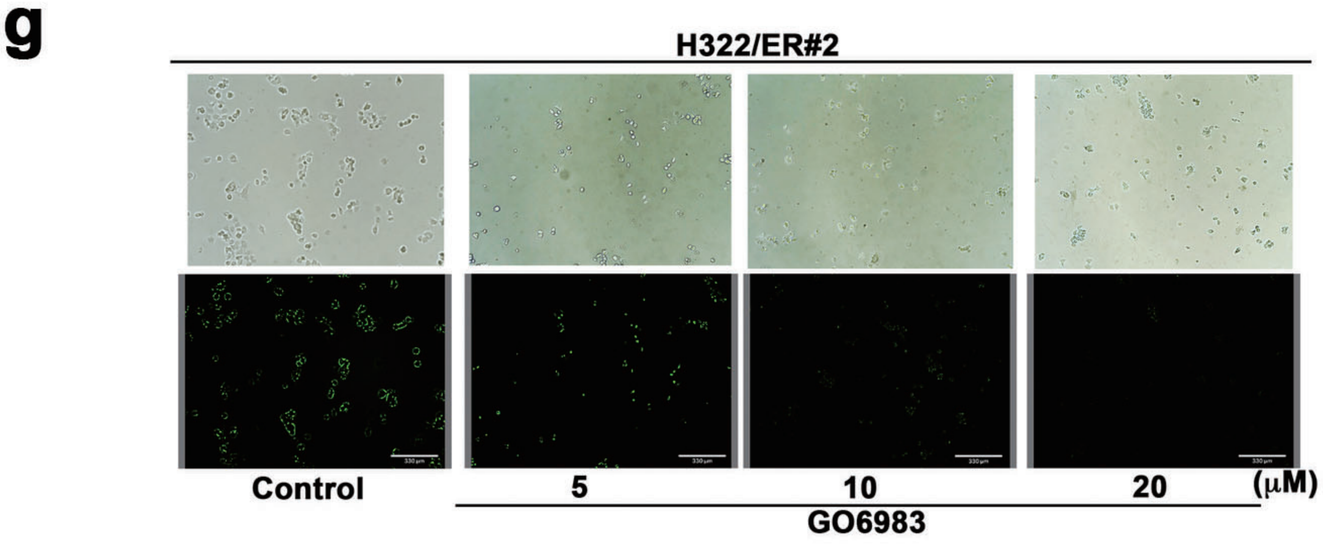
g
H322/ER#2
Control
5
10
20
(μM)
GO6983

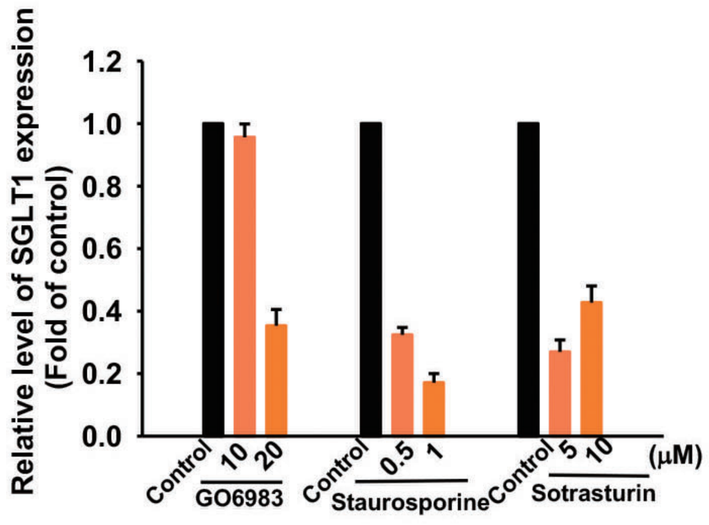
Relative level of SGLT1 expression
(Fold of control)
1.2
1.0
0.8
0.6
0.4
0.2
0.0
Control
10
20
GO6983
Control
0.5
1
Staurosporine
Control
5
10
Sotrasturin
(μM)

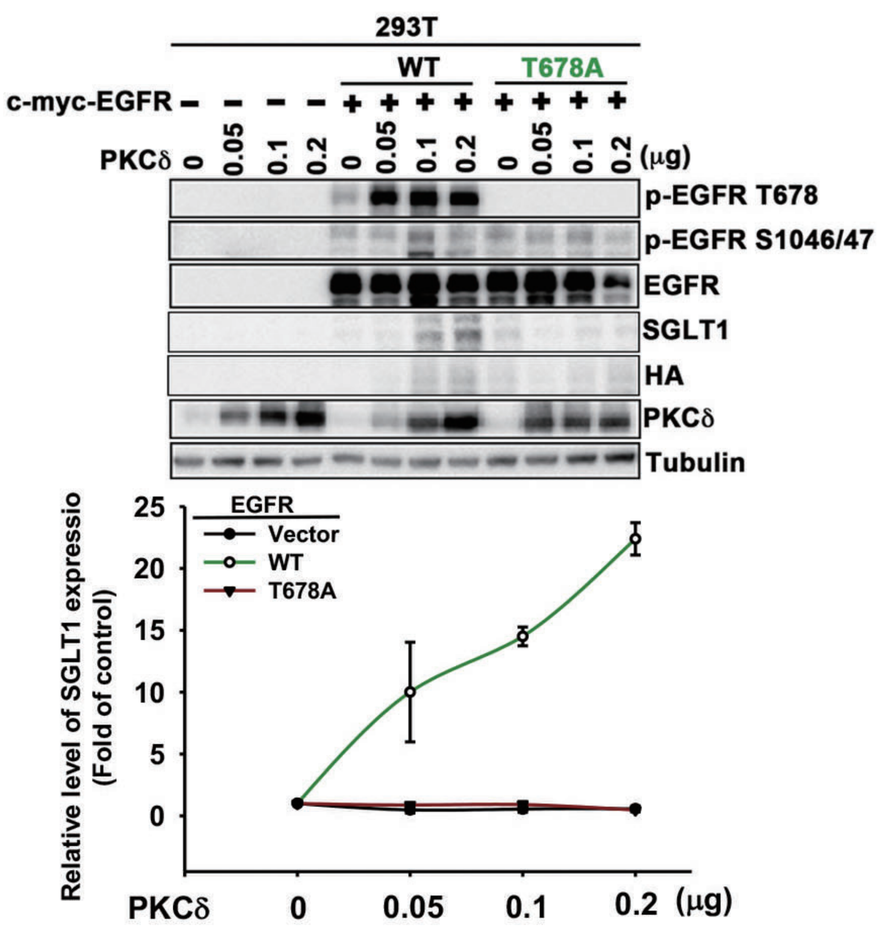
i
293T
WT
T678A
c-myc-EGFR - - - - + + + + + + + +
PKCδ 0 0.05 0.1 0.2 0 0.05 0.1 0.2 0 0.05 0.1 0.2 (μg)
p-EGFR T678
p-EGFR S1046/47
EGFR
SGLT1
HA
PKCδ
Tubulin
EGFR
Vector
WT
T678A
Relative level of SGLT1 expressio
(Fold of control)
25
20
15
10
5
0
PKCδ 0 0.05 0.1 0.2 (μg)

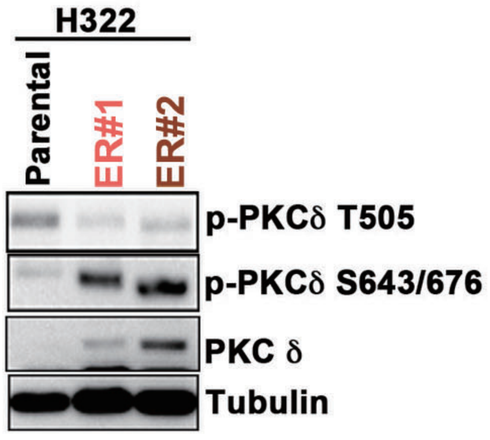
j
H322
Parental
ER#1
ER#2
p-PKCδ T505
p-PKCδ S643/676
PKC δ
Tubulin

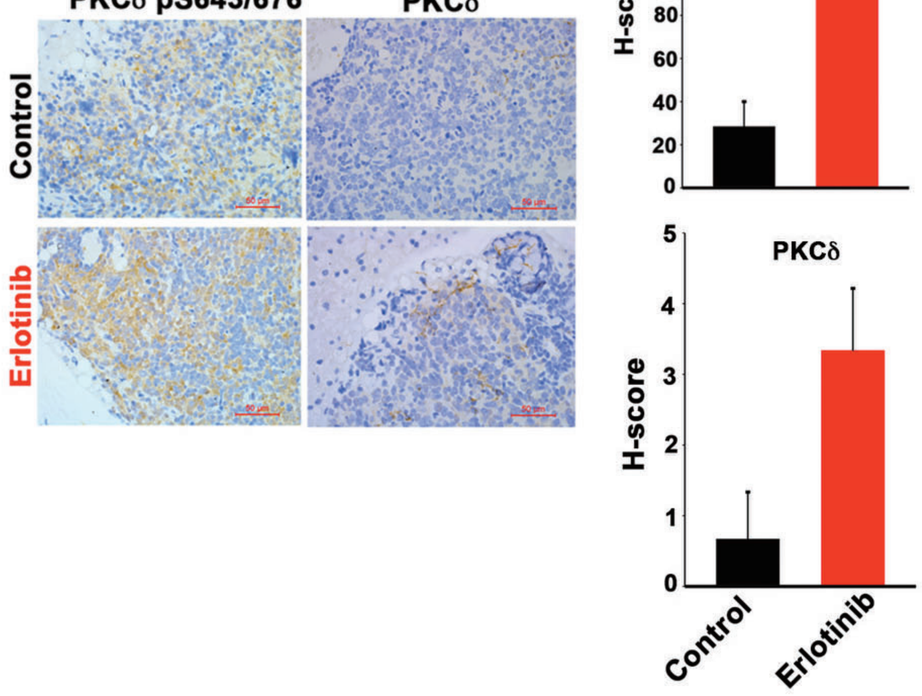
k
PKCδ pS643/676
PKCδ
Control
Erlotinib
PKCδ pS643/676
H-score
160
140
120
100
80
60
40
20
0
PKCδ
H-score
5
4
3
2
1
0
Control
Erlotinib

Figure 8

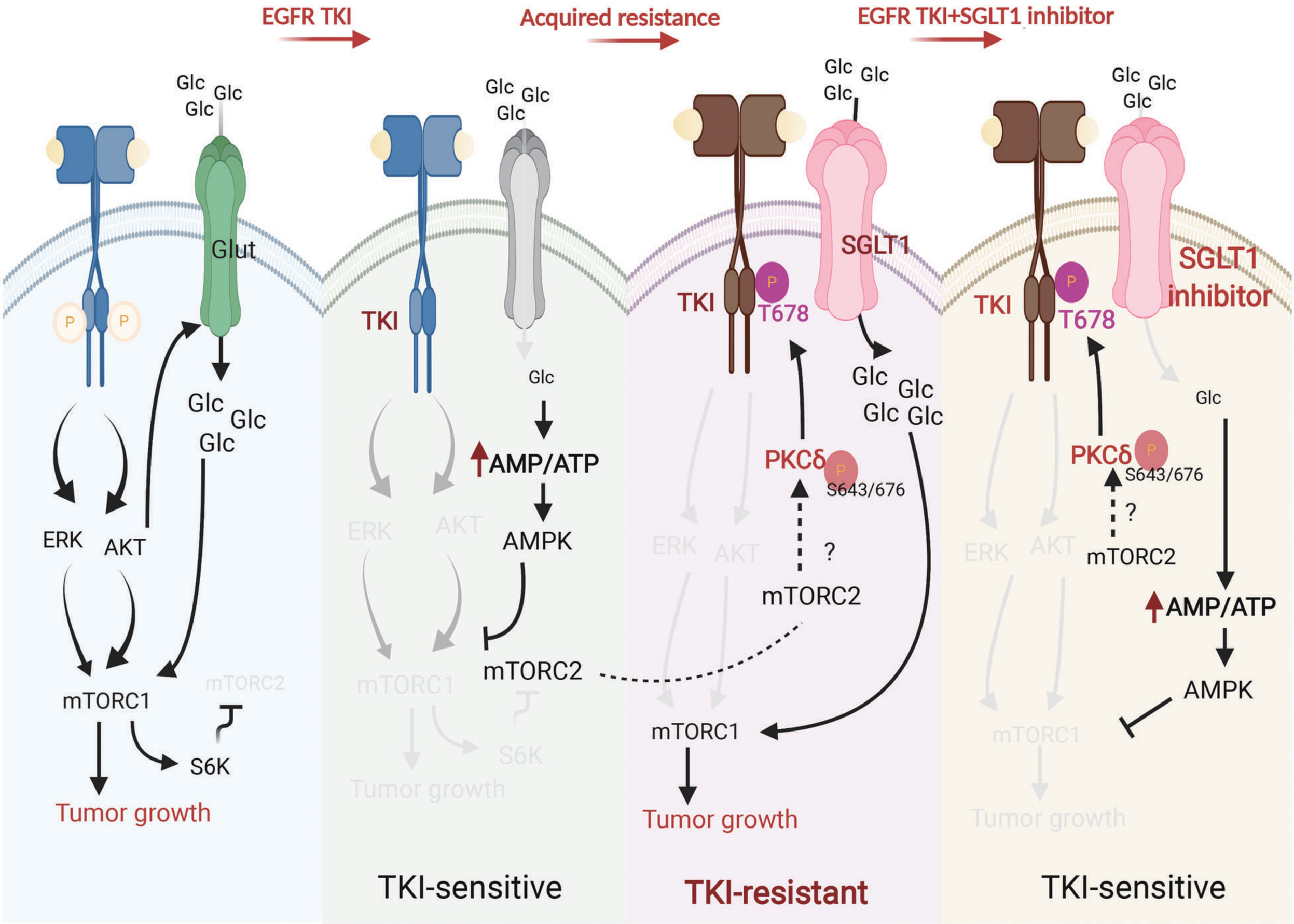
EGFR TKI
Acquired resistance
EGFR TKI+SGLT1 inhibitor
Glc
Glut
SGLT1
SGLT1 inhibitor
TKI
T678
P
PKCδ
S643/676
?
mTORC2
ERK
AKT
mTORC1
S6K
AMP/ATP
AMPK
Tumor growth
TKI-sensitive
TKI-resistant
TKI-sensitive

Supporting Information

PKCδ-mediated SGLT1 upregulation confers the acquired resistance of NSCLC to EGFR TKIs

Chia-Hung Chen, Bo-Wei Wang, Yu-Chun Hsiao, Chun-Yi Wu, Fang-Ju Cheng, Te-Chun Hsia, Chih-Yi Chen, Yihua Wang, Zhang Weihua, Ruey-Hwang Chou, Chih-Hsin Tang, Yun-Ju Chen, Ya-Ling Wei, Jennifer L. Hsu, Chih-Yen Tu, Mien-Chie Hung, Wei-Chien Huang

This file includes:

Materials and Methods

Reagents and plasmids

Erlotinib (#S1023) and gefitinib (#S5098) were obtained from Selleckchem (Houston, TX, USA). SGLT inhibitors phlorizin (# 60-81-1) and LX4211 (# HY-15516) were obtained from PubChem (Bethesda, MD, USA) and MedChem Express (Monmouth Junction, NJ, USA), respectively. D-glucose (#15023-021) was purchased from Thermo Fisher Scientific (Waltham, MA, USA). 2-Deoxy-D-glucose (2-DG) (#MER-25972), 3-methyladenine (3-MA) (#SI-M9281), chloroquine (CQ) (# SI-C6628), propidium iodide (PI) (#P4170), and oligomycin (# 75351) were purchased from Sigma-Aldrich. MG-132 (# 10012628), GO6983 (# 13311), sotrastaurin (#16726), staurosporine (#81590), and everolimus (#11597) were purchased from Cayman Chemical (Ann Arbor, Michigan, USA). HBDDE (#sc-202174) was obtained from Santa Cruz Biotechnology. pLKO-shSGLT1#1(TRCN0000043590), pLKO-shSGLT1#2 (TRCN0000043592), pCMV-ΔR8.91, and pMD.G were purchased from the National RNAi Core Facility of Academia Sinica (Taipei, Taiwan).

The rabbit polyclonal antibodies specific for SGLT1 was generated from LTK BioLaboratories (Taoyuan, Taiwan). The rabbit polyclonal antibodies against EGFR (#sc-03; RRID:AB_631420), HER2 (Neu) (#sc-393712; RRID:AB_2810840), HER3 (#sc-7390; RRID:AB_2262346), HER4 (#sc-283; RRID:AB_2231308), Glut1 (#sc-7903; RRID:AB_2190936) were purchased from Santa Cruz Biotechnology (Dallas, Texas, USA). The rabbit polyclonal antibodies specific for PARP (#9542; RRID:AB_2160739), cleaved PARP (#5625; RRID:AB_10699459), phospho-EGFR S1046/47 (#2238; RRID:AB_331129), phospho-EGFR T669 (#3056; RRID:AB_1264152), phospho-EGFR T678 (#14343; RRID:AB_2798457),

phospho-PKC δ S643/676 (#9376; RRID:AB_2168834), phospho-AMPK T172 (#2531; RRID:AB_330330), phospho-mTOR S2448 (#2971; RRID:AB_330970), mTOR (#2983; RRID:AB_2105622) and caspase 3 (#9662; RRID:AB_331439) were from Cell Signaling Technology (Danvers, MA, USA). LC3 (#NB100-2220SS; RRID:AB_791015) antibody was acquired from Novus Biologicals (Centennial CO, USA). Rabbit polyclonal antibodies specific for PKC δ (#ab182126) and phospho-PKCδ T505 (# ab60992; RRID:AB_944848) were obtained from Abcam (Cambridge, United Kingdom, England). Mouse polyclonal antibody specific for phospho-EGFR Y1068 (#2236; RRID:AB_331792) was purchased from Cell Signaling Technology. Mouse polyclonal antibody specific for Glut3 (sc-74497; RRID:AB_1124974) was acquired from Santa Cruz Biotechnology. The specific rabbit polyclonal antibodies of IHC staining for SGLT1 (#ab14685; RRID:AB_301410) and phospho-EGFR T678 (#ab194733) were purchased from Abcam. Goat polyclonal antibody specific of SGLT2 (#sc-47402; RRID:AB_2189561) was obtained from Santa Cruz Biotechnology. Actin (#A2228; RRID:AB_476697) and Tubulin (#T5168; RRID:AB_477579) were acquired from Sigma-Aldrich (St. Louis, Missouri, USA). HA (#11583816001; RRID:AB_514505) and Ki67 (#RM-9106; RRID:AB_2341197) were purchased from Roche (Basel, Switzerland) and Thermo Fisher Scientific (Waltham, MA, USA), respectively.

Cell culture and establishment of erlotinib-resistant (ER) clones

Human lung cancer H322 (CRL-5806; RRID:CVCL_1556), H292 (CRL1848; RRID:CVCL_0455), A549/Luc, and HCC827 (CRL-2868; RRID:CVCL_2063) cell lines and their erlotinib-resistant (ER) derivatives were cultured in RPMI 1640 medium supplemented with 10% FBS, 100 U/mL penicillin, and 100 mg/mL

streptomycin, with 10 mM HEPES. All cancer cell lines were maintained in a humidified 5% CO_2 incubator at 37 °C. The ER clones of various lung cancer cell lines were established from the parental cells by chronic treatment with gradually increasing concentrations (up to 1μM) of erlotinib.

Cell counting and cell viability assays

Cell viability was carried out in WST-1 colorimetric assays. Briefly, cells seeded in 96-well plates were pretreated with indicated inhibitors or infected with viral shRNA for 24 or 72 hrs followed by the incubation with 10μl/well of WST-1 (Roche, Basel, Switzerland) reagent to the cells already cultured in 100μl/ well (1:10 final dilution) for 1 hr. The relative number of cells was determined by measuring the absorbance at 450 nm.

Clonogenic formation assay

Cells (1×10^4 cells/well) in 12-well plates were grown in the presence of different concentrations of glucose or the indicated inhibitors for 14 days. The colonies were fixed and stained with 30% ethanol containing 1% crystal violet for 30 mins, and then were washed with ddH_2O.

Autophagosome formation assay

Cells seeded in 6-well plates were cultured with different glucose concentrations for 24 hr and were then stained with Cyto-ID® autophagy green dye (Enzo Lifesciences, Farmingdale, NY, USA) at 37 °C for 1 hr. Cells were washed with PBS three times and then fixed with 4% formaldehyde at room temperature for 20 min. The signal of autophagosome was detected by ECHO Revolve (San Diego, CA, USA) or measured

87 in BD FACSCalibur.

88

89 ***Cell cycle analysis***

90 Cell seeded in 6-well plates were cultured with different glucose concentrations or
91 treated with various inhibitors for 24 hr and fixed with ice-cold 70 % ethanol
92 overnight at –20 °C. The cells were spun down and washed with PBS twice, then
93 were stained with propidium iodide (PI) solution (1ml mix of 200 μg/ml RNAse and
94 50 μg/ml PI in PBS) at 37 °C for 30 min with the protection from light. The
95 subpopulation of subG1 was measured in BD FACSCalibur (BD Biosciences, San
96 Jose, CA, USA).

97

98 ***Immunoprecipitation (IP) and Western blot (WB) analysis***

99 Total lysates were prepared with lysis buffer (4 M NaCl,1 M Tris, pH8.0), 10% SDS,
100 Triton X-100, 10% sodium deoxycholate, 0.5 M EDTA), briefly sonicated, and then
101 centrifugated at 15,000 rpm for 20 min at 4 °C followed by the collection of
102 supernatants. For immunoprecipitation, one mg of total lysate incubated with primary
103 antibody for overnight followed the incubation with protein A/G beads for 4 hours at
104 4 °C. The immunoprecipitates were washed with IP buffer (1 M HEPES, 1 M KCl, 1
105 M $MgCl_2$, 5 M NaCl) and eluted with sample dye. Total lysate or immunoprecipitates
106 were subjected to protein separation in 8% or 12% of SDS-PAGE followed by protein
107 transfer to polyvinyl difluoride (PVDF) or nitrocellulose (NC) membranes. The
108 membranes were blocked with 5% milk for 1 hr at room temperature and incubated
109 with primary antibodies at 4 °C overnight followed by the incubation with secondary
110 antibodies in 5% milk for 1 hr at room temperature. The protein amount was
111 developed with enhanced chemiluminescence (Bio-Rad Laboratories, Hercules, CA,

112 USA) reagent and detected in a chemiluminescence system.

113

114 ***Measurement of extracellular acidification rate (ECAR)***

115 The ECAR in lung cancer cells and their ER clones were assessed by using a
116 Seahorse XF®24 Analyzer (Agilent Technologies Inc., Santa Clara, CA, USA).
117 Assays were performed according to the manufacturer's instructions. In brief, cells
118 (2.5×10^4 cells/well) in 24-well XF microplate (Seahorse Biosciences, VIC, Australia)
119 were cultured in glucose-free seahorse XF assay medium. Specific inhibitors,
120 different glucose concentrations, and uncouplers were prepared in XF assay media
121 following the experiment's design for sequential addition at the appropriate final
122 concentrations (10 mM glucose, 1μM oligomycin, and 50 mM 2-DG). The data were
123 normalized with cell numbers.

124

125 ***2-[N-(7-Nitrobenz-2-oxa-1,3-diazol-4-yl) amino]-2-deoxy-D-glucose (2-NBDG)***
126 ***uptake assay***

127 Cells seeded in 6 well plates were pretreated with the indicated inhibitors for 3 days
128 followed by the incubation with glucose-free media for 4 hr and 2-NBDG (100
129 μM/mL; Cayman, Ann Arbor, MI, USA) in PBS for 20 min at 37 °C. The uptake of
130 2-NBDG was detected by ECHO Revolve or measured in BD FACSCalibur.

131

132 ***[14C]-α-methyl-D-glucopyranoside (αMDG) uptake assay***

133 The active glucose uptake ability of cells was determined by measuring the uptake of
134 α-MDG (PerkinElmer, MA, USA), which is a specific subtract for SGLT. Cells
135 seeded in a 12-well plate were cultured with different glucose concentrations or
136 infected with SGLT1 shRNA. After washed with PBS once, the cells were incubated

with Krebs–Ringer–Henseleit (KRH; 120 mM NaCl, 4.7 mM KCl, 1.2 mM $MgCl_2$, 2.2 mM $CaCl_2$, and 10 mM HEPES, pH 7.4 [with Tris]) solution containing [^{14}C]-αMDG (0.1 μCi/ml) for 40 min. Following wash with PBS three times, cells were lysed by 1% Triton and added 2 ml scintillation solution. Then the uptake of [^{14}C]-αMDG was counted and presented as counts per minute (CPM) value in Beckman LS6000 Scintillation Counter (GMI, Ramsey, MN, USA), and the data were normalized with the protein amounts.

Human NSCLC clinical specimens

The acquisition of tumor specimens from NSCLC patients treated with EGFR TKIs were approved by the Ethics Review Board of China Medical University Hospital (DMR101-IRB1-120). Informed written consent was obtained from patients. The tissues were fixed in 10% formalin and embedded in paraffin, and 5μm tissue slides were prepared for IHC staining.

Immunohistochemistry Staining

Five-micrometer thick paraffin wax mouse-tissue sections were dewaxing by xylene and rehydrated by different concentrations of ethanol. These mouse-tissue sections were incubated with the indicated antibodies overnight and then stained with polymer HRP-conjugated secondary antibodies for 30 min followed by reaction with diaminobenzidine (DAB; Leica, Wetzlar, Germany) for 30 sec or 1 min. These slides were counterstained with hematoxylin. According to the H-score system, the immune-intensity of tumor tissue was scored by calculating the percentage of positive cells at different staining intensity levels, and the final score is ranked from 0 to 300. The score of SGLT1 level over than 200 was defined as high expression.

Xenograft tumor growth assay

Animal experiments were performed following a protocol approved by the Institutional Animal Care and Use Committee of China Medical University and Hospital (No. 102-40-N). H292 cells (1×10^6 cells/mouse) were subcutaneously injected into the female severe combined immunodeficient (SCID) mice at 4 weeks of age, and the tumor size was measured with calipers once per week. Once the tumor size reached 100~200 mm^3, mice were treated orally with saline, erlotinib (50 mg/kg), phlorizin (20 mg/kg), LX4211 (60 mg/kg), or the indicated combination for 30 days. A549/Luc cells were intravenously injected into the SCID mice. Tumor volume, as indicated by luciferase intensity, was measured by the Lumina LT In Vivo Imaging System (IVIS; PerkinElmer Inc., Waltham, MA, USA).

Site-directed mutagenesis

The human EGFR T678A, EGFR S1046/47AA mutants were generated by using the QuikChange Site-Directed Mutagenesis kit (Agilent Technologies Inc., Santa Clara, CA, USA) following the manufacturer's protocol. The primers were listed in the Supplementary information. Each mutation was verified by DNA sequencing.

Transient Transfection

Cells with 80% of confluence were subjected to transfection by incubation with DNA/TransIT®-X-2 (Mirus Bio, Madison, WI, USA) complex (ratio of 1:1.2) in serum-free medium for 6 hours followed by the refreshment with complete medium. The cells were harvested and subjected to the experiments after 72 hours of transfection.

187

188 ***Gene silence with shRNA***

189 The shRNA clones against the indicated human genes were purchased from the
190 National RNAi Core Facility at Academia Sinica (Taipei, Taiwan). Briefly, cells were
191 infected with the indicated viral shRNA at the multiplicity of infection (MOI) of 125
192 for 3 days. Cells were refreshed with complete medium and then further subjected to
193 the indicated experiments.

194

195 ***Statistical analysis***

196 Analyses of patient survival and progression-free rates were performed using
197 GraphPad Prism 8. Other statistical analysis was performed by Sigma plot. Data are
198 displayed as the means ± SEM. The significance of the difference between the
199 experimental and control groups was assessed by Student's *t*-test. The difference was
200 considered to be significant if the *P*-value was < 0.05.

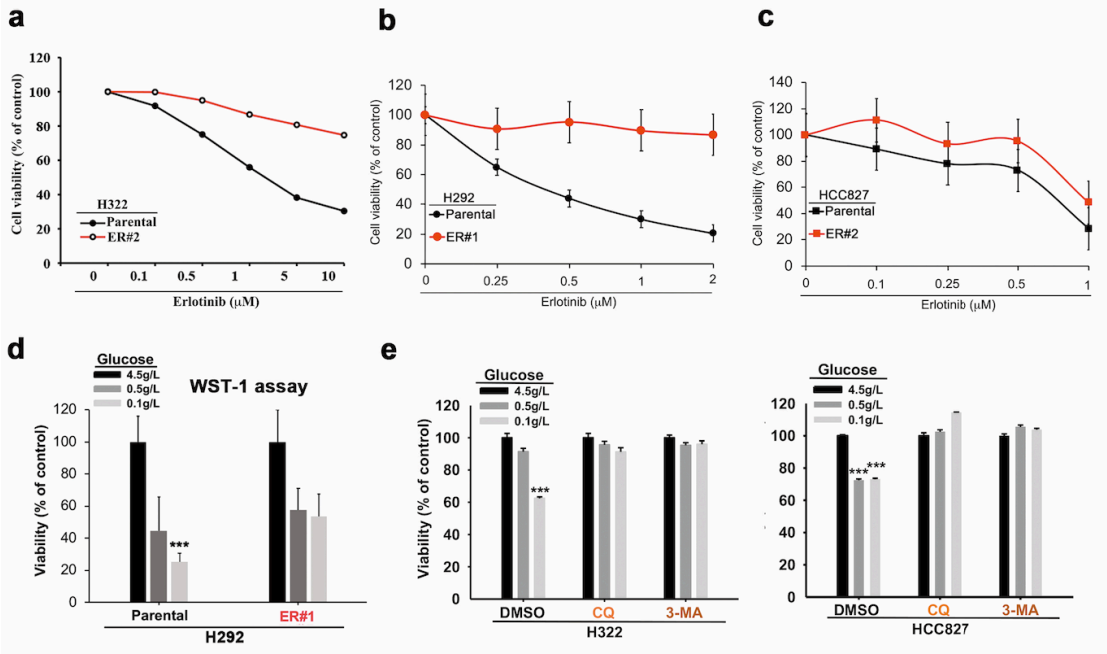

Supplementary Fig S1. The acquired erlotinib-resistant NSCLC cells were more tolerant to glucose deprivation. a-c. H322, H292, and HCC827 cells and their ER clones were treated with different concentrations of erlotinib. The viability was determined by MTT assay. **d**. H292 cells and their ER clone were cultured in different concentrations of glucose. The cell viability was measured in MTT. **e.** The effects of 3-MA or CQ on the glucose deprivation-induced cell death were examined in WST-1 analysis. Data in **(a-e)** represent as mean±s.d. from three independent experiments. **P* < 0.05; ****P*< 0.001 vs control group, Student's t test.

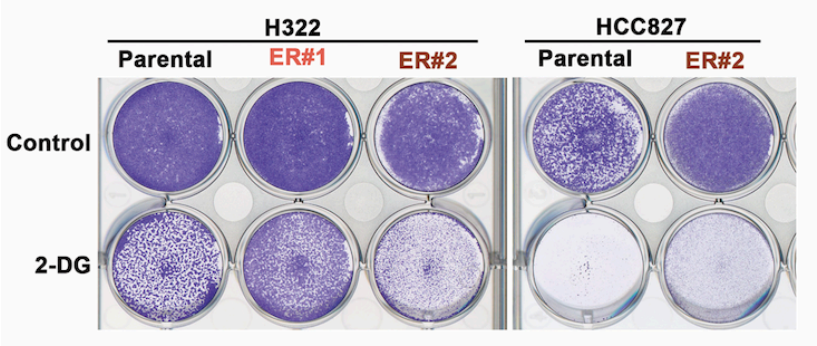

Supplementary Fig S2. Block of glycolysis decreased cell growth.

The inhibitory effects of 2-DG on the viability in H322 and HCC827 cells and their ER clones were measured by clonogenic assay.

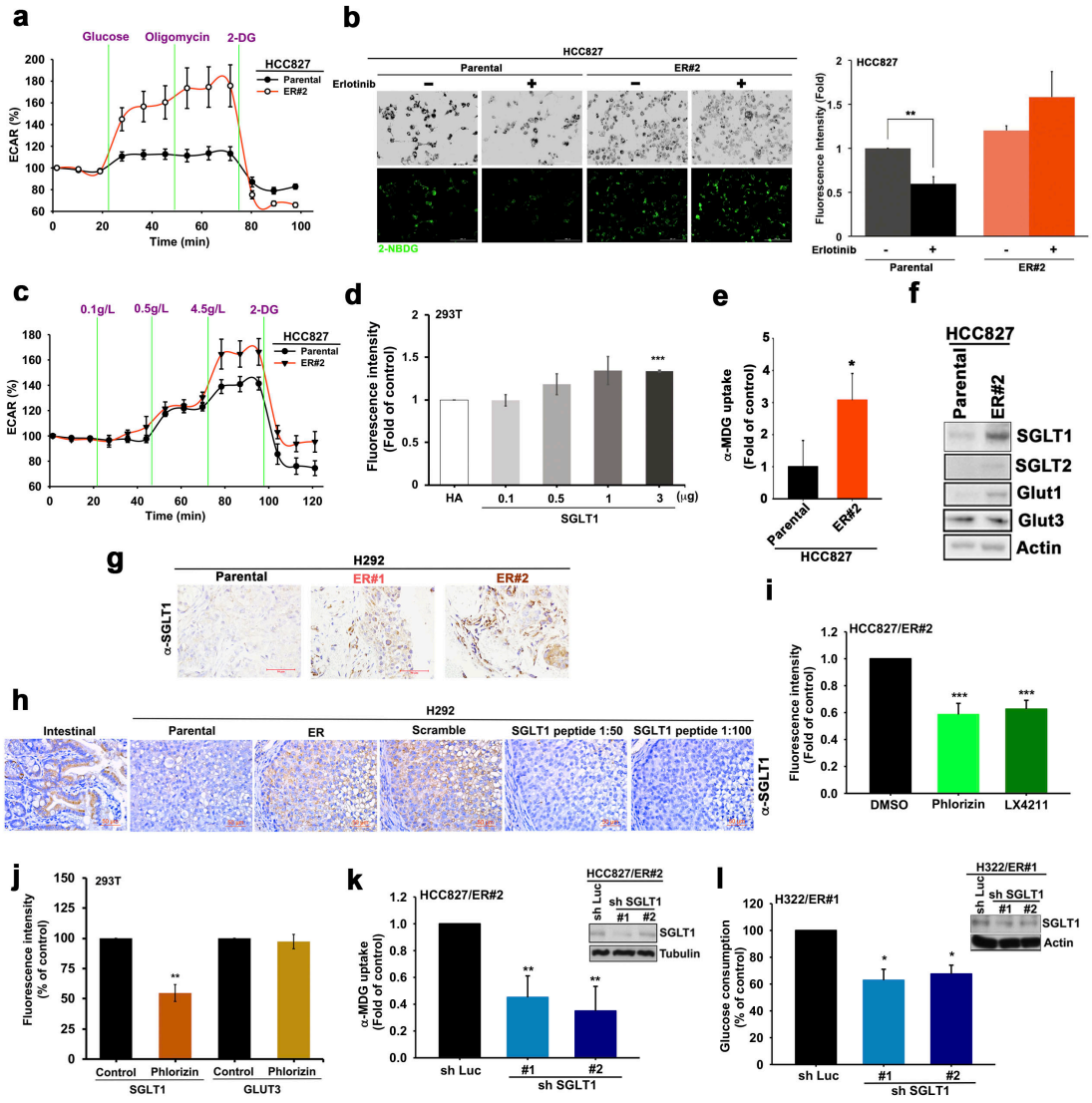

Supplementary Fig S3. The upregulated SGLT1 mediated glucose uptake of the acquired erlotinib-resistant cells. a. Changes in ECAR of HCC827 and their ER clones were measured by using the XF-24 Seahorse extracellular flux analyzer. **b.** 2-NBDG uptake ability of HCC827 and its ER clones under EGFR-TKI treatment were detected by immunofluorescent. Scale bar, 200 μm. **c.** Changes in ECAR in HCC827 and its ER clones in response to different glucose concentrations treatment were analyzed in XF-24 Seahorse extracellular flux analyzer. **d.** HEK-293T cells transfected with increasing amounts of SGLT1 cDNA were subjected to 2-NBDG uptake analysis. **e.** α-MDG uptake ability of HCC827 cells and their ER clones was detected by FACS and Beckman LS6000 Scintillation Counter. **f**. Protein levels of the

indicated glucose transporters in HCC827 and its ER clone cells were detected in WB with the indicted antibodies. **g and h**. Representative images of IHC staining of SGLT1 expression in the tumor sections from H292 and H292/ER cells (g) by using the specific anti-SGLT1 antibody which was validated with competitive peptide corresponding to the epitope sequence of SGLT1 (a.a.601-630) (h). Scale bar, 50 μm. **i.** The effects of 100μM phlorizin or 1μM LX4211 on 2-NBDG uptake ability in HCC827/ER#2 clones under a low glucose concentration condition were examined. **j.** The effects of phlorizin on 2-NBDG uptake ability of SGLT1- or Glut3-transfected HEK-293T cells under a low glucose concentration condition were examined. **k.** The effects of SGLT1 shRNA on the α-MDG uptake ability of HCC827/ER#2 clone were measured under low glucose condition by using Beckman LS6000 Scintillation Counter. **l**. The effects of SGLT1 shRNA on glucose consumption level of H322/ER#1 clone were analyzed. Data shown in **(a)**, and **(c-e),** and **(i-l)** represent as mean±s.d. from three independent experiments. *$P < 0.05$; **<0.01; ***$P < 0.001$ vs control group, Student's t test. Data in **(b)**, **(g)** and **(h)** are representative of three experiments.

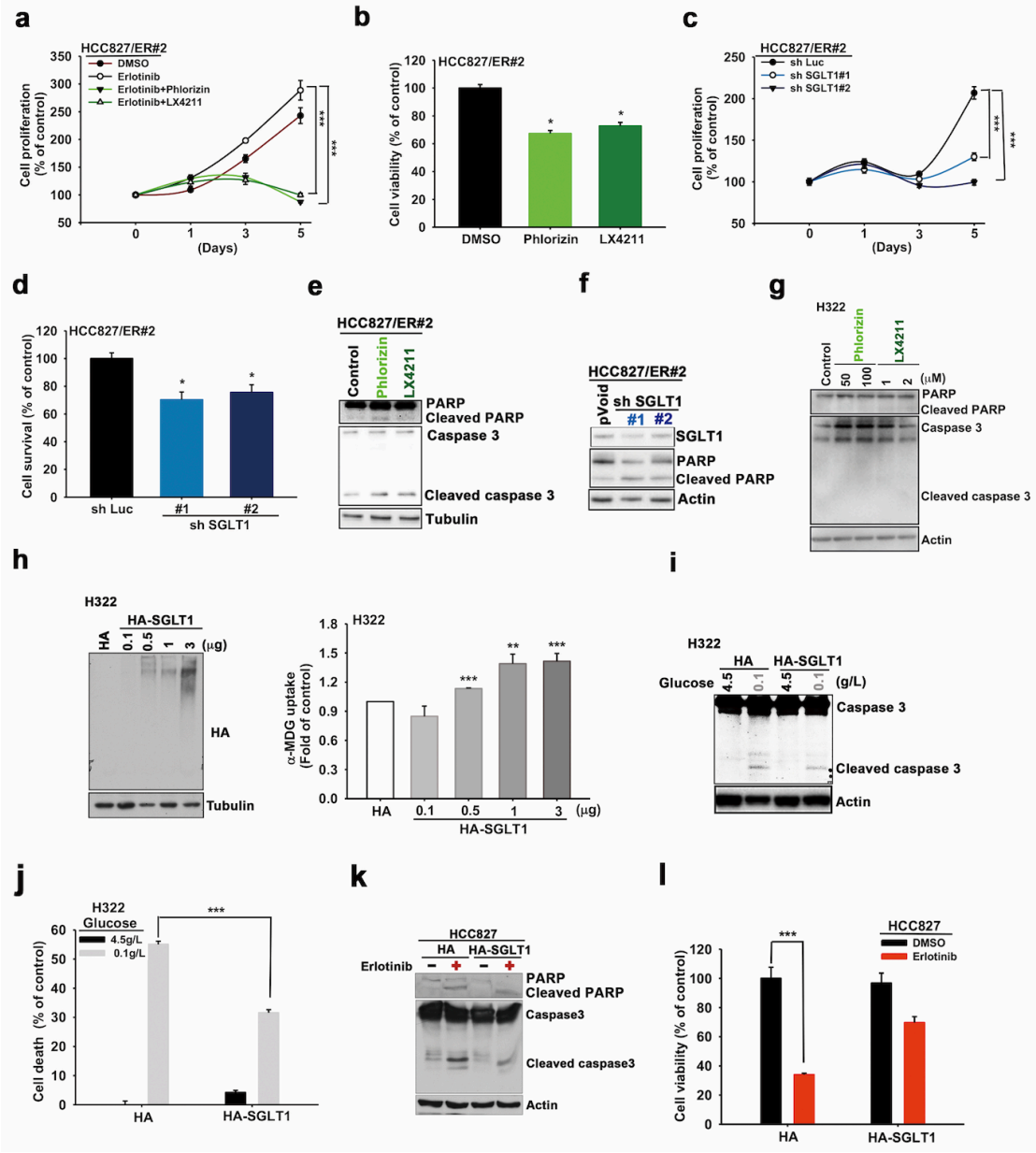

241

242 **Supplementary Fig S4. The upregulated SGLT1 supported the cell viability of**
243 **the acquired TKI-resistant cells. a.** The cell proliferation of HCC827/ER clones in
244 response to erlotinib, phlorizin, or LX4211 were determined in WST-1 analysis. **b.**
245 The effects of phlorizin or LX4211 on cell viability of HCC827/ER#2 clones under
246 low glucose concentration were measured in WST-1 analysis. **c and d.** The effects of
247 SGLT1 shRNA on cell proliferation (c) and viability (d) of HCC827/ER#2 clones
248 under low glucose concentration were determined in cell counting and WST-1
249 analyses, respectively. **e and f.** The effects of SGLT1 inhibitors (e) and shRNA (f) on

PARP cleavages, caspase 3 in HCC827/ER#2 clones were analyzed by WB. **g.** The effects of SGLT1 inhibitors on PARP cleavages, caspase 3 in H322 cells were analyzed by WB. **h**. H322 cells transfected with different amounts of SGLT1 cDNA were subjected to analyze the SGLT1 protein level in WB (left) and to measure α-MDG uptake (right). **i**. The effects of SGLT1 overexpression on caspase 3 cleavage induced by glucose deprivation in H322 cells were analyzed by WB. **j**. The relative cell death of SGLT1-expressing H322 cells in response to glucose deprivation was measured in WST-1 analysis. **k and l.** The effects of SGLT1 overexpression on the erlotinib-induced PARP and caspase 3 cleavages (k) and cell death (l) in HCC827 cells were analyzed in WB and WST-1 analyses, respectively. Data in **(a-d)**, **(h), and (j)** represent the mean and s.d. from three independent experiments. * $p< 0.05$; *** $p< 0.001$ vs control group, Student's t test. Data in **(e-g), (i) and (k)** are representative of three experiments.

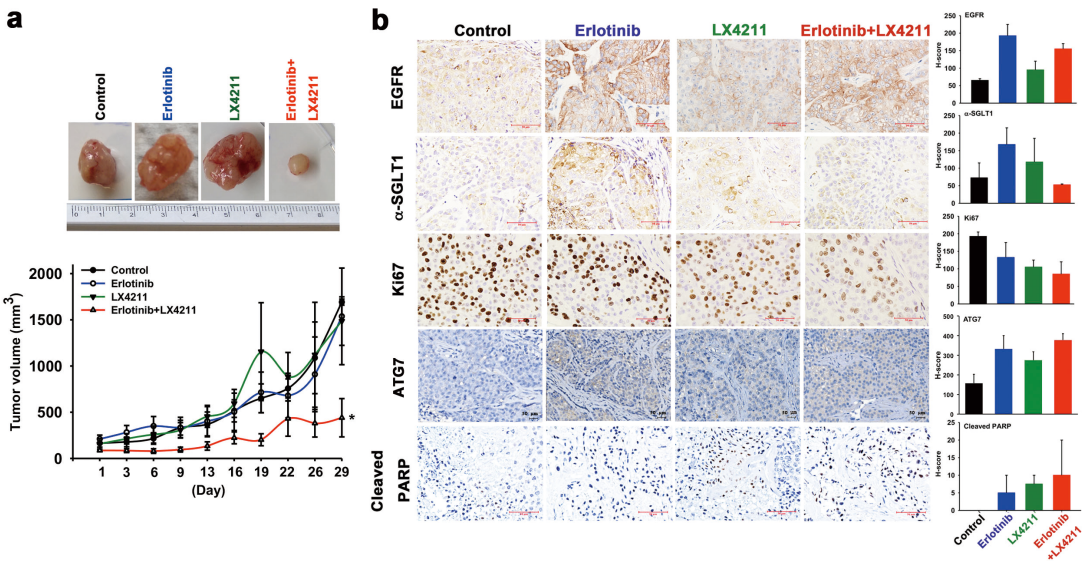

263

264 **Supplementary Fig S5. Targeting SGLT1 reduced the development of acquired**
265 **resistance to EGFR TKI *in vivo*. a.** The growth rate of xenograft tumors of H292
266 cells in response to treatments with erlotinib, LX4211, or the combination of erlotinib
267 and LX4211 was determined by measuring the tumor size. **b**. Representative IHC
268 staining of xenograft tumors from (a) was performed with the indicated antibodies,
269 and the H-score of protein expression was shown. Scale bar, 50 μm. Data represent
270 mean±s.d. * $p< 0.05$ vs control group, Student's t test.

271

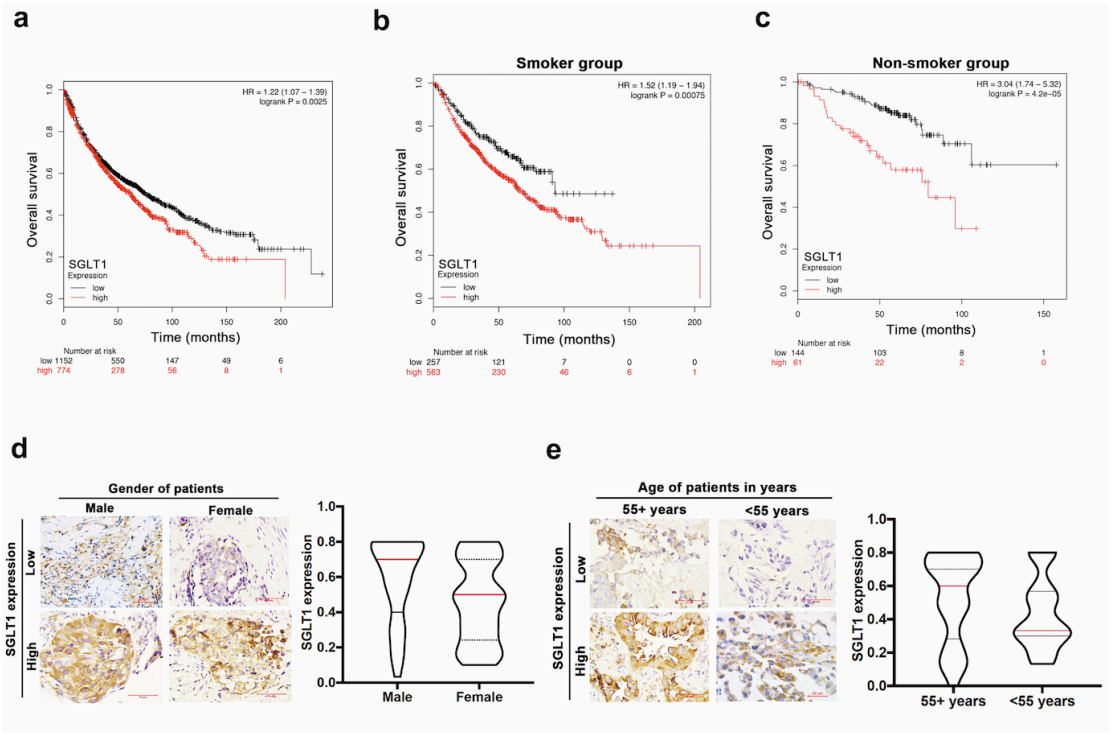

Supplementary Fig S6. SGLT1 expression negatively correlates with the clinical benefits of EGFR TKI in NSCLC patients. **a.** The clinical correlation of SGLT1 mRNA expression with overall survival rate was analyzed in the Kaplan Meier analysis. **b, c.** The SGLT1 mRNA expression was further classified into with (b) and without cigarette smoke (c) groups for Kaplan-Meier overall survival. **d, e.** The SGLT1 protein level in the paired tissues from treatment-naïve tumors and acquired TKI-resistant tumors of 9 lung cancer patients were examined by IHC staining and quantitated. The representative data was shown according to the gender (d) and age (e). Scale bar, 50 μm.

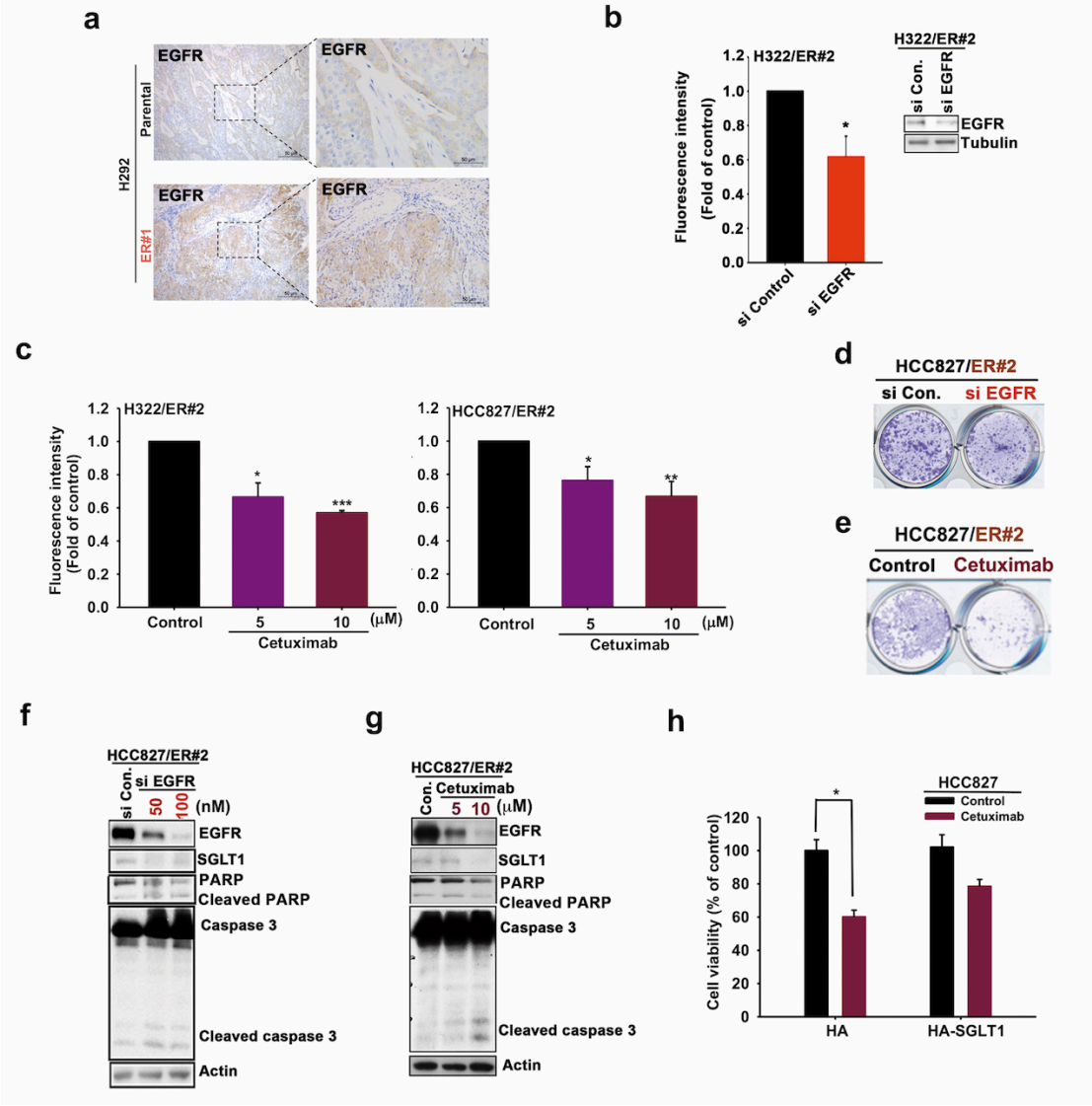

Supplementary Fig S7. **The increased EGFR mediated the glucose uptake and viability of the acquired erlotinib-resistant cells through SGLT1 upregulation. a**. The EGFR protein staining of H292 cells-xenograft tumor sections in response to erlotinib treatment was performed in IHC analysis. Scale bar, 50μm. **b-g**. The effects of monoclonal antibody cetuximab or EGFR siRNA on 2-NBDG uptake (b and c), colony formation (d and e), and caspase and PARP cleavages (f and g) of HCC827/ER#2 cells were determined, respectively. **h**. The effects of SGLT1 overexpression on the cetuximab-induced viability inhibition of HCC827 cells were examined in WST-1 analysis. Data in **(b and c)**, and **(h)** represent as mean±s.d. from three independent experiments. * $p< 0.05$; ** $p< 0.01$; *** $p< 0.001$ vs control group,

293 Student's t test. Data in **(a)** and **(d-g)** were representative of three experiments.

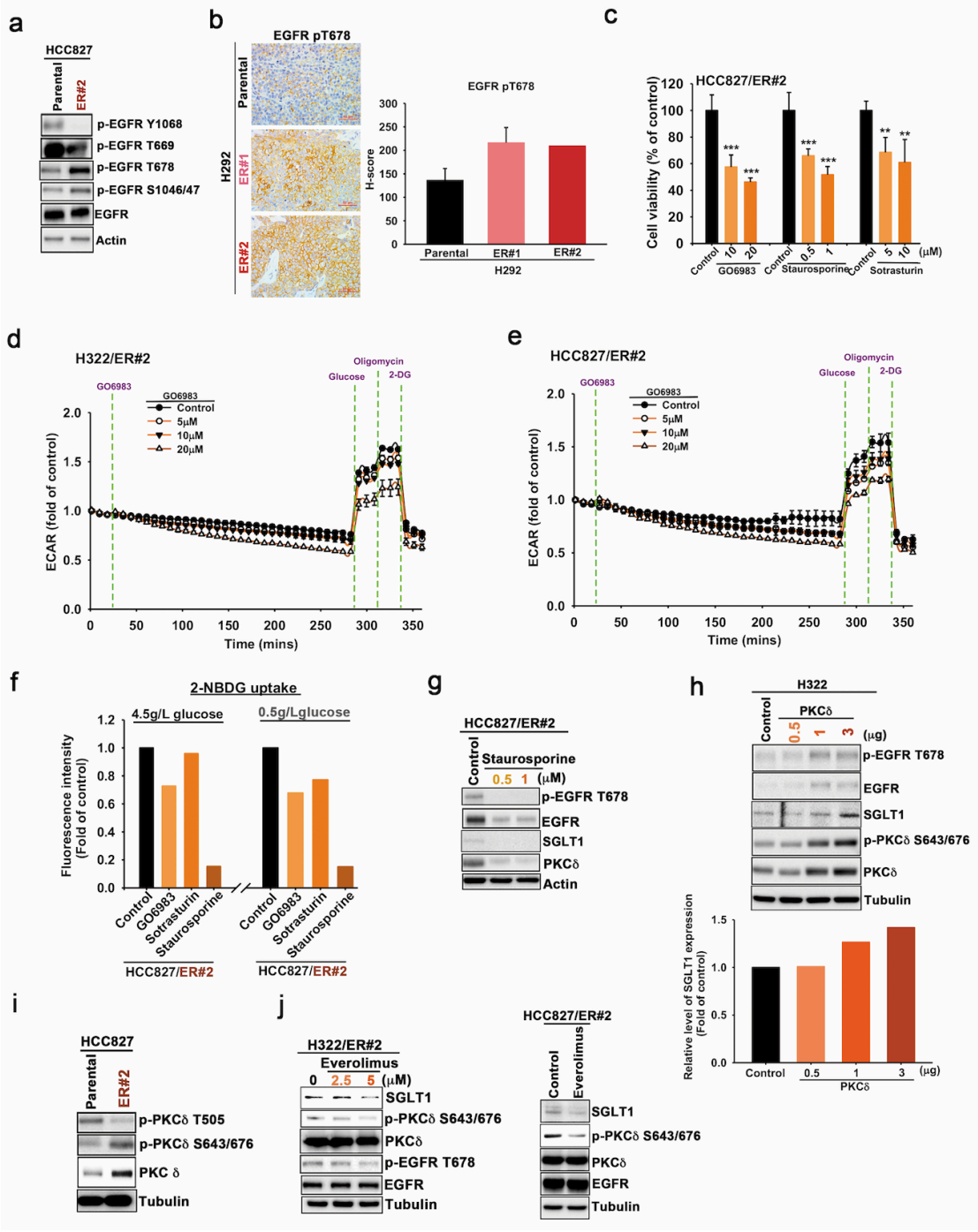

Supplementary Fig S8. **EGFR Thr678 phosphorylation by PKC delta mediated the SGLT1/EGFR interaction for SGLT1 protein stabilization. a**. The protein and phosphorylations of EGFR in HCC827 cells and their ER clones were analyzed in WB analysis. **b**. Representative IHC image and H-score of EGFR p-T678 expression in xenograft tumor sections of H292 cells and their ER clones were shown. Scale bar, 50 μm. **c**. The effects of GO6983, staurosporine, sotrasturin or HBDDE on cell

viability were determined in WST-1 assay. **d, e.** Changes in ECAR in H322/ER#2 (d) and HCC827/ER#2 (e) cells in response to GO6983 treatment for 4 hrs were analyzed in XF-24 Seahorse extracellular flux analyzer. **f**. The effects of various PKC inhibitors treatment on 2-NBDG uptake ability were analyzed by FACS analysis. **g-j.** The total lysates from staurosporine-treated HCC827/ER#2 cells (g), PKCδ-transfected H322 cells (h), HCC827 cells and their ER clones (i), and everolimus-treated H322/ER#2 cells (j) were subjected to WB analysis with the indicated antibodies. Data shown in **(c)**, **(d)**, and **(e-f)** represent as mean±s.d. from three independent experiments. ***$p< 0.001$ as compared with control group using Student's t test. Data in **(a)**, **(b)**, and **(g-j)** were representative of three experiments.

311 Table 1. Association of SGLT1 with clinical characteristics

		Analysis patients' number	SGLT1		*p* value
		Total number (72)	High	Low	
Gender					
	Male	35	18 (51.4%)	17 (48.5)	
	Female	37	9 (24.3%)	28 (75.6)	0.018*
Age (years)					
	≧55	53	26 (49.0%)	27 (50.9%)	
	<55	19	2 (10.5%)	17 (89.4%)	0.003**
Smoke					
	Smoker	26	12 (46.1%)	14 (53.8%)	
	Non-smoker	46	15 (32.6%)	31 (67.3%)	0.254
EGFR status					
WT		33	9 (27.2%)	24 (72.7%)	
Mutation		39	18 (46.1%)	21 (53.8%)	0.099
	del.19	20	10 (50%)	10 (50%)	
	L858R	16	7 (43.7%)	9 (56.2%)	
	del.19/T790M	1	0 (0%)	1 (100%)	
	L816Q	1	1 (100%)	0 (0%)	
	exon 20	1	0 (0%)	1 (100%)	0.552
Clinical T-stage					
	Tx-T0	5	2 (40%)	3 (60%)	
	T1-T2	14	7 (50%)	7 (50%)	
	T3-T4	44	16 (36.3%)	28 (63.6%)	0.662
Clinical N-stage					
	x	4	2 (50%)	2 (50%)	
	0	11	6 (54.5%)	5 (45.4%)	
	1	3	0 (0%)	3 (100%)	
	2	20	9 (45%)	11 (55%)	
	3	26	8 (30.7%)	18 (69.2%)	0.37
Pathological staging (AJCC)					
	Stage I	0	0 (0%)	0 (0%)	
	Stage II	1	1 (100%)	0 (0%)	
	Stage III	5	0 (0%)	5 (100%)	
	Stage IV	44	19 (43.1%)	25 (56.8%)	0.081
TKI drug therapy					
	Gefitinib	36	16 (44.4%)	20 (55.5%)	
	Erlotinib	35	13 (37.1%)	22 (62.8%)	

	Afatinib	2	0 (0%)	2 (100%)	0.417
TKI response CT					
	PR	20	8 (40%)	12 (60%)	
	SD	9	3 (33.3%)	6 (66.6%)	
	PD	38	16 (42.1%)	22 (57.8%)	0.89

312 *$P < 0.05$ and *$P < 0.01$